

17 MEI 1971

HYPERFINE INTERACTIONS OF
RADIOACTIVE NUCLEI STUDIED
WITH NUCLEAR ORIENTATION
AND NMR TECHNIQUES

INSTITUUT-LORENTZ
voor theoretische natuurkunde
Nieuwsteeg 16-Londen-100, Nederland

L. NIESEN

Universiteit Leiden



2 020 084 1

Bibliotheek
Gorlaeus Laboratoria
Universiteit Leiden
Postbus 9502
NL-2300 RA LEIDEN

17 MEI 1971

HYPERFINE INTERACTIONS OF RADIOACTIVE NUCLEI STUDIED WITH NUCLEAR ORIENTATION AND NMR TECHNIQUES

PROEFSCHRIFT

TER VERKRIJGING VAN DE GRAAD VAN DOCTOR IN
DE WISKUNDE EN NATUURWETENSCHAPPEN AAN
DE RIJKSUNIVERSITEIT TE LEIDEN, OP GEZAG VAN
DE RÉCTOR MAGNIFICUS DR. C. SOETEMAN, HOOG-
LERAAR IN DE FACULTEIT DER LETTEREN, TEN
OVERSTAAN VAN EEN COMMISSIE UIT DE SENAAT
TE VERDEDIGEN OP WOENSDAG 19 MEI 1971
TE KLOKKE 15.15 UUR

DOOR

LAMBERTUS NIESEN

geboren te 's-Gravenhage in 1942

INSTITUUT-LORENTZ
voor theoretische natuurkunde
Nieuwsteeg 15-Leiden-Nederland

1971

Drukkerij J. H. Pasmans - 's-Gravenhage

kast dissertaties

Promotor: Prof. Dr. C.J. Gorter

Dit proefschrift is tot stand gekomen onder toezicht van
Dr. W.J. Huiskamp

This investigation is part of the research program of the "Stichting voor Fundamenteel Onderzoek der Materie (F.O.M.)", financially supported by the "Organisatie voor Zuiver Wetenschappelijk Onderzoek (Z.W.O.)"

STELLINGEN

1. De behandeling van de richtingscorrelatie tussen twee in cascade uitgezonden gamma-quanta, waarvan er minstens één een gemengd multipool karakter heeft, geschiedt in een aantal belangrijke overzichtsartikelen op dit gebied onvolledig en daardoor misleidend.

Biedenharn, L.C. en Rose, M.E., *Rev.Mod.Phys.* 25 (1953) 729.
Devons, S. en Goldfarb, L.J., *Handbuch der Physik* 42 (1957) 362.

Frauenfelder, H. en Steffen, R.M., *Alpha-, Beta- and Gamma-Ray Spectroscopy*, ed. K. Siegbahn, North-Holland Publ. Co. (Amsterdam, 1965) 997.

2. Het is te verwachten dat metingen met behulp van het Mössbauer effect, waarbij als bron ^{57}Co kernen worden gebruikt die opgenomen zijn in niet-metallische kristallen, uitgevoerd in het temperatuurgebied 1-300 K, interessante gegevens zullen opleveren over de atomaire effecten optredende na de vangst van een elektron in de ^{57}Co kern.

Wickman, H.H. en Wertheim, G.K., *Chemical Applications of Mössbauer Spectroscopy*, ed. V.I. Goldanskii and R.H. Herber, Academic Press (New York) 1968, 548.

3. Voor het afkoelen van metallische preparaten tot een temperatuur nabij 10^{-3} K verdient de demagnetisatie van een kubische intermetallische Pr-verbinding zoals PrTi_3 de voorkeur boven de kern-demagnetisatie van koper.

Andres, K. en Bucher, E., *Phys. Rev. Letters* 24 (1970) 1181.

4. Het is mogelijk de ladingstoestand van een ion tijdens zijn vlucht door een kristalrooster te bepalen aan de hand van de spectrale verdeling van de door het ion uitgezonden Röntgenstraling.

Burch, D. en Richard, P., *Phys.Rev.Letters* 25 (1970) 983.

5. Het door Stearns voorgestelde model ter verklaring van de gemeten hyperfijnvelden van gastatomen in ijzer bevat een aantal veronderstellingen die deels onaannemelijk, deels onjuist zijn.

M.B. Stearns, *Phys.Letters* 34A (1971) 146.

6. De metingen van Clogston et al. van de Knight shift van ^{51}V in de supergeleidende toestand van V_3Ga en V_3Si moeten met enige reserve worden beschouwd.
- Clogston, A.M., Gossard, A.C., Jaccarino, V. en Yafet, Y., Phys.Rev.Letters 9 (1962) 262.
7. De metingen van de kernorientatie van ^{54}Mn in het systeem CuMn leveren geen overtuigend bewijs voor het bestaan van een spin-gecompenseerde toestand (Kondo toestand) met $T_K = 0.06$ K.
- Campbell, I.A., Compton, J.P., Williams, I.R. en Wilson, G.V.H., Phys.Rev.Letters 19 (1967) 1319.
 Pratt, W.P., Schermer, R.I. en Steyert, W.A., Journ. Low Temp.Phys. 1 (1969) 469.
 Flouquet, J., J.Phys.F., Metal Phys. 1 (1971) 87.
8. Voor de interpretatie van protonresonantiemetingen aan $\text{CuCl}_2 \cdot 2\text{H}_2\text{O}$ in de antiferromagnetische toestand is het van belang de proton-koper wisselwerking in gehydrateerde en magnetisch verdunde koperzouten te bestuderen met de "ligand ENDOR" techniek.
- Poulis, N.J., Hardeman, G.E.G., v.d. Lugt, W. en Hass, W.P.A., Physica 24 (1958) 280.
 V. Ormondt, D., De Beer, R., Brouha, M. en De Groot, F., Z. Naturforsch. 24a (1969) 1746.
9. Brintzinger en Bercaw menen ten onrechte dat met behulp van kernresonantietechnieken geen onderscheid valt te maken tussen de twee door hen voorgestelde structuren van $(\text{C}_{10}\text{H}_9\text{TiH})_2$.
- Brintzinger, H.H. en Bercaw, J.E., Journ.Am.Chem.Soc. 92 (1970) 6182.
10. Om in Nederland een adequaat wetenschapsbeleid mogelijk te maken is het gewenst dat de universiteiten en hogescholen hun begrotingen zodanig gaan inrichten dat duidelijk wordt welke uitgaven worden gedaan ten behoeve van wetenschappelijk onderzoek.
11. Een gemeenschappelijke koffiepauze is van groot belang voor het goed functioneren van een werkgroep voor wetenschappelijk onderzoek.

CONTENTS

INTRODUCTION AND SURVEY	7
I. NUCLEAR MAGNETIC RESONANCE ON ORIENTED NUCLEI IN A DILUTE PARAMAGNETIC CRYSTAL; ^{52}Mn AND ^{54}Mn IN $\text{La}_2\text{Mg}_3(\text{NO}_3)_{12}\cdot 24\text{H}_2\text{O}$.	13
1. Introduction and principle.	13
2. Theory.	15
2.1. Crystal structure, energy levels of ^{52}Mn , ^{54}Mn and Ce in LMN.	15
2.2. Nuclear properties of ^{52}Mn and ^{54}Mn ; angular distribution of gamma rays.	17
2.3. Theory of the NMR-ON process.	19
3. Experimental.	22
3.1. Equipment.	22
3.2. Experimental procedure.	26
4. Experimental results on ^{54}Mn .	28
4.1. Line positions and hfs parameters.	28
4.2. Changes in $W(0)$.	32
4.3. Linewidths.	34
5. Experimental results on ^{52}Mn .	35
5.1. Line positions and hfs parameters.	35
5.2. Changes in $W(0)$, linewidths.	37
6. Discussion.	39
6.1. Hfs parameters; nuclear moments.	39
6.2. Origin of the homogeneous linewidth.	40
6.3. Conclusion.	42
References.	43
II. NUCLEAR MAGNETIC RESONANCE ON ORIENTED NUCLEI IN A DILUTE PARAMAGNETIC CRYSTAL; ^{57}Co , ^{58}Co AND ^{60}Co IN $\text{La}_2\text{Mg}_3(\text{NO}_3)_{12}\cdot 24\text{H}_2\text{O}$.	45
1. Introduction.	46
2. Theory.	48

2.1. Crystal structure; energy levels of Co^{2+} ions in LMN.	48
2.2. Gamma anisotropy parameters for ^{57}Co .	54
2.3. Gamma anisotropy parameters for ^{58}Co .	59
2.4. Gamma anisotropy parameters for ^{60}Co .	61
3. Experimental arrangements.	63
4. Experimental results on ^{60}Co .	64
4.1. Nuclear orientation by means of cross relaxation with Ce spins.	64
4.2. Nuclear spin-lattice relaxation times.	68
4.3. Line positions and hfs parameters.	70
4.4. Linewidths.	73
4.5. Changes in $W(0)$.	74
5. Experimental results on ^{58}Co .	75
5.1. Nuclear orientation by means of cross relaxation with Ce spins.	75
5.2. Line positions and hfs parameters.	76
5.3. Linewidths.	77
5.4. Changes in $W(0)$ and $W(\pi/2)$.	80
6. Experimental results on ^{57}Co .	81
6.1. Nuclear orientation by means of cross relaxation with Ce spins.	81
6.2. Line positions and hfs parameters.	81
6.3. Linewidths.	84
6.4. Multipole mixing ratio of the 122 keV gamma transition in ^{57}Co ; reorientation in the 136 keV state.	84
6.5. Changes in $W(0)$ and $W(\pi/2)$.	87
7. Discussion.	89
7.1. Hfs parameters and nuclear moments.	89
7.2. Comparison of linewidths.	92
7.3. Intermediate state reorientation after electron capture.	94
8. Conclusion.	96
APPENDIX 1. Analysis of errors in the obtained hfs parameters and in the calculated resonance frequencies.	97

APPENDIX 2. Analysis of changes in $W(0)$ during saturation of resonance transitions.	99
References.	100
III. HYPERFINE FIELDS ON ^{133}Xe AND ^{160}Tb NUCLEI IN Fe.	103
1. Introduction.	103
2. Theory.	105
2.1. Decay and magnetic moment of ^{133}Xe . Gamma anisotropy parameters.	105
2.2. Decay and magnetic moment of ^{160}Tb . Gamma anisotropy parameters.	106
2.3. Hyperfine fields on dilute impurities in iron.	108
2.3.1. Hyperfine field on ^{133}Xe in Fe.	108
2.3.2. Hyperfine field on ^{160}Tb in Fe.	111
3. Experimental arrangements.	115
3.1. Foil preparation.	115
3.2. Measuring equipment.	116
4. Results and discussion.	119
4.1. ^{133}Xe in Fe.	119
4.2. ^{160}Tb in Fe.	122
References.	129
SAMENVATTING.	131
STUDIEOVERZICHT.	134

INTRODUCTION AND SURVEY.

Nuclear orientation can be defined as the ordering of nuclear spins in space. Two requirements must be met in order to achieve orientation of nuclear spins I: i) the $2I + 1$ spatial degeneracy must be removed, leading to differences in energy between the associated $2I + 1$ nuclear sublevels, and ii) appreciable differences in occupation numbers of these sublevels have to be realized. If the nuclei to be studied are radioactive and emit gamma rays during their decay, the degree of nuclear orientation can be determined by observing the directional distribution of these gamma rays¹⁾.

Several mechanisms can be used to produce the necessary splittings of the nuclear sublevels. The use of an external magnetic field, interacting with the nuclear magnetic moment μ , is the most obvious. This method, however, has only little practical importance so far, because even in a magnetic field as high as 100,000 Oe, the associated energy differences between the nuclear sublevels, $\frac{\Delta E}{k} = \frac{\mu H}{k}$, are in the milli-Kelvin range. In order to achieve nuclear orientation by a thermal equilibrium method, the nuclear spins must be cooled down to that temperature region. The experimental problems associated with this method (known as "brute force" polarization) are formidable, and up to now only very few experiments have been done in this field.

In nearly all other methods, one uses the hyperfine interaction between the nucleus and the surrounding electrons. This can be

1. The coupling between the nuclear electric quadrupole moment and the electric field gradient at the nucleus, produced by the non spherical electron charge distribution and the lattice potential of the closed shell ions. ("Electric hyperfine structure" or "quadrupole" interaction.)
2. The interaction between the nuclear magnetic dipole moment and the "magnetic field" produced by the surrounding electron cloud ("magnetic hyperfine structure" interaction).

Extensive discussions of these methods can be found in ref. 1, 2 and 3. The practical realization of these methods requires temperatures of the order of 10^{-2} K; sometimes in addition a rather small magnetic

field is used to orient the electronic spins. If one wishes to study hyperfine interactions by means of orientation of radioactive nuclei, one has to measure the directional anisotropy of the emitted gamma rays as a function of the temperature of the sample; sometimes it is useful to vary the external magnetic field also. The parameters in the Hamiltonian which describes the hyperfine structure (hfs) interaction can then be found by curve fitting procedures. In this way, only global information concerning the character of the hfs interaction can be obtained. Moreover, the relative accuracy of the results is not high (1 - 10%), due to the statistical nature of the experiments. On the other hand, the concentration of the radioactive atoms (ions) can be very small (of the order of 10^{-10}), which gives the possibility of "probing" the hyperfine interactions in different environments, thereby obtaining information about the electronic structure of the solid.

Hyperfine interactions can also be studied by resonance techniques, such as electron spin resonance (EPR), nuclear magnetic resonance (NMR) and electron-nuclear double resonance (ENDOR). In this way, detailed, and usually very accurate, information about hfs levels can be obtained (relative accuracy is in the order of $10^{-3} - 10^{-5}$). However, these measurements require a rather high concentration of the studied atoms, which clearly limits the applicability of these methods.

A combination of both resonance and nuclear orientation techniques would thus form a very powerful method to study hyperfine interactions, especially in very dilute systems. This was realized very early; in fact, the first suggestion of this kind was made by Tolhoek and De Groot⁴⁾ in 1951, before the first successful nuclear orientation experiment was performed. The underlying idea is very simple: if an ensemble of radioactive nuclear spins is oriented, and one induces resonance transitions between the hfs levels by means of an r.f. field, these transitions can be detected by the accompanying changes in the directional anisotropy of the emitted gamma rays.

The practical problems associated with this method are considerable, however, and therefore the first attempts to use the technique failed⁵⁾, mainly because of rf heating of the sample, causing a rapid

warm up of the adiabatic demagnetization apparatus. Pipkin and Culvahouse^{6,7)} used the method of rf destruction of nuclear orientation successfully in connection with experiments in which the nuclei were oriented dynamically, a technique that will not be discussed here. The first successful attempt to combine thermal equilibrium nuclear orientation and NMR was made in 1966 by Matthias and Holliday⁸⁾, using ^{60}Co nuclei dissolved in iron metal.

In this thesis, the method of Nuclear Magnetic Resonance on Oriented Nuclei (NMR-ON) is applied to radioactive isotopes, incorporated in a dilute ionic crystal. Chapter I deals with ^{52}Mn and ^{54}Mn nuclei in lanthanum magnesium nitrate (LMN), whereas in Chapter II, measurements are described on ^{57}Co , ^{58}Co and ^{60}Co nuclei in the same salt. Under our experimental conditions (temperatures below 0.1 K, magnetic fields of several kOe), the electronic spins of the Mn^{2+} and Co^{2+} ions are polarized to a high degree, which leads to very long nuclear spin-lattice relaxation times. Therefore nuclear orientation was produced by means of thermal mixing (cross relaxation) with a cold system of cerium spins, the Ce ions replacing about 0.1% of the La ions in the lattice. This method has been described in detail by Lubbers⁹⁾. In this way, one can perform NMR measurements on a strongly polarized nuclear spin system which is thermally isolated from the surroundings. This is very advantageous compared to earlier experiments, since in this way the problem of rf heating is practically eliminated.

Several hfs transitions could be induced separately, and the populations of two adjacent hfs levels could be equalized using only a small rf field (≈ 1 mOe), the frequency of which was swept once through the resonance line. From the measured resonance frequencies, the magnetic moments of the five radioactive isotopes were determined with a precision limited mainly by the precision with which the magnetic moments of the stable isotopes ^{55}Mn and ^{59}Co are known. The electric quadrupole moments of the five isotopes were determined for the first time. In addition, interesting information was obtained about the resonance mechanism itself and the broadening of the resonance lines. For one isotope, ^{57}Co , the multipole character of the emitted 122 keV gamma

transition was determined with high precision; also studied in some detail was the reorientation of the ^{57}Fe nucleus in the excited state at 136 keV following the electron capture in the ^{57}Co nucleus.

Chapter III is devoted to nuclear orientation studies of ^{133}Xe and ^{160}Tb nuclei, implanted in iron foils by means of an isotope separator. The measurements were done in close collaboration with the group of Prof. H. de Waard in Groningen. For this type of samples, all attempts to perform NMR-ON measurements have failed so far, possibly connected with linewidth problems. Therefore only static nuclear orientation measurements were performed, by cooling the samples down to 0.015 K in a magnetic field of about 2kOe, i.e. sufficiently large to orient the domains in the iron foil.

For both nuclides, a large hfs interaction was found. For Xe - a diamagnetic impurity - the magnetic hyperfine field is caused by the fact that the s electrons with their spin directed parallel at the iron magnetization have a different density at the nucleus than the s electrons with their spins in the opposite direction. The experimental results suggest that the overlap between the 3d wave functions of the iron host and the s electron wave functions of the Xe atoms is responsible for the observed hyperfine interaction.

The results on ^{160}Tb in Fe can be explained satisfactorily by assuming that the Tb impurities behave as Tb^{3+} ions, and that the hfs interaction of the free ion is responsible for the major part of the observed interaction. Both magnetic and electric hfs interaction is present in this case, which results in some ambiguity in the interpretation of the measurements.

The method of ion implantation - which is the only available technique to bring these ions into the iron lattice - presents additional difficulties in the data analysis. From several experiments it is known that not all ions end up in substitutional positions, hence no unique hyperfine field for all ions is to be expected. Nevertheless, meaningful results were obtained by combining the data with the results of Mössbauer experiments on ^{133}Cs (the daughter nucleus of ^{133}Xe) and on ^{161}Dy in Fe, performed in Groningen.

The significance of the results is discussed in the context of the systematic study of hyperfine structure interactions of dilute impurities in ferromagnetic metals, a topic that has recently received much experimental and theoretical interest^{10,11}.

Summarizing one may say that the work in this thesis forms part of the rapidly growing field of hyperfine structure interactions detected by nuclear radiations. The main theme is the development of sensitive methods for measuring the magnitude of the hfs interactions, and the precise determination of the magnetic moments of radioactive nuclei. One may expect that this will stimulate the use of radioactive nuclei as probes for further study of atomic structure. Accurate measurements of the hyperfine interactions of several nuclides of the same element may provide future possibilities for studying isotope effects in various solids.

Chapter I of this thesis has been published in *Physica* 50 (1970) 259; Chapter II will be published in the same journal.

References

1. De Groot, S.R., Tolhoek, H.A. and Huiskamp, W.J., *Alpha- Beta and Gamma-Ray Spectroscopy*, ed. K. Siegbahn, North-Holland Publ. Co. (Amsterdam, 1965) p. 1199 c.f.
2. Daniels, J.M., *Oriented Nuclei*, Academic Press, New York (1965).
3. Shirley, D.A., *Thermal Equilibrium Nuclear Orientation*, *Ann.Rev. Nucl.Sci.* 16 (1966) 89.
4. Tolhoek, H.A. and De Groot, S.R., *Physica* 17 (1951) 81.
5. Bloembergen, N. and Temmer, G.M., *Phys.Rev.* 89 (1953) 883.
6. Pipkin, F.M. and Culvahouse, J.W., *Phys.Rev.* 109 (1958) 1423.
7. Pipkin, F.M., *Phys.Rev.* 112 (1958) 935.
8. Matthias, E. and Holliday, R.J., *Phys.Rev.Letters* 17 (1966) 897.
9. Lubbers, J., thesis, Leiden (1967); Lubbers, J. and Huiskamp, W.J., *Physica* 34 (1967) 193. (*Commun. Kamerlingh Onnes Lab., Leiden No. 353b*).
10. Shirley, D.A., Rosenblum, S.S. and Matthias, E., *Phys.Rev.* 170 (1968) 363.
11. De Waard, H., *Ned.Tijdschr. voor Natuurkunde* 35 (1969) 253.

The first part of the paper is devoted to the study of the interaction of the electron with the field of a plane wave in the case of a relativistic electron. The results of the calculations are given in the form of explicit formulas. The second part of the paper is devoted to the study of the interaction of the electron with the field of a plane wave in the case of a non-relativistic electron. The results of the calculations are given in the form of explicit formulas. The third part of the paper is devoted to the study of the interaction of the electron with the field of a plane wave in the case of a relativistic electron in the presence of a magnetic field. The results of the calculations are given in the form of explicit formulas. The fourth part of the paper is devoted to the study of the interaction of the electron with the field of a plane wave in the case of a non-relativistic electron in the presence of a magnetic field. The results of the calculations are given in the form of explicit formulas. The fifth part of the paper is devoted to the study of the interaction of the electron with the field of a plane wave in the case of a relativistic electron in the presence of a magnetic field and a scalar potential. The results of the calculations are given in the form of explicit formulas. The sixth part of the paper is devoted to the study of the interaction of the electron with the field of a plane wave in the case of a non-relativistic electron in the presence of a magnetic field and a scalar potential. The results of the calculations are given in the form of explicit formulas. The seventh part of the paper is devoted to the study of the interaction of the electron with the field of a plane wave in the case of a relativistic electron in the presence of a magnetic field and a scalar potential. The results of the calculations are given in the form of explicit formulas. The eighth part of the paper is devoted to the study of the interaction of the electron with the field of a plane wave in the case of a non-relativistic electron in the presence of a magnetic field and a scalar potential. The results of the calculations are given in the form of explicit formulas. The ninth part of the paper is devoted to the study of the interaction of the electron with the field of a plane wave in the case of a relativistic electron in the presence of a magnetic field and a scalar potential. The results of the calculations are given in the form of explicit formulas. The tenth part of the paper is devoted to the study of the interaction of the electron with the field of a plane wave in the case of a non-relativistic electron in the presence of a magnetic field and a scalar potential. The results of the calculations are given in the form of explicit formulas.

CHAPTER I

NUCLEAR MAGNETIC RESONANCE ON ORIENTED NUCLEI
IN A PARAMAGNETIC CRYSTAL,
 ^{52}Mn AND ^{54}Mn IN $\text{La}_2\text{Mg}_3(\text{NO}_3)_{12} \cdot 24\text{H}_2\text{O}$ **Synopsis**

Transitions between hyperfine-structure levels of oriented ^{52}Mn and ^{54}Mn ions included in lanthanum magnesium nitrate were induced by radiofrequency irradiation. The Mn ions were oriented by cross relaxation with Ce ions, partly replacing the La ions ($\text{Ce} : \text{La} = 1 : 10^3$). Changes in the directional anisotropy of the gamma rays emitted by the nuclear spin system were utilized to detect the rf resonance transitions.

Different hfs transitions could be induced separately. Complete saturation of each transition was accomplished by slowly sweeping the frequency of the rf field across the resonance, the rf field amplitude being as low as 10^{-4} Oe. A theoretical description of the process is given in which the enhancement of the rf amplitude at the position of the nucleus through the intermediary of the electronic spin plays a major role. The agreement with the experimental results is satisfactory.

The observed resonance lines were very narrow; their width was mainly determined by the inhomogeneity of the external magnetic field. Also a homogeneous linewidth was shown to be present; it is argued that it originates from the protons surrounding the Mn ions.

By taking data at various field strengths and directions very accurate values of the hfs parameters were obtained. By comparing these with the data on the stable isotope ^{55}Mn the magnetic moments of ^{52}Mn and ^{54}Mn were derived with a precision determined only by the error in the value of the magnetic moment of ^{55}Mn . The quadrupole moments of both radioactive isotopes were determined for the first time.

1. *Introduction and principle.* Nuclear orientation may be achieved at very low temperatures by establishing a Boltzmann equilibrium over nuclear Zeeman levels under the influence of an external magnetic field or through the intermediary of hyperfine coupling in a paramagnetic ion.

In the case that the oriented nuclei are radioactive, a measurement of the anisotropy in the angular distribution of the emitted gamma rays (hereafter called gamma anisotropy) provides a means of detecting the degree of nuclear orientation.

It was suggested by Bloembergen and Temmer¹⁾ that saturation of the radiofrequency transitions between the nuclear Zeeman levels, thereby equalizing the population density of the nuclear magnetic substates, would destroy the gamma anisotropy, thus providing an easy method to detect

the resonance. We will call this method NMR-ON; nuclear magnetic resonance on oriented nuclei.

The first successful NMR-ON experiment was done in 1966 by Matthias and Holliday²⁾ who detected the resonance frequency of ^{60}Co nuclei dissolved in an iron lattice. Several experiments have been done since, in all cases on nuclei in metallic ferromagnets. They can be found in a recent review article by Shirley³⁾.

The main experimental difficulties of these experiments are:

a. A rather short (typically 1 min) nuclear spin-lattice relaxation time, which means that the spin system is practically in thermal equilibrium during the measurements. The rf power must be kept so low that the lattice does not warm up, because otherwise the nuclear orientation would diminish and eventually vanish.

b. The inhomogeneous broadening of the resonance line makes it necessary to sweep the frequency through the resonance in a period short compared to the spin-lattice relaxation time. Moreover, this means that the amplitude of the rf field must be enhanced compared to the situation without broadening, because one individual nucleus is in resonance only part of the time. A discussion of these problems has been given by Shirley⁴⁾.

In the experiments reported here these difficulties do not exist. By using a dilute paramagnetic crystal, the nuclear spin-lattice relaxation time can be made quite long: in a field of a few kOe and at $T < 0.1$ K the nuclear spins are effectively thermally isolated from their surroundings. In addition, the resonance lines are narrower than those from ferromagnetic samples, so that very accurate measurements are possible.

In the present paper we are dealing with samples consisting of diamagnetic $\text{La}_2\text{Mg}_3(\text{NO}_3)_{12} \cdot 24\text{H}_2\text{O}$ (hereafter called LMN) in which about 0.1% of the La ions are replaced by Ce ions. ^{52}Mn or ^{54}Mn ions are present as radioactive impurities in the relative concentrations of $\text{Mn} : \text{Mg} \approx 1 : 10^{10}$. The energy level schemes of these ions are discussed in section 2.1.

For orienting the ^{52}Mn or ^{54}Mn nuclear spins we used the scheme described in detail by Lubbers⁵⁾ and we mention here only the essential features. The Ce spins were first precooled to about 0.05 K by thermal contact with a K-Cr refrigerator in an adiabatic demagnetization apparatus in the presence of a magnetic field oriented in a direction in which the g value of the Ce spins was large. The field was subsequently rotated to a direction in which the g value was much smaller. By doing this adiabatically, the Ce ions were cooled. If the Zeeman splitting of the Ce ions became equal to the hfs splittings of the Mn ions, a fast thermal mixing between both

spin systems occurred which oriented the Mn nuclei. When, hereafter, the splittings were made unequal, the two spin systems were again thermally isolated from each other. In this way it was possible to obtain a highly polarized Mn nuclear-spin system which was practically isolated from the lattice.

The NMR experiment following this procedure consisted simply of varying the frequency of the rf field linearly in time until the frequency matched the difference of the lowest two levels of the Mn energy scheme. If an rf field of sufficient amplitude was used, the population of both levels were equalized. The frequency variation therefore led to a marked change in the gamma anisotropy, detected by two counters parallel to the magnetic field direction.

In a similar way the distance between higher lying levels could be found when the accompanying change in gamma intensity was large enough to be discernible.

2. Theory. 2.1. Crystal structure, energy levels of ^{52}Mn , ^{54}Mn and Ce in LMN. The crystal structure of the double nitrates is rather well known⁶). The divalent ions occupy two sites, one (type II) being twice as prevalent as the other type (type I). At both sites the divalent ion is surrounded by an octahedron of water molecules, which is somewhat distorted along that body diagonal which coincides with the trigonal crystal axis. The trivalent ion is surrounded by six nitrate groups. All these sites have trigonal symmetry, site I also has inversion symmetry.

The energy levels of the various ions in the crystal can be described by the following hamiltonian:

$$\begin{aligned} \mathcal{H} = & g_{\parallel}\mu_B H_z S_z + g_{\perp}\mu_B (H_x S_x + H_y S_y) + D\{S_z^2 - \frac{1}{3}S(S+1)\} \\ & + B_4^0\{35S_z^4 - 30S(S+1)S_z^2 + 25S_z^2 - 6S(S+1) + 3S^2(S+1)^2\} \\ & + AI_z S_z + B(I_x S_x + I_y S_y) - g_N \mu_N (1 - \sigma) \mathbf{H} \cdot \mathbf{I} \\ & + P\{I_z^2 - \frac{1}{3}I(I+1)\}. \end{aligned} \quad (1)$$

The z axis is chosen so as to coincide with the trigonal axis of the crystal. Values of the parameters appearing in this hamiltonian are listed in table I. All constants are measured directly, except the hfs parameters A and B , which are calculated using the known parameters of ^{55}Mn ⁷) and the ratios between the magnetic moments of ^{52}Mn , ^{54}Mn and ^{55}Mn .

For the ^{52}Mn and ^{54}Mn ions the following remarks can be made. The effective spin formalism cannot be used because of the relatively small influence of the crystalline field on the 6S_5 ground state of the Mn ion. The B_4^0 term consists of two contributions. One is the diagonal part of the cubic

field term which originates in the water octahedron around the Mn ion and the other comes from the axial distortion of this cubic field. The D term contains only the effect of this axial distortion. The off-diagonal part of the cubic field can be estimated, but it has a negligible effect on the distances

TABLE I

Spin hamiltonian parameters for ^{52}Mn , ^{54}Mn and Ce in LMN							
parameter	^{52}Mn		^{54}Mn		ref.	Ce	ref.
	site I	site II	site I	site II			
S	$\frac{5}{2}$	$\frac{5}{2}$	$\frac{5}{2}$	$\frac{5}{2}$		$\frac{1}{2}$	
I	6	6	3	3		0	
g_{\parallel}	2.0007(7)	2.0007(7)	2.0007(7)	2.0007(7)	9	0.0235(9)	5, 13
g_{\perp}	2.0007(7)	2.0007(7)	2.0007(7)	2.0007(7)	9	1.8264(13)	13
D/hc (10^{-4} cm^{-1})	-220.1(3)	-49.4(3)	-220.1(3)	-49.4(3)	9	-	
$B_{\frac{1}{2}}^0/hc$ (10^{-4} cm^{-1})	-0.045(2)	-0.054(2)	-0.045(2)	-0.054(2)	9	-	
A/hc (10^{-4} cm^{-1})	-33.419(5)*	-33.257(5)*	-71.55(13)*	-71.21(13)*	9, 10, 12	-	
B/hc (10^{-4} cm^{-1})	-33.35(8)*	-33.23(8)*	-71.40(14)*	-71.14(15)*	9, 10, 12	-	
g_N	+0.5088(3)*	+0.5088(3)*	+1.109(2)*	+1.109(2)*	10, 12	-	
σ	+0.0196	+0.0196	+0.0196	0.0196	11	-	

The values marked with an asterisk are calculated from the given references using $\mu (^{55}\text{Mn}) = +3.4432(16) \mu_N$.

between the various hyperfine levels and consequently has been omitted. For a discussion of the crystal field effects in this salt we refer to ref. 8. σ represents the diamagnetic shielding effect, its value is taken from ref. 11.

The resulting 78×78 resp. 42×42 matrices were diagonalized with the aid of the IBM 360/50 computer of the University of Leiden. The time necessary to calculate the eigenvalues for a fixed value and direction of the magnetic field was roughly 10 min for ^{52}Mn and 2 min for ^{54}Mn .

The dependence of the resonance lines on small changes of the parameters could be analysed most easily with the aid of closed forms obtained from perturbation theory. In a field of a few kOe the electronic Zeeman term dominates and by choosing a representation in which the magnetic field is diagonal one obtains for the differences of two successive energy levels of the lowest hfs multiplet ($S_z = -\frac{5}{2}$):

$$E_{-\frac{1}{2}, m+1} - E_{-\frac{1}{2}, m} = -\frac{5}{2}A + \frac{5}{2} \frac{mA^2}{g\mu_B H - 4D(\frac{3}{2} \cos^2 \theta - \frac{1}{2})} - g_N(1 - \sigma) \mu_N H + P(\frac{3}{2} \cos^2 \theta - \frac{1}{2})(2m + 1). \quad (2)$$

In this formula m is the nuclear magnetic quantum number and θ the angle between the field direction and the trigonal crystal axis. The B_4^0 term has

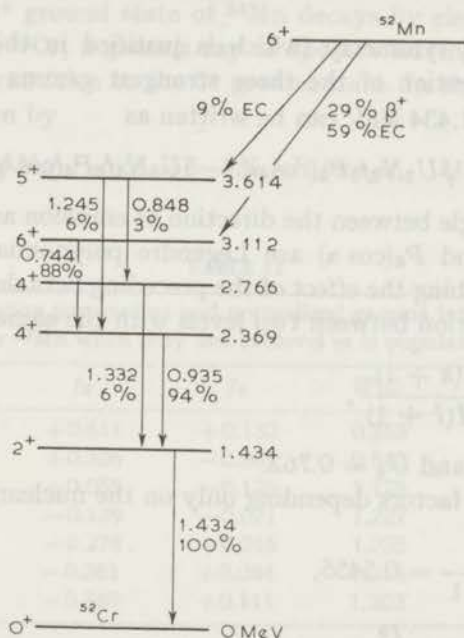


Fig. 1. Decay scheme of ^{52}Mn , taken from ref. 14. Only the important levels are shown.

been neglected; furthermore it has been assumed that the hyperfine interaction is isotropic ($A = B$). For $A \neq B$ and $B_4^0 \neq 0$ the expressions obtained are more complicated and it was found that the expression used above was sufficient to analyse the effect of small variations in the parameters.

The Ce ions have even-even nuclei, hence $I = 0$. The crystalline field splits up the 2F_3 ground state into 3 doublets. The spacing between the lowest two doublets is $\approx 24 \text{ cm}^{-1}$. Therefore higher order Zeeman effects are negligible in our considerations and only the lowest doublet is populated at temperatures below 1 K.

2.2. Nuclear properties of ^{52}Mn and ^{54}Mn ; angular distribution of emitted gamma rays. a. ^{52}Mn . The decay scheme is taken from

ref. 14. Only the important levels are shown (fig. 1). The main beta decay feeds the 6^+ level of ^{52}Cr at 3.112 MeV. The most precise measurement¹⁵⁾ of the Fermi admixture in the predominantly Gamow-Teller transition using the technique of beta-circularly polarized gamma directional correlation gives for the ratio of the matrix elements $C_{\text{FM}}/C_{\text{AMGT}} = +0.007 \pm 0.013$. This is in reasonable agreement with the beta-asymmetry experiments on oriented ^{52}Mn nuclei¹⁶⁾. We conclude that the Fermi admixture is negligible.

Assuming axial symmetry (which is justified in the case of Mn), the directional distribution of the three strongest gamma rays with energies 0.744, 0.935 and 1.434 MeV can be written as

$$W(\alpha) = 1 - \frac{1}{7}U_2N_2f_2P_2(\cos \alpha) - 5U_4N_4f_4P_4(\cos \alpha), \quad (3)$$

where α is the angle between the direction of emission and the quantization axis. $P_2(\cos \alpha)$ and $P_4(\cos \alpha)$ are Legendre polynomials. U_2 and U_4 are coefficients describing the effect of the preceding beta decay. For a Gamow-Teller beta transition between two levels with the same spin I one has:

$$U_k = 1 - \frac{k(k+1)}{2I(I+1)}, \quad (4)$$

thus $U_2 = 0.929$ and $U_4 = 0.762$.

N_2 and N_4 are factors depending only on the nuclear spin $I = 6$:

$$N_2 = \frac{I}{2I-1} = 0.5455, \quad (5)$$

$$N_4 = \frac{I^3}{(I-1)(2I-1)(2I-3)} = 0.4364.$$

f_2 and f_4 are so-called orientation parameters. In the case that the nuclear energy eigenvectors are also eigenvectors of I_z (i.e. $m = I_z$ is a good quantum number), they are given by:

$$f_2 = (1/I^2) \left\{ \sum_{m=-I}^{+I} m^2 a_m - \frac{1}{3}I(I+1) \right\}, \quad (6)$$

$$f_4 = (1/I^4) \left\{ \sum_{m=-I}^{+I} m^4 a_m - \frac{1}{7}(6I^2 + 6I - 5) \sum_{m=-I}^{+I} m^2 a_m + \frac{3}{35}I(I-1)(I+1)(I+2) \right\}, \quad (7)$$

in which a_m is the normalized population density of the level characterized by m . If m is not a good quantum number the summations $\sum_m m^k a_m$ are replaced by $\sum_{i=1}^{2I+1} \langle I_z^k \rangle a_i$ in which i runs over the energy states.

Combining expressions (3), (4) and (5) one finds:

$$W(\alpha) = 1 - 0.087f_2P_2(\cos \alpha) - 1.66f_4P_4(\cos \alpha) \quad (8)$$

for the three strong electric quadrupole (E2) transitions in cascade.

Using formulae (6), (7) and (8) it is possible to obtain the values of $W(0)$ resp. $W(\pi/2)$ for the case that only one level is populated. The results are given in table II, together with values for f_2 and f_4 .

b. ^{54}Mn . The 3^+ ground state of ^{54}Mn decays by electron capture to a 2^+ excited state of ^{54}Cr ; a gamma ray of 834 keV having E2 multipolarity is emitted in the transition to the 0^+ ground state. In this case the angular distribution is given by

$$W(\alpha) = 1 - \frac{15}{7}N_2f_2P_2(\cos \alpha) - 5N_4f_4P_4(\cos \alpha), \quad (9)$$

TABLE II

Orientation parameters and normalized gamma intensities for ^{52}Mn when only one sublevel m is populated				
m	f_2	f_4	$W(0)$	$W(\pi/2)$
± 6	+0.611	+0.132	0.253	1.212
± 5	+0.306	-0.087	0.840	1.187
± 4	+0.055	-0.126	1.125	1.091
± 3	-0.139	-0.071	1.227	0.973
± 2	-0.278	+0.015	1.235	0.864
± 1	-0.361	+0.084	1.214	0.790
0	-0.389	+0.111	1.203	0.763

TABLE III

Orientation parameters and normalized gamma intensities for ^{54}Mn when only one sublevel m is populated				
m	f_2	f_4	$W(0)$	$W(\pi/2)$
± 3	+0.556	+0.064	0.000	1.250
± 2	0.000	-0.149	1.667	1.250
± 1	-0.333	+0.021	1.333	0.750
0	-0.444	+0.127	1.000	0.500

with $N_2 = 0.300$ and $N_4 = 0.900$. In table III one finds $W(0)$ and $W(\pi/2)$ for the case that only one sublevel m is populated; also f_2 and f_4 are given.

2.3. Theory of the NMR-ON process. The description of the resonance mechanism will be given with the aid of a specific example. Consider

a ^{54}Mn ion in a magnetic field H of a few kOe, the direction of which coincides with the trigonal axis of the crystal. In this case one can use perturbation theory to find the eigenvectors of the lowest two hfs levels in a representation in which S_z and I_z are diagonal:

$$|\psi_1\rangle = |-\frac{5}{2}, -3\rangle,$$

$$|\psi_2\rangle = \frac{1}{\sqrt{(1 + \varepsilon^2)}} |-\frac{5}{2}, -2\rangle + \frac{\varepsilon}{\sqrt{(1 + \varepsilon^2)}} |-\frac{3}{2}, -3\rangle, \quad (10)$$

with

$$\varepsilon = \frac{B\sqrt{30}}{g\mu_B H - 4D}. \quad (11)$$

For $H = 3$ kOe we find $\varepsilon = 0.13$, so $\sqrt{(1 + \varepsilon^2)} \approx 1$.

For small fields diagonalization of the hamiltonian would be required, but for all the situations encountered in our experiments the perturbation calculation is sufficiently accurate.

To describe the rf transitions between these states we use the fact that the measured resonance line is inhomogeneously broadened and thus consists of many individual "spin packets" with Larmor frequencies centered around ν_0 . The distribution of these spin packets is given by the distribution function $g(\nu_0)$, such that

$$\int_{-\infty}^{+\infty} g(\nu_0) d\nu_0 = 1.$$

If one uses an rf field perpendicular to the static field H , having an amplitude H_1 and a frequency ν , one calculates for the transition probability between the two states

$$W = (2\pi/\hbar) \frac{1}{4} |\langle \psi_2 | g\mu_B H_1 (S_+ + S_-) + g_N \mu_N H_1 (I_+ + I_-) | \psi_1 \rangle|^2 \rho(E), \quad (12)$$

where $\rho(E)$ gives the density of final states. For each individual spin packet one can write $\rho(E) dE = f(\nu - \nu_0) d\nu_0$, where $f(\nu - \nu_0)$ gives the distribution of Larmor frequencies within the spin packet.

For the total line this gives:

$$W = \int_{-\infty}^{+\infty} (2\pi/\hbar) \frac{1}{4} |\langle \psi_2 | g\mu_B H_1 (S_+ + S_-) + g_N \mu_N H_1 (I_+ + I_-) | \psi_1 \rangle|^2 f(\nu - \nu_0) g(\nu_0) d\nu_0. \quad (13)$$

If we take $H = 5$ kOe, it follows that the S_{\pm} term contributes much more to W than does the I_{\pm} term. This situation can be considered as enhancement of the strength of the resonance field through the action of the

electronic spin, *i.e.* "paramagnetic enhancement", which may be compared to "ferromagnetic enhancement" in the case of nuclei dissolved in a ferromagnetic medium⁴).

Recalling that the spin-lattice relaxation time for the Mn nuclei is very long, the rate equation for the population of the state $|\psi_2\rangle$ is given by

$$\frac{da_2}{dt} = W(a_1 - a_2), \quad (14)$$

where a_1 and a_2 are the normalized populations of the states $|\psi_1\rangle$ and $|\psi_2\rangle$.

This can be integrated to yield

$$(a_1 - a_2)_t = (a_1 - a_2)_{t=0} e^{-2p}, \quad (15)$$

where $p = \int W dt$ is integrated over the total time that the system is in resonance. The value of p can easily be estimated if we are sweeping the frequency of H_1 at a constant rate $\dot{\nu}$, since then the linewidth vanishes from the transition probability:

$$\iint f(\nu - \nu_0) g(\nu_0) d\nu_0 dt = \frac{1}{\dot{\nu}} \iint f(\nu - \nu_0) d\nu g(\nu_0) d\nu_0 = \frac{1}{\dot{\nu}}, \quad (16)$$

which gives:

$$p = \frac{75\pi^2 B^2 H_1^2}{2h^2 H^2} \frac{1}{\dot{\nu}}. \quad (17)$$

Some remarks may be added on the validity of eq. (12), which is based on time-dependent perturbation theory. If the applied rf field rotates in a plane perpendicular to the external field, the spin precession of the gamma ray emitting nuclei may under certain conditions become coherent with the rf field. If this were the case in our experiment, the degree of nuclear orientation could no longer be described by the parameters f_2 and f_4 . Instead, a more complicated description would be required. Such a description could be based on the density matrix formalism dealing with spin systems which do not have rotational symmetry about the quantization direction¹⁷). In that case expectation values such as $\langle I_x^2 \rangle$ will not necessarily be zero.

Shirley⁴) has utilized a somewhat different description of the nuclear orientation by the introduction of time and rf field dependent Majorana factors. From his qualitative examples it is easily seen that in our case, where the ratio of the paramagnetically enhanced rf field to the hyperfine field is extremely small ($10^{-7} - 10^{-8}$), the above coherence effect would be discernible in the degree of nuclear orientation only at a very narrow in-

terval $\Delta\nu_1$ around the common resonance frequency ν_0 ($\Delta\nu_1/\nu_0 = 10^{-7}$ – 10^{-8}).

However, due to the inhomogeneity of the static field and the presence of nearby protons the resonance line is inhomogeneously broadened, as will be discussed in section 4.3. Borrowing from the results of that section we remark that the linewidth $\Delta\nu$ is of the order of 50 kHz in a field of 5 kOe. So $\Delta\nu/\nu_0 = 10^{-4}$, which is very large compared to the ratio $\Delta\nu_1/\nu_0 = 10^{-7}$ to 10^{-8} .

Hence, averaging the density matrix over all nuclei in the sample, expectation values such as $\langle I_x^2 \rangle$ and $\langle I_x^4 \rangle$ – which are necessary to calculate the gamma anisotropy – will be zero due to the spread in Larmor frequencies of the Mn ions. Therefore the use of perturbation theory, which neglects the off-diagonal matrix elements, is justified.

3. *Experimental.* 3.1. *Equipment.* A schematical view of the experimental setup is sketched in fig. 2. The equipment consisted of the following parts.

a. A glass adiabatic demagnetization apparatus was mounted in a liquid He cryostat. The inner part is drawn in fig. 3. The cooling salt consisted of a slurry of K–Cr–alum powder, mixed with a saturated solution of K–Cr–alum in water and glycerol, in which many thin insulated copper wires were placed. The copper-to-alum contact area in these experiments was in the order of 200 cm².

The tin heat switch provided two widely different values of the thermal contact between the cooling salt and the sample. In the normal – heat conducting – state, temperatures from 0.025 K to 0.15 K could be obtained without exhausting the cooling capacity of the K–Cr–alum, whereas this range was 0.15 K to 0.6 K when the switch was in the superconducting state. The switch could be operated by means of a Nb coil around the pumping tube.

In the first experiments the apparatus described in ref. 18 was used. The copper rf coil consisted of a single loop, placed around the pumping tube between the upper susceptibility coils and the heater coil. In the later version the upper susceptibility coils were removed and the rf coil was placed at the top of the apparatus, as can be seen in fig. 3. It consisted then of two parallel loops, the power leads being symmetrically connected with respect to these loops. The loop diameter was 40 mm and the distance between the loops was 20 mm. In this way the rf field was made more homogeneous.

The platinum-glass seals at the bottom of the apparatus were used to connect a resistance heater and a Speer resistor. The resistance of the latter,

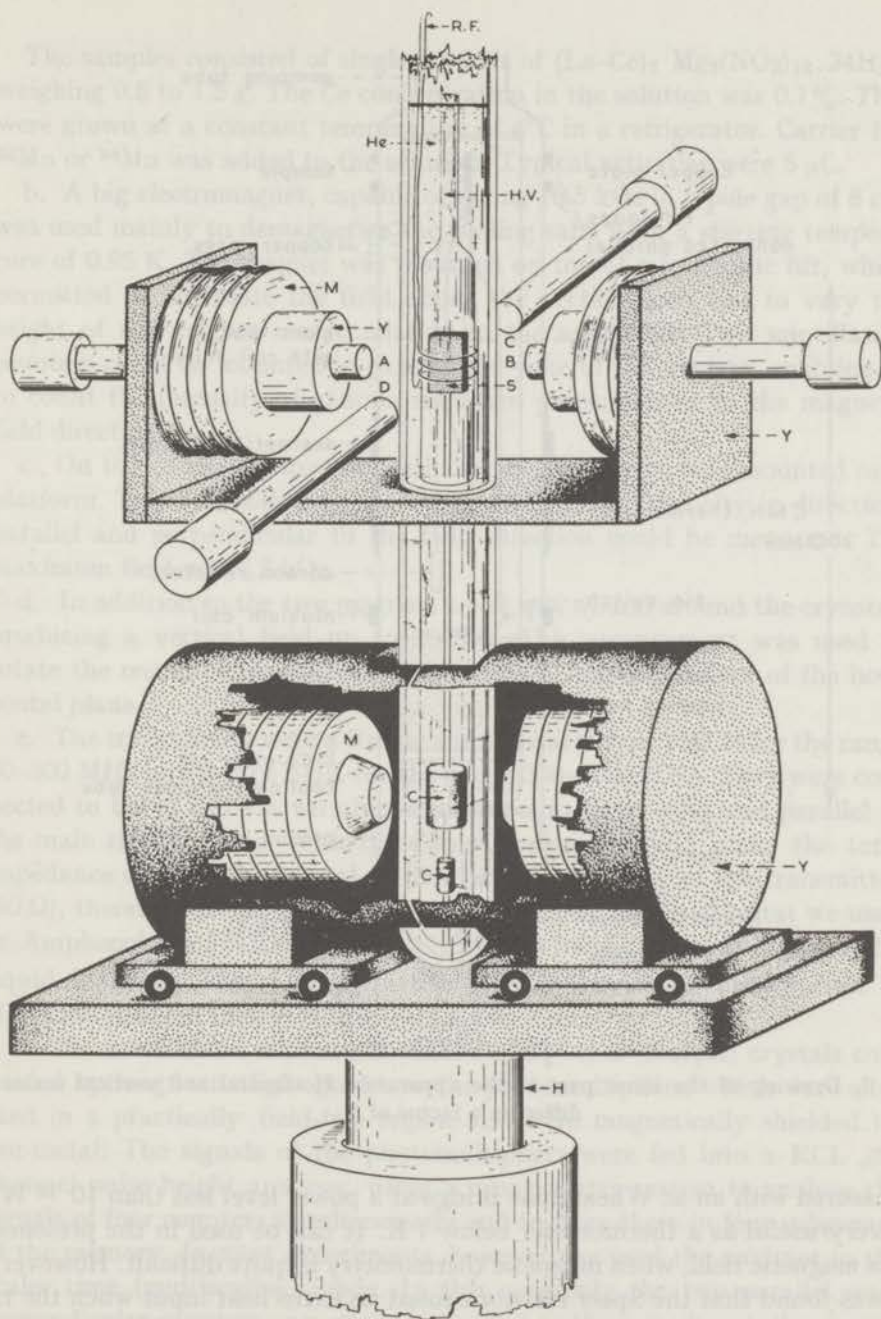


Fig. 2. Sketch of the experimental setup. A, B, C, D scintillation counters, C cooling salt, M magnet coils, He liquid He, Y magnet yoke, H.V. high vacuum, S sample, R.F. radiofrequency coil, H hydraulic lift.

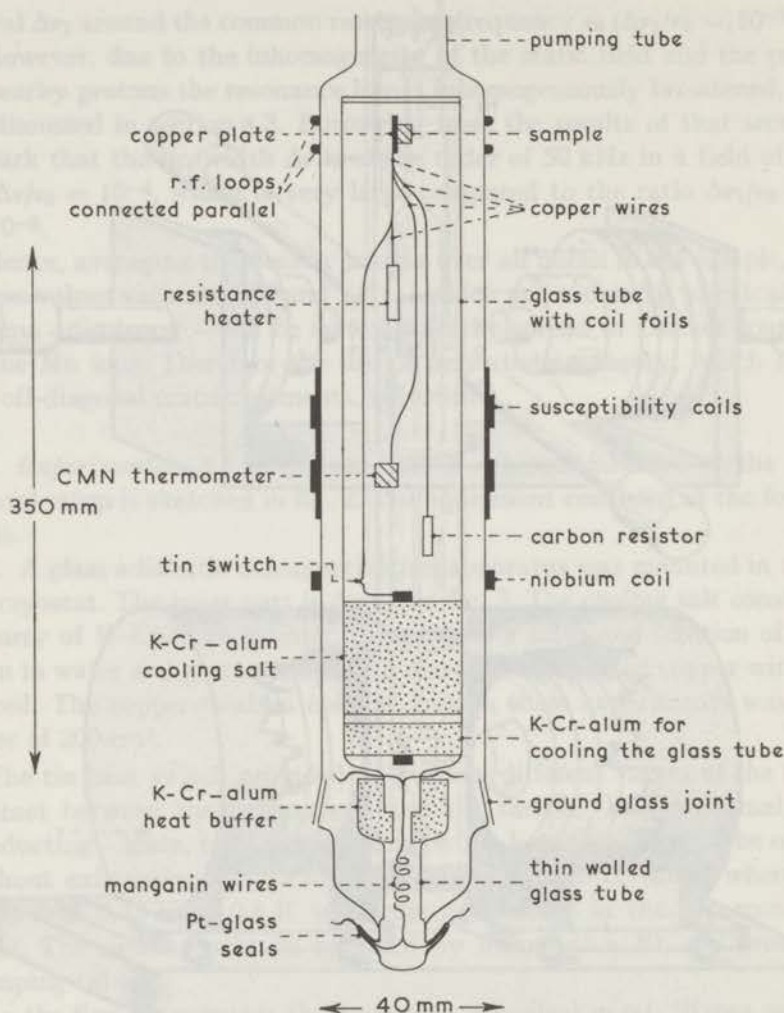


Fig. 3. Drawing of the inner part of the apparatus. Horizontal and vertical scales differ by a factor of 3.

measured with an ac Wheatstone bridge at a power level less than 10^{-12} W, is very useful as a thermometer below 1 K. It can be used in the presence of a magnetic field, when magnetic thermometry is quite difficult. However, it was found that the Speer resistor caused an extra heat input when the rf field was on, of a magnitude depending on the frequency in a very capricious way. Therefore the resistor was omitted during most of the resonance experiments.

The samples consisted of single crystals of $(\text{La-Ce})_2 \text{Mg}_3(\text{NO}_3)_{12} \cdot 24\text{H}_2\text{O}$, weighing 0.5 to 1.5 g. The Ce concentration in the solution was 0.1%. They were grown at a constant temperature of 4°C in a refrigerator. Carrier free ^{52}Mn or ^{54}Mn was added to the solution. Typical activities were $5 \mu\text{C}$.

b. A big electromagnet, capable of giving 18.5 kOe in a pole gap of 8 cm, was used mainly to demagnetize the cooling salts from a starting temperature of 0.95 K. The magnet was mounted on top of a hydraulic lift, which permitted us to rotate the field about the vertical axis and to vary the height of the magnet centre relative to the apparatus. Two scintillation counters could be mounted in gaps in the yoke of the magnet, enabling us to count the intensity of gamma radiation perpendicular to the magnetic field direction.

c. On top of the big magnet a smaller electromagnet was mounted on a platform. This had hollow poles, so that the gamma intensity in directions parallel and perpendicular to the field direction could be measured. The maximum field was 5.5 kOe.

d. In addition to the two magnets a coil was wound around the cryostat, producing a vertical field up to 200 Oe. This arrangement was used to rotate the resultant magnetic field direction a few degrees out of the horizontal plane.

e. The transmitters were a Rohde and Schwartz type SMLM for the range 30–300 MHz and a type SDR for the range 300–1000 MHz. They were connected to the rf coil via variable impedances in series with and parallel to the main rf power line. With these components we could make the total impedance of the circuit equal to the output impedance of the transmitter (50Ω), thereby providing maximum power output. In the cryostat we used an Amphenol RG 174/U "mini-coax" cable to reduce the heat input to the liquid He bath. The rf losses in this cable were not disturbing even at 500 MHz. The maximum rf field was about 1 mOe.

f. The scintillation counters consisted of $1\frac{3}{4} \times 2$ " NaI(Tl) crystals connected by long lucite light guides to the photomultipliers, which were situated in a practically field-free region and were magnetically shielded by mu-metal. The signals of the photomultipliers were fed into a RCL 256 channel pulse height analyser, using a mixer-router system to analyse the signals of four counters simultaneously and to store them in four subgroups of the memory. In most experiments, however, we used the analyser in the scaler time (multiscaling) mode. In this case only the two parallel resp. perpendicular counters were used, connected to the same input, the system now serving as a single channel analyser. In this way we could conveniently measure the counting rate as a function of time.

A few remarks must be made about some difficulties encountered during the experiments. It turned out that the cryostat axis and the axis of rotation of the magnets did not coincide exactly, which implies that the sample moved relative to the magnet during rotation of the latter. During the measurements it was impossible to measure the field strength at the position of the sample. Using an NMR method, only the field in the centre of the magnet could be measured accurately. This gave an uncertainty in the magnetic field at the sample which we estimated to be of the order of 0.1%.

A special problem was encountered in the measurements at high fields using the big magnet. As can be seen in tables II and III the resonance transitions between the lowest levels gave no change in the gamma-ray intensity perpendicular to the field direction. Therefore these transitions could not be detected in this magnet. However, by placing the counters somewhat off the perpendicular direction, as far as could be permitted by the gaps in the yoke, the detection of the transitions proved to be feasible.

3.2. Experimental procedure. The determination of an rf transition consisted of the following steps. First, the cooling salts were demagnetized and the sample was precooled to a temperature below 0.1 K in a magnetic field of a few kOe, the direction of which was perpendicular to the trigonal axis. After a few minutes the magnet was rotated to the region around the trigonal axis, where the field direction was varied in discrete steps.

After each step $W(0)$ was measured. The result of this procedure is shown in fig. 4 for a field of 4710 Oe. It is seen that the orientation of the nuclear spins by thermal mixing with the Ce spins is a very sharp function of the angle θ .

By approaching the mixing region from the other side the projection of the crystal axis on the horizontal plane could be determined very accurately. A small misalignment could be determined with the use of the vertical coil. By varying the field in this coil while a static horizontal field was present, the direction of the resultant field was varied in a vertical plane, so that in that plane the thermal mixing also could be observed. From these measurements the position of the crystal axis could be established with an accuracy of 0.1 degree.

After the nuclear orientation had been accomplished, the magnetic field was adjusted to the desired direction and strength. Then the resonance measurement was started by varying the frequency of the transmitter at a rate of about 1 kHz/s, meanwhile counting the gamma-ray intensity $W(0)$ by using the scaler time mode of the analyser. Curves so obtained are shown in fig. 5. Two transitions are visible; they are indicated in the figure.

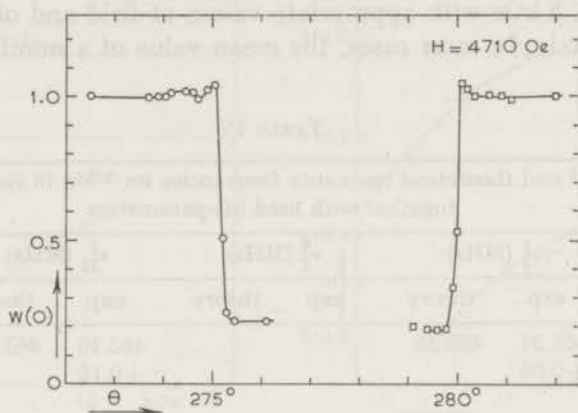


Fig. 4. Two typical experimental runs showing the gamma radiation intensity $W(0)$ for ^{54}Mn in LMN when the angle θ between the direction of the magnetic field and the c axis was varied in discrete steps, taken every 20 s.

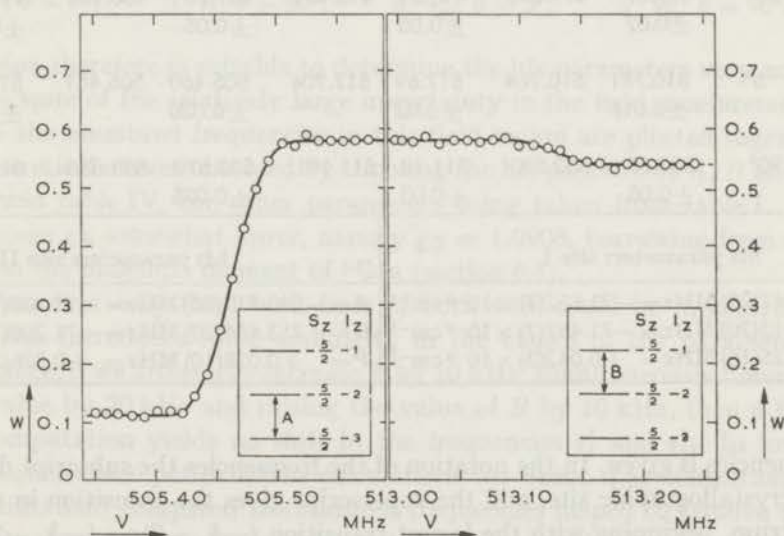


Fig. 5. Typical resonance series showing the change in $W(0)$ for ^{54}Mn in LMN obtained by continuously increasing the frequency. Points were taken every 10 s. Two resonance transitions are clearly visible. Their position in the energy level scheme is indicated in the inserts.

4. *Experimental results on ^{54}Mn .* 4.1. Line positions and hfs parameters. In table IV we give a survey of the measured resonance frequencies for $H < 5$ kOe with appropriate values of field and of angle between field and c axis. In most cases, the mean value of a number of measured

TABLE IV

Experimental and theoretical resonance frequencies for ^{54}Mn in fields up to 5kOe, together with used hfs parameters									
H (Oe)	θ	ν_{I}^1 (MHz)		ν_{I}^2 (MHz)		ν_{II}^1 (MHz)		ν_{II}^2 (MHz)	
		exp	theory	exp	theory	exp	theory	exp	theory
1471	5°	485.31 ± 0.05	485.35			463.10 ± 0.10	463.23		
1471	90°					447.11 ± 0.12	447.22		
2795	5°	501.483 ± 0.025	501.491	511.40 ± 0.03	511.406	491.80 ± 0.04	491.832	503.47 ± 0.03	503.508
2795	90°	479.07 ± 0.07	479.090	493.39 ± 0.05	493.434	487.00 ± 0.05	486.954	499.53 ± 0.03	499.547
4710	5°	510.751 ± 0.015	510.764	517.69 ± 0.02	517.704	505.460 ± 0.020	505.481	513.14 ± 0.02	513.157
4710	90°	502.65 ± 0.05	502.593	511.18 ± 0.03	511.191	503.670 ± 0.025	503.656	511.60 ± 0.03	511.586
hfs parameters site I					hfs parameters site II				
$A = -214.747(20)$ MHz = $-71.632(7) \times 10^{-4}$ cm $^{-1}$					$A = -213.712(20)$ MHz = $-71.287(7) \times 10^{-4}$ cm $^{-1}$				
$B = -214.313(20)$ MHz = $-71.487(7) \times 10^{-4}$ cm $^{-1}$					$B = -213.454(20)$ MHz = $-71.200(7) \times 10^{-4}$ cm $^{-1}$				
$P = +0.125(10)$ MHz = $+0.042(3) \times 10^{-4}$ cm $^{-1}$					$P = +0.078(10)$ MHz = $+0.026(3) \times 10^{-4}$ cm $^{-1}$				

frequencies is given. In the notation of the frequencies the subscript denotes the crystallographic site, and the superscript gives the transition in the hfs spectrum, beginning with the lowest transition $(-\frac{5}{2}, -3) \rightarrow (-\frac{5}{2}, -2)$.

The region around 12 kOe is of special interest, because the resonance frequencies ν_{I}^1 and ν_{II}^1 have a maximum as a function of the field strength. The reason for this maximum can be seen from a numerical consideration of eq. (2): the effects of the second and third term cancel at $H \approx 12$ kOe.

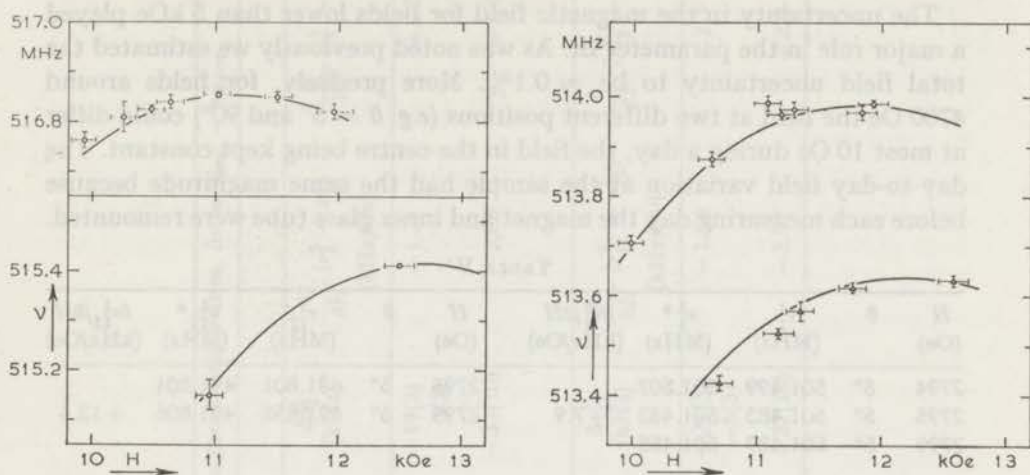


Fig. 6. Hfs resonance frequencies for ^{54}Mn at both sites I, II of LMN measured as a function of the magnetic field strength H for two values of θ , the angle between the direction of H and the c axis. The drawn curves represent the results of calculations using the hfs parameters given in table IV.

$$\circ \nu_{\text{I}}^1, \theta = 5^\circ; \quad \square \nu_{\text{I}}^1, \theta = 90^\circ; \quad \diamond \nu_{\text{II}}^1, \theta = 5^\circ; \quad \triangle \nu_{\text{II}}^1, \theta = 90^\circ.$$

This region therefore is suitable to determine the hfs parameters very accurately in spite of the relatively large uncertainty in the field measurement. In fig. 6 the measured frequencies in this field region are plotted together with theoretical curves obtained by choosing the hfs parameters A , B and P as given in table IV, the other parameters being taken from table I. We have chosen g_N somewhat lower, namely $g_N = 1.0908$, borrowing from our results on the magnetic moment of ^{54}Mn (section 6.1).

The fact that only the lowest lines of both sites could be measured in those fields introduces some ambiguity in the choice of the parameters. For instance, if we arbitrarily increase P by 10 kHz, simultaneously lowering the A value by 20 kHz and raising the value of B by 10 kHz, then a first order computation yields no shift in the frequencies ν_{I}^1 and ν_{II}^1 . In lower fields, higher-order perturbation calculations (or exact diagonalization of the hamiltonian) compared to measured frequencies helped to remove this ambiguity; nevertheless it turned out that there remained a considerable uncertainty in the parameters as long as we looked only at ν_{I}^1 and ν_{II}^1 . The ambiguity could be removed to a considerable extent by comparing ν_{I}^2 to ν_{I}^1 and ν_{II}^2 to ν_{II}^1 , measured at the same angle and field strength. The influence of ΔP on $\nu_{\text{I,II}}^2$ is only $\frac{2}{3}$ of that on $\nu_{\text{I,II}}^1$, which enabled us to distinguish between several sets of parameters (A , B , P).

The uncertainty in the magnetic field for fields lower than 5 kOe played a major role in the parameter fit. As was noted previously we estimated the total field uncertainty to be $\approx 0.1\%$. More precisely, for fields around 4700 Oe the field at two different positions (*e.g.* $\theta = 5^\circ$ and 90°) could differ at most 10 Oe during a day, the field in the centre being kept constant. The day-to-day field variation at the sample had the same magnitude because before each measuring day the magnet and inner glass tube were remounted.

TABLE V

H (Oe)	θ	ν_I^1 (MHz)	ν_I^{1*} (MHz)	$\partial\nu_I^1/\partial H$ (kHz/Oe)	H (Oe)	θ	ν_{II}^1 (MHz)	ν_{II}^{1*} (MHz)	$\partial\nu_{II}^1/\partial H$ (kHz/Oe)
2794	5°	501.499	501.507		2795	5°	491.801	491.801	
2795	5°	501.483	501.483	+7.9	2799	5°	491.855	491.806	+12.4
2799	5°	501.489	501.458						
2794	90°	479.16	479.18		2795	90°	487.100	487.100	
2799	90°	479.10	479.02	+21.2	2795	90°	487.080	487.080	+15.8
2799	90°	479.08	479.00		2799	90°	486.970	486.907	
4707	5°	510.755	510.764		4707	5°	505.464	505.476	
4711	5°	510.755	510.752	+3.0	4711	5°	505.464	505.460	+4.2
4712	5°	510.753	510.747		4712	5°	505.446	505.438	
4714	5°	510.757	510.745		4715	5°	505.481	505.460	
4707	90°	502.598	502.616		4707	90°	503.664	503.679	
4711	90°	502.754	502.748	+6.0	4711	90°	503.717	503.712	+4.9
4712	90°	502.680	502.668		4715	90°	503.640	503.626	
4714	90°	502.580	502.556						

The columns labelled with ν_I^1 resp. ν_{II}^1 give the measured resonance frequencies. The columns marked with an asterisk give the same frequencies, but now calculated as if they were measured at one of the two standard fields, $H = 2795$ Oe or $H = 4710$ Oe. This is done with the aid of the columns denoted by $\partial\nu_I^1/\partial H$ and $\partial\nu_{II}^1/\partial H$. They show to which extent the frequencies are influenced by field variations.

This clearly affected the reproducibility of the results, as can be seen in the fourth and ninth column of table V. We remark that for $\theta = 5^\circ$ the irreproducibility can be easily accounted for by the field uncertainty, whereas for $\theta = 90^\circ$ the variations were too large by a factor of two. Probably we have underestimated the field variations at this position.

We estimated the error in the experimental points in table IV mainly on the basis of this field uncertainty.

The irreproducibility at $\theta = 5^\circ$ being less than at other angles, together with the fact that at this angle the dependence on P was strongest, led us to consider only the points at $\theta = 5^\circ$, $H = 4700$ Oe resp. 2795 Oe when comparing $\nu_{I,II}^2$ to $\nu_{I,II}^1$. Table VI gives the relevant experimental values

TABLE VI

Comparison of the two measured lines of each site with theory, for two magnetic field values. $\Delta v = v_{\text{exp}} - v_{\text{theor}}$.									
Site I									
H (Oe)	θ	$v_{\text{I}^2}^{\text{exp}}$ (MHz)	$v_{\text{I}^2}^{\text{theor}}$ (MHz)	Δv_{I^2} (kHz)	$v_{\text{I}^1}^{\text{exp}}$ (MHz)	$v_{\text{I}^1}^{\text{theor}}$ (MHz)	Δv_{I^1} (kHz)	$\frac{\partial}{\partial H} \{v_{\text{I}^2} - v_{\text{I}^1}\}$ (kHz/Oe)	$\frac{\partial}{\partial P} \{v_{\text{I}^2} - v_{\text{I}^1}\}$
4710	5°	517.673(10)	517.704	-31(10)	510.751(3)	510.764	-19(3)	-1.21	+2.0
4710	5°	517.705(10)	517.704	+1(10)	510.764(3)	510.764	0(3)		
2795	5°	511.40(3)	511.406	-6(30)	501.458(10)	501.491	-33(10)	-2.65	+2.0
Site II									
H (Oe)	θ	$v_{\text{II}^2}^{\text{exp}}$ (MHz)	$v_{\text{II}^2}^{\text{theor}}$ (MHz)	Δv_{II^2} (kHz)	$v_{\text{II}^1}^{\text{exp}}$ (MHz)	$v_{\text{II}^1}^{\text{theor}}$ (MHz)	Δv_{II^1} (kHz)	$\frac{\partial}{\partial H} \{v_{\text{II}^2} - v_{\text{II}^1}\}$ (kHz/Oe)	$\frac{\partial}{\partial P} \{v_{\text{II}^2} - v_{\text{II}^1}\}$
4710	5°	513.147(10)	513.157	-10(10)	505.460(3)	505.481	-21(3)	-1.56	+2.0
4710	5°	513.138(10)	513.157	-18(10)	505.476(3)	505.481	-5(3)		
2795	5°	503.467(10)	503.508	-39(10)	491.806(10)	491.832	-27(10)	-3.97	+2.0

together with the theoretical values. Also the variations in $\nu_{\text{I}}^2 - \nu_{\text{I}}^1$, resp. $\nu_{\text{II}}^2 - \nu_{\text{II}}^1$ caused by a variation of the field strength are shown. We should like to point out that the two lines of each site were measured in sequence at exactly the same field and angle. Also the variation in $\nu_{\text{I,II}}^2 - \nu_{\text{I,II}}^1$ due to a variation in P is given.

The resulting uncertainty in P was taken as ± 10 kHz for both sites. This in turn determined the uncertainty in A and B . For A we found an error of ± 20 kHz; for B we found ± 10 kHz. In view of the spread of the points at $\theta = 90^\circ$ we took the final error in B also as ± 20 kHz.

4.2. Changes in $W(0)$. The change in $W(0)$ caused by the resonance process was studied in experiments during which we used a relatively high rf field ($\approx 0.2 \times 10^{-3}$ Oe) and a low frequency sweep rate (1 kHz/s). As will be discussed below, this was sufficient to saturate the lines. The resulting changes in $W(0)$ are shown in table VII. We concentrated on the transitions between the lowest levels of both sites (ν_{I}^1 and ν_{II}^1), the changes there being much larger than in the following transitions.

TABLE VII

Changes in $W(0)$ of ^{54}Mn due to saturation of resonance transitions									
site I (ν_{I}^1)					site II (ν_{II}^1)				
H (Oe)	θ	$W(0)_i$	$W(0)_f$	$W(0)_f^{\text{th}}$	H (Oe)	θ	$W(0)_i$	$W(0)_f$	$W(0)_f^{\text{th}}$
2795	5°	0.204	0.423	0.430	2799	5°	0.182	0.599	0.599
2794	5°	0.368	0.524	0.535	2799	5°	0.117	0.567	0.575
4715	5°	0.127	0.386	0.381	2799	90°	0.149	0.584	0.587
4715	90°	0.210	0.410	0.434	4714	5°	0.174	0.588	0.595
					4714	90°	0.115	0.553	0.574

ν_{II}^1 and ν_{I}^1 in sequence						
H (Oe)	θ	$W(0)_1$	$W(0)_2$	$W(0)_2^{\text{th}}$	$W(0)_3$	$W(0)_3^{\text{th}}$
4711	5°	0.095	0.558	0.567	0.815	0.833
4712	5°	0.221	0.620	0.614	0.835	0.833

For the case that ν_{II}^1 and ν_{I}^1 were saturated in sequence, $W(0)_1$ gives the value of $W(0)$ at the start of the experiment. $W(0)_2$ is the value of $W(0)$ obtained after saturating transition ν_{II}^1 , whereas $W(0)_3$ is the value of this quantity after saturating ν_{I}^1 . The calculated values $W(0)_2^{\text{th}}$ and $W(0)_3^{\text{th}}$ are also given.

For a given value of $W(0)$ before resonance, $W(0)_i$, it is possible to derive $W(0)_f$, the value after line saturation, on the basis of the following simple model. We assume that the orientation process gives a final state in which

only the levels characterized mainly by $(-\frac{5}{2}, -3)$ and $(-\frac{5}{2}, -2)$ are populated. This is justified by the observation that $W(\pi/2) \approx 1.25$ if $W(0) < 0.2$. By inspection of table III we see that under these circumstances the higher levels are not significantly populated.

After saturation of a resonance line (for instance ν_{II}^1) we have a situation in which ions of type II have the population numbers $a_1 = a_2 = 0.5$ whereas the population distribution of type I ions is not disturbed. Then, only the ratio of the two types of ions needs to be known. By saturating ν_{II}^1 and ν_I^1 in sequence we found this ratio to be 1 : 1.8, that is, 36% of the ^{54}Mn ions are in site I and 64% in site II. This ratio can be compared with the ratio 1 : 1.7 found by Van Ormondt¹⁹), by E.P.R. in the same salt. The crystallographic ratio is 1 : 2, hence it is seen that there exists a slight preference for lattice site I.

With the aid of table III we can easily calculate $W(0)_I^{\text{th}}$, the value of $W(0)$ to be expected assuming complete saturation of the line. These calculated values are also listed in table VII. The agreement with the experiment is very satisfactory in view of the uncertainty of about 0.01 in the measured $W(0)$. For the transitions ν_I^2 and ν_{II}^2 , we expect maximum changes in $W(0)$ of -0.030 and -0.053 resp. Experimentally we found -0.024 and -0.042 . The difference is probably due to insufficient saturation.

The theory of the NMR-ON process (see section 2.3) has been tested by sweeping through the transition ν_{II}^1 at a controlled speed and power level and measuring $W(0)_I$ and $W(0)_I$ as a function of these variables. The quantities $W(0)_I$ and $W(0)_I$ can be related to $(a_1 - a_2)_I$ and $(a_1 - a_2)_I$ by means of the following formulae, which are derived on basis of table III and the ratio of type I ions to type II ions.

$$(a_1 - a_2)_I = 1 - \frac{W(0)_I}{0.833}, \quad (18)$$

$$(a_1 - a_2)_I = 1 - \frac{W(0)_I - 0.36W(0)_I}{0.64 \times 0.833}. \quad (19)$$

With the aid of (15) we can then find $\dot{\phi}$. Making use of the linear dependence of H_1 on the output voltage V of the transmitter, eq. (17) would predict $\dot{\phi}$ to be a linear function of $V^2/\dot{\nu}$ ($\dot{\nu}$ being the sweep rate). The results of the measurements are shown in fig. 7. The linear dependence on $\dot{\nu}^{-1}$ is seen to be obeyed but the quadratic dependence on V is not seen.

Assuming $H_1 = \alpha V$ and taking the mean slope of the lines in fig. 7 we find $\alpha = 2.7 \times 10^{-4}$ Oe/V at the position of the sample. At room temperature, using a pickup loop, we estimated α in the centre of the rf loop to be

5×10^{-4} Oe/V. The discrepancy can be partly accounted for by the fact that the centre of the sample did not coincide exactly with the centre of the loop, giving a reduction of about 20% in the field at the sample. The rest may be caused by imperfect impedance matching during the experi-

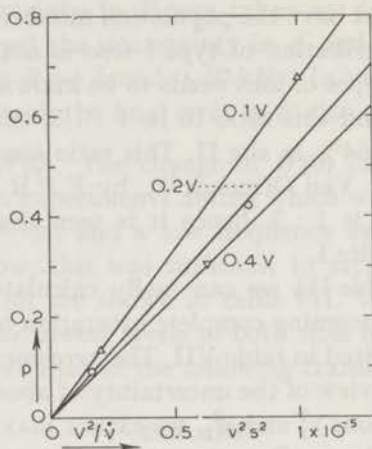


Fig. 7. Relation between $p = \int W dt$ and $V^2/\dot{\nu}$, in which W is the rf transition probability, V is the voltage of the transmitter and $\dot{\nu}$ is the frequency sweep rate.

Δ $V = 0.1$ V; \circ $V = 0.2$ V; ∇ $V = 0.4$ V.

ment. The reason for the deviation from quadratic dependence of p on V is not quite clear.

In conclusion we may remark that the theory describes the experiments reasonably well in view of the rather rough nature of the experimental determination of p .

4.3. Linewidths. Our method of measuring resonance lines is not suitable to determine the precise line shape. Therefore it was assumed that the shape was gaussian, which is not unreasonable in view of the fact that the inhomogeneous broadening greatly exceeds the homogeneous broadening, as will be seen below.

Throughout the further discussion the linewidth $\Delta\nu$ is defined as the frequency width in which 68% of the total change in $W(0)$ occurred. For a gaussian line this is the same as the width between the inflexion points, *i.e.* two times the standard deviation.

In table VIII a selection of the measured lines is presented. Only the experiments in which we measured ν_{I}^1 and ν_{II}^1 at exactly identical circumstances are used, since it appeared that there were day-to-day variations far outside the experimental error (about 5%), which must be attributed to

TABLE VIII

Linewidths for ^{54}Mn in LMN							
H (Oe)	θ	$\Delta\nu_{\text{I}}^1$ (kHz)	$\partial\nu_{\text{I}}^1/\partial H$ (kHz/Oe)	ΔH_{I} (Oe)	$\Delta\nu_{\text{II}}^2$ (kHz)	$\partial\nu_{\text{II}}^1/\partial H$ (kHz/Oe)	ΔH_{II} (Oe)
4712	5°	41	3.01	13.6	57	4.15	13.7
4711	5°	24	3.01	8.0	36	4.15	8.7
4707	5°	31	3.01	10.3	42	4.15	10.1
4711	90°	48	5.94	8.1	37	4.86	7.6
4707	90°	54	5.94	9.0	40	4.15	9.6
2795	5°	49	7.86	6.2	78	13.35	6.3
1471	5°	115	19.9	5.8	250	41.2	6.1

differences in the sample position with respect to the centre of the magnetic field. Assuming that the linewidth is entirely due to the field inhomogeneity ΔH we can calculate this quantity on basis of the measured values of $\Delta\nu_{\text{I}}^1$ and $\Delta\nu_{\text{II}}^1$ together with the quantities $\partial\nu_{\text{I}}^1/\partial H$ and $\partial\nu_{\text{II}}^1/\partial H$ which are derived with the aid of perturbation theory. The results of this approach are also listed in table VIII. It is seen that although $\Delta\nu_{\text{I}}^1$ and $\Delta\nu_{\text{II}}^1$ differ quite clearly for different field and angles, the derived values of ΔH are equal if ν_{I}^1 and ν_{II}^1 are measured under identical circumstances. This justifies the assumption made above.

In regions where ν_{I}^1 and ν_{II}^1 reached a maximum as a function of the magnetic field, we measured linewidths smaller than 4 kHz. This signifies that the spread in the hyperfine parameters A and B is very small.

Some information about the homogeneous broadening was obtained by keeping the frequency constant ($\Delta\nu < 1$ kHz) in the centre of the ν_{II}^1 line. At a low power level ($V < 0.02$ V) there was no change in $W(0)$. For high power levels $W(0)$ started to rise, reaching a practically constant value within 1 to 2 min (fig. 8). The rate of change in $W(0)$ as well as the total change increased somewhat as the power level was made higher, but the differences were not large. The ratio of the observed change in $W(0)$ and the total possible change varied between 14% and 19%. The total width of the line was 40 kHz, so by simple scaling we obtain a homogeneous width of the line lying between 5.6 kHz and 7.4 kHz. Expressed in terms of a fluctuating field on the Mn ions this amounts to 1.3–1.8 Oe. The origin of this width will be discussed in section 6.2.

5. *Experimental results on ^{52}Mn .* 5.1. Line positions; hfs parameters. Table IX lists the measured resonance frequencies obtained in an LMN crystal in which 5 μC of ^{52}Mn was present at the beginning of the measuring period. The measurements were hampered by the occurrence of a λ leak,

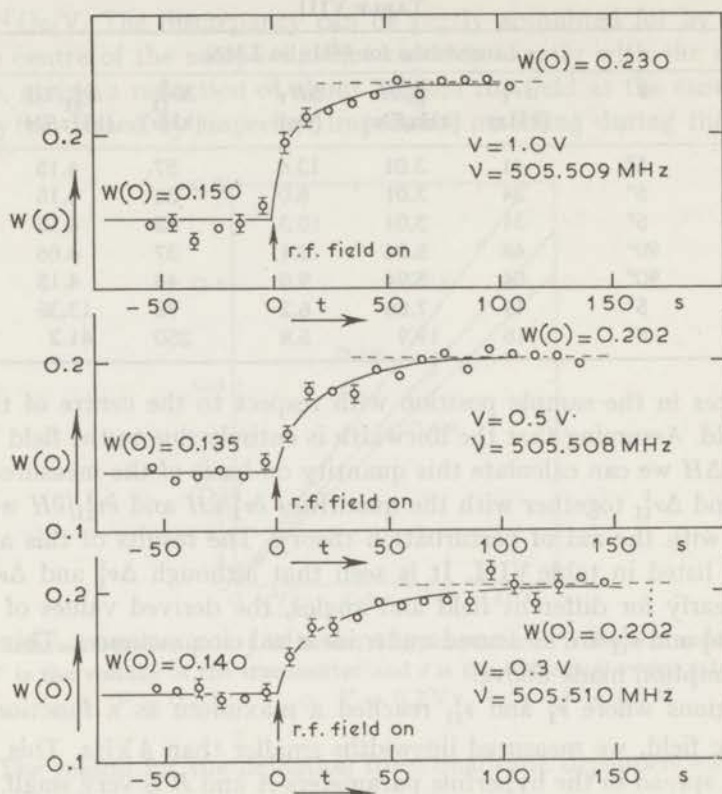


Fig. 8. Change in $W(0)$ for ^{54}Mn in LMN as a function of time when an rf field of constant amplitude was applied at the sample, the frequency being kept constant in the centre of the resonance line. The values of $W(0)$ at the start of the irradiation as well as the final values are given. The frequency and the voltage of the transmitter are also shown.

which forced us to demagnetize at a starting temperature of 2.2 K. Consequently only temperatures above 0.08 K were reached, and the whole apparatus warmed up rather quickly ($\approx 1 \text{ h}$) to 0.2 K, which was approximately the upper limit permitting reliable measurements in view of the spin-lattice relaxation time.

Together with the measurements the results of computer calculations are shown; the values of the hfs parameters in the spin hamiltonian, as found in an optimal fit to the experimental data, are also given in this table.

The procedure of obtaining these parameters is the same as used for ^{54}Mn (section 4.1). The quoted errors are conservative estimates based on the error in the differences of two measured frequencies, e.g. $\nu_1^2 - \nu_1^1$. It follows

TABLE IX

Experimental and theoretical resonance frequencies for ^{52}Mn together with used hfs parameters									
H (Oe)	θ	ν_{I}^1 (MHz)		ν_{I}^2 (MHz)		ν_{II}^1 (MHz)		ν_{II}^2 (MHz)	
		exp	theory	exp	theory	exp	theory	exp	theory
4691	5°	238.968 ± 0.007	239.968	240.499 ± 0.010	240.498	236.700 ± 0.009	236.700	238.371 ± 0.010	238.371
4691	90°	235.759 ± 0.013	235.760	237.62 ± 0.02	237.592	236.107 ± 0.010	236.104	237.809 ± 0.012	237.803
hfs parameters site I					hfs parameters site II				
$A = -100.225(30)$ MHz = $-33.431(10) \times 10^{-4} \text{cm}^{-1}$					$A = -99.734(20)$ MHz = $-33.268(7) \times 10^{-4} \text{cm}^{-1}$				
$B = -100.032(30)$ MHz = $-33.367(10) \times 10^{-4} \text{cm}^{-1}$					$B = -99.631(20)$ MHz = $-33.233(7) \times 10^{-4} \text{cm}^{-1}$				
$P = +0.044(7)$ MHz = $+0.015(2) \times 10^{-4} \text{cm}^{-1}$					$P = +0.025(5)$ MHz = $0.0083(17) \times 10^{-4} \text{cm}^{-1}$				

from the analysis that the uncertainty in P is related to the quoted errors in A and B .

5.2. Changes in $W(0)$, linewidths. The experiments on ^{52}Mn in LMN were done by setting the window of the single channel analyser such as to accept pulses arising from the three strongest gamma transitions in the decay of ^{52}Cr . However, this implied that we also counted the weaker 0.847 MeV and 1.246 MeV gamma transitions from the 5^+ level of ^{52}Cr at 3.614 MeV. These are mixed M1 + E2 transitions, the anisotropy of which is measured relative to that of the E2 transitions by Kaplan and Shirley²⁰).

Moreover, this energy region included parts of the Compton distributions of the various lines, of which the anisotropy is generally lower than that of the corresponding photopeaks. All these effects gave rise to an attenuation of the gamma anisotropy. It turned out to be practically impossible to determine this attenuation in a theoretical way, so we tried to determine it experimentally by looking at the lowest values of $W(0)$ reached by thermal mixing of ^{52}Mn and Ce spins and comparing these with experimental results on ^{54}Mn -Ce mixing.

Given the initial conditions of the Ce spin system ($H = 4700$ Oe, $\theta = 90^\circ$, $T = 0.09$ K) we estimated on basis of the latter experiments the resulting population densities of the ^{52}Mn spin system. These can be described by a Boltzmann factor $e^{-\beta}$ with $\beta = 3 \pm 1$. (Strictly speaking we do not expect a Boltzmann distribution, but at these high degrees of orientation the difference between a Boltzmann distribution and the true population density distribution will be very small).

On the other hand, the lowest value of $W(0)$ attained is $W(0) = 0.41$. This gives an estimate for the attenuation coefficient G of the gamma anisotropy, this quantity being 1 in the absence of attenuation and 0 in case of complete attenuation of the gamma anisotropy; experimentally $G = 0.70^{+0.05}_{-0.03}$.

Using this value, it is possible to analyse the observed changes in $W(0)$ due to resonance saturation in the way described in 4.2. The results are

TABLE X

Changes in $W(0)$ for ^{52}Mn due to saturation of resonance transitions								
Resonance transition	$W(0)_I$	$\Delta W(0)_{\text{exp}}$	$G = 0.70$			$G = 0.67$		
			$W(0)_{\text{min}}$	$\Delta W(0)_{\text{max}}$	$\Delta W(0)_{\text{th}}$	$W(0)_{\text{min}}$	$\Delta W(0)_{\text{max}}$	$\Delta W(0)_{\text{th}}$
$\nu_{\text{I}}^{\text{I}}$	0.414	0.079(6)	0.382	0.086	0.075	0.409	0.084	0.082
$\nu_{\text{II}}^{\text{I}}$	0.448	0.0132(10)	0.382	0.153	0.111	0.409	0.149	0.126

given in table X for two values of G , 0.70 and 0.67. The following notation is used:

$W(0)_I$ is the observed value of $W(0)$ before resonance;

$W(0)_{\text{min}}$ is the value of $W(0)$ in case of complete orientation of the ^{52}Mn spin system;

$\Delta W(0)_{\text{max}}$ is the maximal obtainable change in $W(0)$ by crossing the resonance (assuming $W(0)_I = W(0)_{\text{min}}$);

$\Delta W(0)_{\text{th}}$ is the calculated change in $W(0)$ due to resonance saturation taking into account the difference between $W(0)_I$ and $W(0)_{\text{min}}$;

$\Delta W(0)_{\text{exp}}$ is the observed change in $W(0)$ due to the passage through resonance.

From the table it is seen that the measurements are consistent with complete saturation and an attenuation coefficient of 0.67 rather than 0.70. Higher values of G and/or incomplete saturation always lead to lower values of $\Delta W(0)_{\text{th}}$ and consequently are not compatible with the data. As can be seen, $G = 0.67$ implies nearly complete orientation of the nuclear spin system after thermal mixing with the Ce spin system.

The obtained linewidths were somewhat smaller than in the case of ^{54}Mn . However, if analysed in terms of a magnetic field varying over the sample, the obtained values scattered around 15 Oe, which is somewhat more than in the case of ^{54}Mn . This result is not surprising, because the volume of the ^{52}Mn crystal was about two times the average volume of the ^{54}Mn crystals. No attempts were made to measure the homogeneous linewidth.

6. Discussion. 6.1. hfs parameters; nuclear moments. The obtained hfs parameters of $^{52}\text{Mn}^{2+}$ and $^{54}\text{Mn}^{2+}$ in LMN, combined with the ENDOR values of De Beer *et al.*⁷⁾ on ^{55}Mn in the same salt, enabled us to find values

TABLE XI

Isotope	A_I/hc	A_{II}/hc	B_I/hc	B_{II}/hc	P_I/hc	P_{II}/hc
$^{52}\text{Mn}^a$	-33.431(10)	-33.268(7)	-33.367(10)	-33.233(7)	+0.015(2)	+0.0083(17)
$^{54}\text{Mn}^a$	-71.632(7)	-71.287(7)	-71.487(7)	-71.200(7)	+0.042(3)	+0.026(3)
$^{55}\text{Mn}^b$	-90.448(3)	-90.009(3)	-90.26(7)	-89.93(7)	+0.065(3)	+0.038(2)
$^{52}\text{Mn}/^{55}\text{Mn}$	+0.36962(11)	+0.36961(8)	+0.3697(3)	+0.3695(3)	+0.23(4)	+0.22(5)
$^{54}\text{Mn}/^{55}\text{Mn}$	+0.79197(8)	+0.79200(8)	+0.7920(6)	+0.7917(6)	+0.65(9)	+0.68(13)
$^{52}\text{Mn}/^{54}\text{Mn}$	+0.46676(14)	+0.46668(11)	+0.46676(14)	+0.46676(11)	+0.35(6)	+0.32(8)
Ratios	g_N	μ	Q			
$^{52}\text{Mn}/^{55}\text{Mn}$	0.36961(7)	+0.88706(15)	+1.5(2)			
$^{54}\text{Mn}/^{55}\text{Mn}$	0.79199(6)	+0.95039(7)	+0.99(10)			

^a This work.

^b Measurements of De Beer⁷⁾.

for the magnetic dipole and electric quadrupole moment ratios of the three nuclei. In table XI the hfs parameters for ^{52}Mn and ^{54}Mn in the two sites are listed together with the parameters of De Beer⁷⁾. The obtained ratios of the parameters are seen to be the same for the two sites; moreover the ratio of the A 's equals that of the B 's. This indicates that the hyperfine anomaly is negligible and that we can calculate moment ratios of for instance ^{54}Mn and ^{55}Mn with the aid of

$$\frac{{}^{54}A}{{}^{55}A} = \frac{{}^{54}B}{{}^{55}B} = \frac{{}^{54}g_N}{{}^{55}g_N} = \frac{{}^{54}\mu^{55}I}{{}^{55}\mu^{54}I} = \frac{5}{6} \frac{{}^{54}\mu}{{}^{55}\mu} \quad (20)$$

and

$$\frac{{}^{54}P}{{}^{55}P} = \frac{{}^{54}Q}{{}^{55}Q} \frac{{}^{55}I(2 \times {}^{55}I - 1)}{{}^{54}I(2 \times {}^{54}I - 1)} = \frac{2}{3} \frac{{}^{54}Q}{{}^{55}Q}. \quad (21)$$

The ratio of ^{52}Mn to ^{54}Mn parameters serves only as a check on the obtained B values; for the determination of the magnetic moment ratios only the values of A were used. The obtained results will now be compared with other measurements.

a) ${}^{54}\mu/{}^{55}\mu$. Templeton and Shirley¹²⁾ measured the resonance frequency of ^{54}Mn dissolved in Fe with the same technique. Compared with the reso-

nance frequency of ^{55}Mn in Fe^{21}) this gives $^{54}\mu/^{55}\mu = 0.9521$ (15). The difference between their result and ours is just outside the experimental error. Another result is quoted by Shirley²²): $^{54}\mu/^{55}\mu = -0.952$ (18). Apart from the sign this is in agreement with our experiment. The magnetic moment of ^{55}Mn is known to be positive, so a negative ratio would imply $^{54}\mu < 0$ and consequently ^{54}A and $^{54}B > 0$. This is incompatible with our measurements, considering the known signs of the crystal field parameters. The field dependence of $\nu_{\text{I}}^{\text{I}}$ and $\nu_{\text{II}}^{\text{I}}$ would be certainly incorrect if one assumes ^{54}A and $^{54}B > 0$. We conclude that μ (^{54}Mn) is positive, in agreement with the result of Bauer *et al.*²³).

The magnetic moment of ^{55}Mn has been determined by several authors²⁴⁻²⁶). If we use the weighted average $^{55}\mu = +3.4432$ (16) μ_{N} , the magnetic moment of ^{54}Mn is found to be: $^{54}\mu = +3.2724$ (15) μ_{N} .

b) $^{54}Q/^{55}Q$. To our knowledge no other determinations of this quantity are found in the literature. If we take from ref. 27

$$^{55}Q = +0.35 \text{ (5) barn,}$$

then we find

$$^{54}Q = +0.35 \text{ (6) barn.}$$

We note, however, that no correction for the atomic Sternheimer anti-shielding factor has been applied in ref. 27. This introduces an uncertainty of roughly 30% in the final result²⁸).

c) $^{52}\mu/^{55}\mu$. This quantity was determined by Ädelroth *et al.*¹⁰) with an atomic beam method, using the atomic hyperfine structure constant for ^{55}Mn measured by Woodgate and Martin²⁹). Their result, $^{52}\mu/^{55}\mu = +0.88678$ (12), is not affected by a new determination of the atomic hyperfine structure of ^{55}Mn by Evans *et al.*³⁰). Our result is $^{52}\mu/^{55}\mu = +0.88706$ (15). The difference between the two measurements is just the combined experimental error. Again using $^{55}\mu = +3.4432$ (16) μ_{N} , we arrive at $^{52}\mu = +3.0543$ (15) μ_{N} , whereas the ratio of Ädelroth gives $^{52}\mu = +3.0534$ (14) μ_{N} .

d) $^{52}Q/^{55}Q$. The hitherto unknown quadrupole moment of ^{52}Mn can be determined from the measured ratio. Taking $^{55}Q = +0.35$ (5) barn²⁷), we find $^{52}Q = +0.53$ (11) barn.

Again, no antishielding correction has been applied.

6.2. Origin of the homogeneous linewidth. The experiments on the homogeneous linewidth are discussed in 4.3. The results can be expressed in terms of a fluctuating field at the Mn ion, its value being 1.8 Oe for the highest rf power level. In the experiments one observes the growing of $W(0)$ when the frequency of the rf field is constant and in the centre of the

inhomogeneously broadened line, $\nu = \nu_c$. The increase of $W(0)$ takes place in a time of the order of 10 s. In this section we shall try to show that this field very probably originates from the protons surrounding the Mn ion.

Let us consider the following situation. Each Mn ion is placed in a field composed of a static component (4700 Oe) and a component varying in time arising from the fluctuating dipole fields of the protons around the ion. The fields due to Ce or other Mn spins are negligible. Due to the fluctuations the Larmor frequency of one individual Mn ion varies and can be equal to ν_c for a certain time, creating a transition of type ν_{II}^1 . According to this picture the value of the fluctuating component of the proton field determines the fraction of Mn ions for which such a transition is feasible. By the fluctuating component we mean the fraction of the protons that can make spin flips in a time less than 10 s. Therefore the protons nearest to the Mn ion will give no contribution, their spin flips being hindered due to the fact that their Larmor frequencies are shifted by the presence of the Mn dipole field. In view of the experiments described in section 4.3 we estimate the fluctuating proton field to be 1.8 Oe.

If we want to estimate the homogeneous width theoretically we must know the probability W of a simultaneous spin flip of two protons with unequal Larmor frequencies. W is roughly given by³⁰⁾:

$$W \approx W_0 \int_{-\infty}^{+\infty} G_1(\nu_1 + u) G_2(\nu_2 + u) du / G_1(\nu_1), \quad (22)$$

where W_0 is the probability of an energy conserving spin flip and G_1 and G_2 are the normalized shape functions for the two protons centered around ν_1 and ν_2 respectively. Assuming G_1 and G_2 to be gaussian, W is a gaussian function of $\nu_1 - \nu_2$, hence one can estimate the spin flip rate W as a function of $\nu_1 - \nu_2$.

Van Ormondt^{32,33)} has measured the resonance frequencies of proton groups in the vicinity of both Mn sites with the Ligand-ENDOR technique. From his work one obtains the linewidth of the proton groups together with the distances between the centres of these lines. This enables an estimation of which proton groups are able to perform mutual spin flips within 10 s and thus contribute to the homogeneous linewidth.

More quantitatively, the total width between the inflexion points of the ENDOR lines is about 50 kHz. Accordingly, we neglected the proton groups with Larmor frequencies differing more than 120 kHz from those of at least one other proton group, because for $\nu_1 - \nu_2 = 120$ kHz we find $W \approx 0.1$ assuming gaussian line shapes. Following this line of reasoning one may neglect nine of the twelve protons in the complex $[\text{Mn}(\text{H}_2\text{O})_6]^{2+}$ and also

some other proton groups at greater distances. We can now calculate M_2 , the second moment of the Mn EPR line due to the remaining protons. All protons within 40 Å were taken into account. The result is $M_2 = 0.545 \text{ Oe}^2$ which gives for the total width between the inflexion points 1.48 Oe. This figure agrees reasonably well with the experimental value, 1.8 Oe, in view of the crudeness of the model. We conclude therefore that the observed homogeneous linewidth originates from the protons.

In the model given above we made the assumption that, once a Mn ion has an energy splitting matching exactly the frequency of the rf field, the probability of the transition $W(\nu_{II}^1)$ is sufficiently high that

$$W(\nu_{II}^1) \Delta t \gg 1, \quad (23)$$

Δt being the time during which the Mn ion has the required energy. So in fact one calculates the homogeneous width for a very high rf power level. To analyse the observed dependence of the width on the rf power level and the rate at which $W(0)$ grows would require a much more sophisticated approach than is presented here.

6.3. Conclusion. In this article we described magnetic resonance experiments on oriented radioactive nuclei detected by changes in the directional anisotropy of the emitted gamma rays. The accuracy and the detailed information obtained with NMR methods are combined with a very sensitive detection technique, using the signals emitted by the individual nuclei. Accordingly the concentration of the resonant spin system can be kept very small, in the order of magnitude of 10^{-8} – 10^{-10} . Hence the method may be very attractive also for the study of very dilute alloys, for instance by experiments on the Kondo effect³⁵⁾ or in the case of hyperfine fields on impurities in a ferromagnetic metal³⁴⁾. The main experimental problems – skin effect, rf heating – can be overcome by using a very thin sample (1–10 μ).

In our experiments we showed that the method is also very useful if the nuclei are incorporated in a dilute paramagnetic crystal. The hfs levels turn out to be quite sharp and the nuclear spin-lattice relaxation time is very long if the electronic spins are sufficiently polarized at very low temperatures. The paramagnetic impurity ions are utilized to provide nuclear orientation via the process of thermal mixing during a level crossing. The long nuclear relaxation time and the use of a dilute paramagnetic crystal eliminates the difficult problem of rf heating occurring in previous experiments on nuclei dissolved in a ferromagnetic metal.

In the resonance process a major role is played by the enhancement of the rf field at the position of the radioactive nucleus through the action of

the electronic spin. A quantitative description of this effect in the case of a paramagnetic ion is given. Experimentally this is very important because it enabled us to saturate the hfs transitions by means of an rf field having an amplitude as low as $\approx 10^{-4}$ Oe.

The usefulness of the method to determine hfs constants has been demonstrated for ^{52}Mn and ^{54}Mn . The precision obtained is in principle the same as in ENDOR measurements, however, in practice it is limited somewhat by the fact that one can measure only a few lines of the hfs spectrum. By comparing the results with ENDOR results on stable isotopes in the same host one can derive very accurate values for the magnetic moments of the radioactive isotopes as well as values for their quadrupole moments.

In addition the gamma anisotropies can be studied in some detail. Due to the orientation process and the resonance saturation, it is possible to deduce the gamma anisotropy for each hfs level separately. This is in contrast to conventional nuclear orientation measurements, in which a Boltzmann distribution over the hfs levels is obtained.

REFERENCES

- 1) Bloembergen, N. and Temmer, G. M., *Phys. Rev.* **89** (1953) 883.
- 2) Matthias, E. and Holliday, R. J., *Phys. Rev. Letters* **17** (1966) 897.
- 3) Shirley, D. A., *Proceedings XVth Colloque Ampère, Grenoble, 1968*, ed. P. Averbuch, North-Holland Publ. Co. (Amsterdam, 1969) p. 81.
- 4) Shirley, D. A., *Hyperfine Structure and Nuclear Radiations*, ed. E. Matthias and D. A. Shirley, North-Holland Publ. Co. (Amsterdam, 1968) p. 843.
- 5) Lubbers, J. and Huiskamp, W. J., *Physica* **34** (1967) 193 (Commun. Kamerlingh Onnes Lab. Leiden No. 353b).
- 6) Zalkin, A., Forrester, J. D. and Templeton, D. H., *J. chem. Phys.* **39** (1963) 2881.
- 7) De Beer, R. and Van Ormondt, D., *Phys. Letters* **27A** (1968) 475.
- 8) Van Ormondt, D., Thesis, Delft (1968).
- 9) Van Ormondt, D., Thalhammer, T., Holland, J. and Brandt, B. M. M., *Proceedings XIVth Colloque Ampère*, ed. R. Blinc, North-Holland Publ. Co. (Amsterdam, 1967) p. 272.
- 10) Ådelroth, K. E., Lindgren, I., Djay, R. and Rosén, A., *Arkiv. Fys.* **31** (1966) 549.
- 11) Shirley, V. S., ref. 4, p. 1016.
- 12) Templeton, J. E. and Shirley, D. A., *Phys. Rev. Letters* **18** (1967) 240.
- 13) Abragam, A. and Borghini, M., *Progress in low Temp. Phys.* vol. 4 ed. C. J. Gorter, North-Holland Publ. Co. (Amsterdam, 1964) p. 418.
- 14) Wilson, R. R., Bartlett, A. A., Kraushaar, J. J., Mc Cullen, J. D. and Ristinen, R. A., *Phys. Rev.* **125** (1962) 1655.
- 15) Mann, L. G., Camp, D. C., Miskel, J. A. and Nagle, R. J., *Phys. Rev.* **137B** (1965) 1.
- 16) Huiskamp, W. J. and Tolhoek, H. A., *Progress in low Temp. Phys.* vol. 3 ed. C. J. Gorter, North-Holland Publ. Co. (Amsterdam, 1961) p. 360.

- 17) Cox, J. A. M. and De Groot, S. R., *Physica* **19** (1953) 683.
- 18) Lubbers, J. and Huiskamp, W. J., *Physica* **34** (1967) 166 (*Commun. Kamerlingh Onnes Lab., Leiden No. 353a*).
- 19) Van Ormondt, D., Thesis, Delft (1968) p. 160.
- 20) Kaplan, M. and Shirley, D. A., *Nuclear Phys.* **37** (1962) 522.
- 21) Edmonds, D. T., quoted in ref. 12.
- 22) Shirley, V. S., ref. 4, p. 1012.
- 23) Bauer, R. W. and Deutsch, M., *Phys. Rev.* **120** (1960) 946.
- 24) Mims, W. B., Devlin, G. A., Geschwind, S. and Jaccarino, V., *Phys. Letters* **24A** (1967) 481.
- 25) Deyer, G. L. and Woonton, G. A., *Canad. J. Phys.* **45** (1967) 2975.
- 26) Eskes, Y. H. and De Wijn, H. W., *Phys. Letters* **25A** (1967) 553.
- 27) Walther, H., *Z. Physik* **170** (1962) 507.
- 28) Sternheimer, R. M., *Phys. Rev.* **164** (1964) 10.
- 29) Woodgate, G. K. and Martin, J. S., *Proc. Phys. Soc.* **70** (1957) 485.
- 30) Evans, L., Sandars, P. H. G. and Woodgate, G. K., *Proc. Roy. Soc.* **289A** (1965) 108.
- 31) Abragam, A., *The principles of Nuclear Magnetism*, Clarendon Press (Oxford, 1961).
- 32) Van Ormondt, D. and Visser, H., *Phys. Letters* **26A** (1968) 343.
- 33) Van Ormondt, D., Thesis, Delft (1968) p. 120.
- 34) Shirley, D. A., Rosenblum, S. S. and Matthias, E., *Phys. Rev.* **170** (1968) 363.
- 35) Heeger, A. J., in *Solid State Physics* **23**, ed. F. Seitz, D. Turnbull and H. Ehrenreich, Academic Press (New York, 1969) p. 283.

CHAPTER II

NUCLEAR MAGNETIC RESONANCE ON ORIENTED NUCLEI IN A DILUTE PARAMAGNETIC CRYSTAL; ^{57}Co , ^{58}Co and ^{60}Co in $\text{La}_2\text{Mg}_3(\text{NO}_3)_{12}\cdot 24\text{H}_2\text{O}$.Synopsis

The method of nuclear magnetic resonance on radioactive nuclei, oriented in a dilute paramagnetic crystal, was applied to three Co isotopes, incorporated in single crystals of lanthanum magnesium nitrate (LMN). Nuclear orientation was achieved by means of cross relaxation with Ce ions, partly replacing the La ions. Resonance transitions between successive hfs levels were detected by observing changes in the directional anisotropy of the emitted gamma rays.

Resonance transitions could be observed only for Co ions at site II of the LMN crystal. From the observed changes in the gamma anisotropy it was concluded that 58% of the Co ions occupy site II, which is somewhat lower than 2/3, the relative abundance of this site.

The width of the resonance lines was ascribed to a spread in the hfs parameters A and B. The contribution of homogeneous broadening to the total linewidth could not be observed.

From the measured resonance frequencies accurate values of the hfs parameters could be derived. By comparing these with the hfs parameters of stable ^{59}Co in the same salt, accurate values for the magnetic moments of ^{57}Co , ^{58}Co and ^{60}Co were obtained: $\mu(^{57}\text{Co}) = + 4.722 \pm 0.017$ n.m., $\mu(^{58}\text{Co}) = + 4.035 \pm 0.008$ n.m. and $\mu(^{60}\text{Co}) = + 3.790 \pm 0.008$ n.m. The quadrupole moments of the three Co isotopes could be determined for the first time: $Q(^{57}\text{Co}) = + 0.49 \pm 0.09$ barn, $Q(^{58}\text{Co}) = + 0.21 \pm 0.03$ barn and $Q(^{60}\text{Co}) = + 0.42 \pm 0.05$ barn.

In the case of ^{57}Co , a considerable attenuation of the gamma anisotropy was observed, which must be attributed to reorientation during the 8.7 ns lifetime of the excited state of ^{57}Fe at 136 keV. From the anisotropy measurements the mixing ratio $\delta(E2/M1)$ of the 122 keV transition was obtained. This result, $\delta = + 0.1071 \pm 0.0022$, is considerably lower than that from previous determinations.

1. Introduction

The method of nuclear magnetic resonance on oriented nuclei (NMR-ON) was developed for nuclei dissolved in ferromagnetic metals. Recently¹⁾ we applied the method to nuclei incorporated in a dilute paramagnetic crystal, i.e. ^{52}Mn and ^{54}Mn in $\text{La}_2\text{Mg}_3(\text{NO}_3)_{12}\cdot 24\text{H}_2\text{O}$ (lanthanum magnesium nitrate, hereafter called LMN). We will refer to that chapter as I.

In this chapter we are dealing with three radioactive Co isotopes, ^{57}Co , ^{58}Co and ^{60}Co , incorporated in the same salt. In contrast to the Mn^{2+} ion, which has a $^6\text{S}_{5/2}$ ground state, the electronic orbital angular momentum plays an important role in the interaction of the Co^{2+} ion with its surroundings. Therefore we may expect different characteristics with respect to relaxation times, linewidths, etc., compared to Mn^{2+} . Investigations on both ions will thus give an impression to what extent the method of NMR-ON in dilute paramagnetic crystals is generally applicable. Moreover, since the hfs parameters of stable ^{59}Co in this host crystal are known^{2,3)}, we can derive information about the nuclear moments of the three radioactive isotopes.

A detailed treatment of a typical NMR-ON experiment is given in I, and we will give here only a brief description. The experiment consists of two parts.

- a. Nuclear orientation by means of cross relaxation (thermal mixing) between a cold electron spin system and the hfs system of the Co^{2+} ions. The cold electron spin system is formed by Ce ions, partly replacing the La ions in the LMN lattice. By means of precooling to $T < 0.1$ K the Ce ions can be magnetized to a high degree if a magnetic field is applied in a direction along which the g value is large. Rotating the field adiabatically to a direction where the g value is small, causes cooling of the Ce ions. If the Ce Zeeman splitting equals the energy differences of the lowest hfs multiplet in the Co^{2+} system, a fast thermal mixing between both spin systems occurs, leading to a high degree of orientation of the Co nuclei.

b. After the direction and the strength of the magnetic field have been adjusted to the desired values, an rf field of sufficient amplitude (typical 1 mOe) is applied to the sample. The frequency ν of the rf field is swept at a rate of ≈ 1 kHz/s through the region where $h\nu$ equals the energy difference between the lowest two hfs levels of the Co^{2+} ion. Transitions induced between these two levels are detected as a marked change in the gamma anisotropy as the frequency is varied in the region of the resonance. Because the nuclear spin-lattice relaxation times are very long under the experimental conditions ($T < 0.1$ K), we can equalize the populations of both levels (saturation) using only a low rf field. After saturation, the populations will remain equal. In a similar way, transitions between another pair of levels can be detected, at least if the accompanying change in the gamma anisotropy is large enough to be discernible. An example of such a measurement is shown in fig. 1.

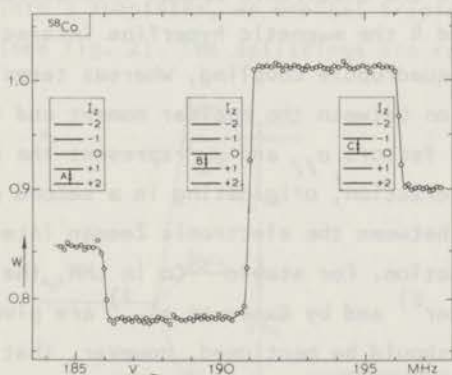


fig. 1. Example of a typical NMR-ON experiment, ^{58}Co in LMN. The changes in W , the normalized gamma intensity in the magnetic field direction, which are induced by varying the frequency ν of the r.f. field at a rate of ≈ 1 kHz/s, clearly show the presence of three transitions. These are indicated in the inserts.

2. Theory

2.1. Crystal structure; energy levels of Co^{2+} ions in LMN.

The crystal structure of the double nitrates is known from the work of Zalkin et al.⁴⁾ The divalent Co ion can occupy two sites, denoted by I and II. Site II is twice as prevalent as the other site. The Co^{2+} ions are surrounded by six water molecules, forming an octahedron which is somewhat distorted along that body diagonal that coincides with the c-axis of the crystal. Both sites have trigonal symmetry, site I has inversion symmetry as well.

To describe the energy levels of the Co^{2+} ion we used the following spin Hamiltonian, in which the z-axis is aligned along the trigonal axis (c-axis) of the LMN crystal:

$$\begin{aligned}
 H = & g_{//} \mu_B H_z S_z + g_{\perp} \mu_B H_x S_x + AS_z I_z + B(S_x I_x + S_y I_y) \\
 & + P \left\{ I_z^2 - \frac{1}{3} I(I+1) \right\} + (1 + \sigma_{//}) g_N \mu_N H_z I_z + (1 + \sigma_{\perp}) g_N \mu_N H_x I_x .
 \end{aligned} \quad (1)$$

Terms 1 and 2 denote the electronic Zeeman interaction in the lowest doublet; terms 3 and 4 the magnetic hyperfine interaction; term 5 gives the electric quadrupole coupling, whereas terms 6 and 7 describe the interaction between the nuclear moment and the external magnetic field. The factors $\sigma_{//}$ and σ_{\perp} represent the so called "pseudo-Zeeman" interaction, originating in a second order effect due to cross terms between the electronic Zeeman interaction and the magnetic hfs interaction. For stable ^{59}Co in LMN, the parameters as determined by De Beer²⁾ and by Gager et al.³⁾ are given in Table I for both sites. It should be mentioned, however, that the ENDOR measurements of De Beer were not completely consistent with the Hamiltonian given. The value of A obtained if H was parallel to the c-axis was not the same as that obtained if H was perpendicular to it; the same holds for B. The values given in the table correspond to the most precise determination, i.e. A was derived from data in which H // c-axis, and B from data in which H \perp c-axis.

The derivation of the before mentioned spin Hamiltonian, starting from the known configuration $3d^7$ for the Co^{2+} ions, has been

TABLE I

Hfs parameters for stable Co^{2+} in LMN							
Site	$g_{//}$	g_{\perp}	A/hc (10^{-4} cm^{-1})	B/hc (10^{-4} cm^{-1})	P/hc (10^{-4} cm^{-1})	$\sigma_{//}$	σ_{\perp}
1 ^a	7.23 (1)	2.31 (2)	+279(6)	≤ 1			
11 ^b	4.043(2)	4.432(2)	+79.096(4)	+103.911(4)	+0.0720(4)	0.406(3)	0.438(5)

^a EPR measurements by Gager et al., ref. 3.

^b ENDOR measurements by De Beer, ref. 2.

given for the first time by Abragam and Pryce⁵⁾. The Coulomb repulsion between the 3d electrons of the Co^{2+} ion gives rise to an ionic 4F ground state and an excited state 4P at about 14000 cm^{-1} . Abragam and Pryce start by considering the effect of the octahedral crystal-line field arising from the six water molecules, which splits up the 4F ground state into 3 substates, an orbital triplet characterized by Γ_4 being lowest (see fig. 2). The splittings are respectively $10 Dq$

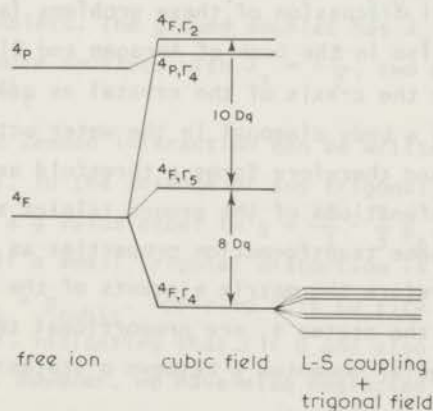


fig. 2. Energy level scheme of the Co^{2+} ion in a crystalline electric field of cubic (octahedral) symmetry. For the lowest orbital level, the triplet $|{}^4F, \Gamma_4\rangle$, the splitting under spin-orbit coupling and under a trigonal distortion of the cubic field is indicated.

and $8 Dq$, Dq being $\approx 900 \text{ cm}^{-1}$. The excited 4P state has the same transformation properties as the Γ_4 ground state and consequently the real ground state will be of the form

$$\varepsilon |{}^4F, \Gamma_4\rangle + \tau |{}^4P, \Gamma_4\rangle, \quad (2)$$

where $\varepsilon \approx 1$ and τ is small.

At this point we may note that the cubic field splittings are of the same order of magnitude as the term splittings of the free ion. Therefore the so called "intermediate field" perturbation procedure described here is not correct. An alternative method, known as "strong field", would be to apply the crystalline field perturbation to the individual d electrons and thereafter take into account the Coulomb repulsion between them. Such an approach has been given for Co^{2+} in an octahedral field by Thornley et al.⁶⁾ It yields the same expression (2) for the ground state of the Co^{2+} ion, but the level pattern of fig. 2 is strongly changed. The excited state corresponding to $|{}^4P, \Gamma_4\rangle$ in the intermediate field approach is at about $20,000 \text{ cm}^{-1}$. Other levels are at about 9000 cm^{-1} of the ground level, but these play a role only if there are important distortions from cubic symmetry. A very useful discussion of these problems (and of the following) can be found also in the book of Abragam and Bleaney⁷⁾.

We will choose the c -axis of the crystal as quantization direction. The c -axis is a body diagonal in the water octahedron surrounding the Co ions, and therefore forms a threefold axis of symmetry. The resulting eigenfunctions of the ground triplet are denoted by ϕ_i ; they have the same transformation properties as real p functions, denoted by p_i . Therefore the matrix elements of the angular momentum operator \underline{L} between the states ϕ_i are proportional to those of an effective orbital angular momentum $\underline{\tilde{L}}$ between p states:

$$\langle \phi_i | \underline{L} | \phi_j \rangle = \tilde{g}_{\tilde{L}} \langle p_i | \underline{\tilde{L}} | p_j \rangle, \quad (3)$$

in which $\tilde{L} = 1$.

The value of $\tilde{g}_{\tilde{L}}$ depends on τ and on the presence of covalent bonding,

which reduces the effective orbital momentum⁶⁻⁸⁾. For $\tau = 0$ and absence of covalency effects, $\tilde{g}_l = -1.5$.

The correspondence between Φ_i and ρ_i is correct only for cubic symmetry. If a trigonal distortion is taken into account we must write $L_z = \tilde{g}_{l_z} \tilde{l}_z$; $L_x = \tilde{g}_{l_x} \tilde{l}_x$; $L_y = \tilde{g}_{l_y} \tilde{l}_y$, where $\tilde{g}_{l_x} = \tilde{g}_{l_y}$. Within the ground manifold the trigonal field distortion and the spin-orbit coupling can be written as

$$H_T + H_{S.O.} = \Delta(\tilde{l}_z^2 - \frac{2}{3}) + \lambda \tilde{g}_{l_z} \tilde{l}_z S_z + \lambda \tilde{g}_{l_x} (\tilde{l}_x S_x + \tilde{l}_y S_y) \quad (4)$$

where Δ is a measure of the trigonal field splitting, and λ is the spin-orbit coupling constant. The free ion value, $\lambda = 180 \text{ cm}^{-1}$, can be used in a first approximation, neglecting for instance covalency effects.

This Hamiltonian splits the ground state into six Kramers doublets. The ground doublet can be written in the \tilde{l}_z, S_z representation as

$$|\Phi_{\pm}\rangle = a_1 | \bar{1}, \pm \frac{3}{2} \rangle + a_2 | 0, \pm \frac{1}{2} \rangle + a_3 | \pm 1, \mp \frac{1}{2} \rangle \quad (5)$$

We note that $\tilde{J}_z = \tilde{l}_z + S_z$ commutes with $H_T + H_{S.O.}$, so that we can use \tilde{J}_z to label the doublets. The ground doublet has $\tilde{J}_z = \pm \frac{1}{2}$; in addition there will be two more doublets with $\tilde{J}_z = \pm \frac{1}{2}$, two with $\tilde{J}_z = \pm \frac{3}{2}$ and one with $\tilde{J}_z = \pm \frac{5}{2}$.

The electronic Zeeman interaction can be written as

$H_z = \mu_B H (\tilde{g}_l \tilde{l}_z + 2S_z)$. In the absence of any trigonal distortion the ground doublet has a g value equal to $g = \frac{10}{3} - \frac{2}{3} \tilde{g}_l$. For $\tilde{g}_l = -1.5$ we find $g = 4.33$. If a small trigonal distortion is present, one can write $\frac{1}{3} g_{//} + \frac{2}{3} g_{\perp} = g_{\text{cubic}}$. Applying this to site II, we have $\frac{1}{3} g_{//} + \frac{2}{3} g_{\perp} = 4.30$, indicating that $\tau = 0$ and also that covalency effects are small. However, we have also neglected second order effects of $H_{S.O.}$ between the ground state $|^4F, ^4\Gamma_4\rangle$ and higher lying states such as $|^4F, ^4\Gamma_5\rangle$. Therefore we must be careful in drawing conclusions from the observed g values on the basis of the simple theory sketched here.

The Hamiltonian H_h describing the hyperfine interaction is⁹⁾

$$H_h = P\{\underline{L} \cdot \underline{I} + [\xi L(L+1) - \kappa] \underline{S} \cdot \underline{I} - \frac{3}{2} \xi [(\underline{L} \cdot \underline{S})(\underline{L} \cdot \underline{I}) + (\underline{L} \cdot \underline{I})(\underline{L} \cdot \underline{S})]\}, \quad (6)$$

where

$$P = 2 \mu_B g_N \mu_N \langle r^{-3} \rangle. \quad (7)$$

$\langle r^{-3} \rangle$ is the mean inverse third power of the electron distance from the nucleus, averaged over the electronic wave functions. For Co^{2+} , Freeman and Watson¹⁰⁾ give $\langle r^{-3} \rangle = 6.04$ a.u.

ξ is given by

$$\xi = \frac{2\ell + 1 - 4S}{S(2\ell - 1)(2\ell + 3)(2L - 1)}, \quad (8)$$

which for $\ell = 2$, $L = 3$ and $S = \frac{3}{2}$, gives $\xi = -\frac{2}{315}$.

The first term of (6) describes the coupling between the electronic orbital angular momentum and the spin of the nucleus; the term $-\kappa P \underline{S} \cdot \underline{I}$ gives the Fermi "contact" interaction, whereas the other terms originate in the dipole-dipole coupling between electronic and nuclear spin. Within the ground doublet the hfs interaction can be written as $A S_z I_z + B(S_x I_x + S_y I_y)$, S now being a fictitious spin $\frac{1}{2}$. Expressions for the coefficients A and B in terms of the constants of (6) are given in ref. 5, 6 and 8. It turns out that the dipole-dipole mechanism gives only a small contribution, and that κ is about 0.325 for the Co^{2+} ion.

Some remarks will be made here about the "pseudo" nuclear Zeeman interaction coefficients $\sigma_{//}$ and σ_{\perp} . These terms are a direct consequence of the fact that the electronic Zeeman interaction $H_z = \mu_B H (\underline{L} + 2\underline{S})$ and the hyperfine interaction H_h both have matrix elements between the various Kramers doublets within the orbital triplet $|^4F, ^4\Gamma_4\rangle$. Therefore H_z and H_h give rise to admixtures of these excited states in the ground doublet. To second order the change in energy of the ground state is given by

$$E' = \sum_{i=1}^5 \frac{|\langle 0 | (H_z + H_h) | i \rangle|^2}{E_0 - E_i}, \quad (9)$$

where i runs over the various Kramers doublets. The terms quadratic in H_z give rise to a shift proportional to H^2 , which is associated with the Van Vleck temperature independent paramagnetism. The terms quadratic in H_h are small and can be neglected. The cross terms are linear in H and I , the major contributions coming from cross-products of $\mu_B H \cdot L$ and $P L \cdot I$, and of $2\mu_B H \cdot S$ and $-kPS \cdot I$. The final result can be written in the form $H \cdot \underline{\sigma} \cdot I$, in which $\underline{\sigma}$ is a diagonal tensor having components $\sigma_{//}$, σ_{\perp} and σ_{\perp} . The calculation of $\sigma_{//}$ and σ_{\perp} is lengthy but straightforward, provided the wave functions of the Kramers doublet are known. For tetragonal $\text{Co}(\text{NH}_4)_2(\text{SO}_4)_2 \cdot 6\text{H}_2\text{O}$, Choh and Seidel¹¹⁾ have evaluated the σ terms, using essentially the wave functions of Abragam and Pryce, and compared them to their EPR and NMR data on the same compound. The agreement is satisfactory. Unpublished calculations of Nijman and De Beer²⁾ on Co^{2+} in LMN, site II, based upon this second order effect, are in agreement with their ENDOR results.

Although we fitted the measured resonance frequencies to the Hamiltonian using a computer for diagonalization of the matrix, we made use of perturbation expressions to study the influence of small parameter variations on the resonance frequencies. For magnetic fields of several kOe, the electronic Zeeman interaction is the most important term in the Hamiltonian; therefore we used a representation in which this term is diagonal. We distinguish between two cases:

1) $H // c$ -axis. The Hamiltonian is written as

$$H_{//} = g_{//} \mu_B H S_z + A I_z S_z + \frac{1}{2} B \{S_+ I_- + S_- I_+\} + P \{I_z^2 - \frac{1}{3} I(I+1)\} + (1 + \sigma_{//}) g_N \mu_N H I_z \quad (10)$$

2) $H \perp c$ -axis, say, $H // x$. We apply the transformation $x \rightarrow z$, $y \rightarrow y$, $z \rightarrow -x$. The Hamiltonian then becomes

$$H_{\perp} = g_{\perp} \mu_B H S_z + B S_z I_z + \frac{1}{4} (A+B) \{S_+ I_- + S_- I_+\} + \frac{1}{4} (A-B) \{S_+ I_+ + S_- I_-\} - \frac{1}{2} P \{I_z^2 - \frac{1}{3} I(I+1)\} + \frac{1}{4} P \{I_+^2 + I_-^2\} + (1 + \sigma_{\perp}) g_N \mu_N H I_z \quad (11)$$

Applying second order perturbation theory to these expressions gives

for the energy levels in the lowest hfs multiplet ($-\frac{1}{2}, m$) :

1) For $H // c$ -axis:

$$E_{-\frac{1}{2}, m} = -\frac{1}{2} g_{//} \mu_B H - \frac{1}{2} A m - \frac{1}{4} \frac{B^2 \{I(I+1) - m^2 + m\}}{g_{//} \mu_B H + (m - \frac{1}{2}) A} + P \{m^2 - \frac{1}{3} I(I+1)\} + (1 + \sigma_{//}) g_N \mu_N H m. \quad (12)$$

2) For $H \perp c$ -axis:

$$E_{-\frac{1}{2}, m} = -\frac{1}{2} g_{\perp} \mu_B H - \frac{1}{2} B m - \frac{1}{16} \frac{(A+B)^2 \{I(I+1) - m^2 + m\}}{g_{\perp} \mu_B H + (m - \frac{1}{2}) A} - \frac{1}{16} \frac{(A-B)^2 \{I(I+1) - m^2 - m\}}{g_{\perp} \mu_B H + (m + \frac{1}{2}) A} - \frac{1}{2} P \{m^2 - \frac{1}{3} I(I+1)\} + (1 + \sigma_{\perp}) g_N \mu_N H m, \quad (13)$$

in which one term of the order P^2/B has been omitted.

2.2. Gamma anisotropy parameters for ^{57}Co .

The decay scheme of ^{57}Co is given in fig. 3. The 14.4 keV gamma radiation was not observed in our experiments, because it was absorbed

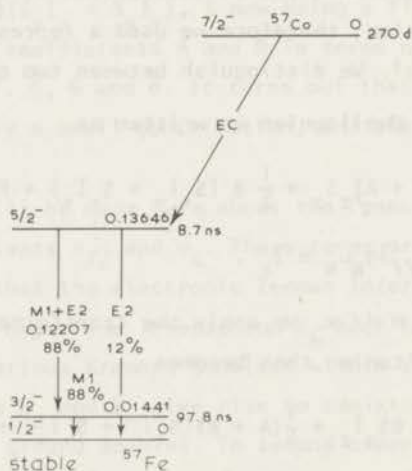


fig. 3. Nuclear decay scheme for ^{57}Co . All energies are given in MeV.

The half lives and the spins of the various states are indicated.

in the cryostat walls. The 122 keV line is a mixed M1-E2 transition; the quadrupole-dipole mixing ratio $\delta(E2/M1)$ has been determined by several authors¹²⁻¹⁴⁾, using the angular correlation of the 122 keV - 14.4 keV cascade and assuming that the last transition has purely magnetic dipole (M1) character. This assumption is justified by K and L subshell conversion measurements of Ewan et al.¹⁵⁾, who state that $|\delta| < 0.01$.

The directional distribution of gamma rays emitted at an angle α with respect to the magnetic field direction can be given by

$$W(\alpha) = 1 + A_2 f_2(j_i) P_2(\cos \alpha) + A_4 f_4(j_i) P_4(\cos \alpha). \quad (14)$$

f_2 and f_4 are so called orientation parameters, depending on the relative populations a_m of the substates m of the initial state having nuclear spin j_i :

$$f_2 = \frac{1}{j_i^2} \left[\sum_m m^2 a_m - \frac{1}{3} j_i (j_i + 1) \right]. \quad (15)$$

$$f_4 = \frac{1}{j_i^4} \left[\sum_m m^4 a_m - \frac{1}{7} (6j_i^2 + 6j_i - 5) \sum_m m^2 a_m + \frac{3}{35} j_i (j_i - 1) (j_i + 1) (j_i + 2) \right]. \quad (16)$$

The populations are normalized according to $\sum_m a_m = 1$. $P_2(\cos \alpha)$ and $P_4(\cos \alpha)$ are Legendre polynomials. The coefficients A_2 and A_4 depend on the spins of the initial and final state and on the multipole character of the transition. For the 136 keV E2 transition one has¹⁶⁾

$$j_i = 5/2, \\ A_2 = -\frac{15}{7} N_2(j_i) = -1.339, \quad (17)$$

$$A_4 = -5 N_4(j_i) = -6.511. \quad (18)$$

Eq. 14 is valid only for the case that the Hamiltonian has rotational symmetry with respect to the quantization axis. This condition is, strictly speaking, fulfilled only if \mathbf{H} is aligned along the c -axis of the crystal. However, if we quantize along the magnetic field direction, the deviation from rotational symmetry may be neglected in all

cases in view of the fairly large values of the magnetic field and in view of the restriction to type II ions, for which the hfs interaction is not very anisotropic.

For the 122 keV transition we have

$$A_2 = \frac{1}{1+\delta^2} \left[\frac{3}{2} - 3 \left\{ \frac{15(j_i - 1)}{j_i + 1} \right\}^{\frac{1}{2}} \delta + \frac{15}{14} \frac{j_i - 5}{j_i + 1} \delta^2 \right] N_2(j_i) \quad (19)$$

$$= \frac{1}{1+\delta^2} [0.9375 - 4.756 \delta - 0.479 \delta^2] ,$$

$$A_4 = 10 \frac{2j_i - 3}{j_i + 1} \frac{\delta^2}{1 + \delta^2} N_4(j_i) = 7.45 \frac{\delta^2}{1 + \delta^2} . \quad (20)$$

However, we want to know also the directional distribution $W(\alpha)$ expressed in terms of the orientation parameters $f_k(I)$ of the parent nucleus ^{57}Co , having $I = 7/2$. We neglect the spin precession during the 8.7 ns half life of the excited state of ^{57}Fe at 136 keV (see, however, section 6.4.). The relation between $f_k(I)$ and $f_k(j_i)$ can be written as

$$f_k(j_i) = U_k(j_i, I) f_k(I) , \quad (21)$$

where the coefficient U_k describes the influence of the beta decay on the nuclear orientation.

In this case

$$U_k(j_i, I) = N_k(I) / N_k(j_i) , \quad (22)$$

which gives $U_2 = 0.933$ and $U_4 = 0.549$.

Consequently we have for the 136 keV transition:

$$W(\alpha) = 1 - 1.251 f_2(I) P_2(\cos \alpha) - 3.573 f_4(I) P_4(\cos \alpha) . \quad (23)$$

This expression can be employed to calculate the values of $W(0)$ and $W(\pi/2)$, in particular for the case that only one sublevel m of the ground state of ^{57}Co is populated ($a_m = \delta_{mm}$). The results are shown in Table II.

At this point some remarks must be made concerning the sign of the multipole mixing parameter δ , as appearing in formulas (19) and

TABLE II

Orientation parameters and normalized gamma intensities in two directions for the 136 keV transition in ^{57}Fe , if only one sublevel m of the ground state of ^{57}Co is populated.

m	f_2	f_4	$W(0)$	$W(\pi/2)$
$\pm 7/2$	+ 0.5714	+ 0.0800	0.000	1.250
$\pm 5/2$	+ 0.0816	- 0.1485	1.429	1.250
$\pm 3/2$	- 0.2449	- 0.0343	1.429	0.893
$\pm 1/2$	- 0.4082	+ 0.1028	1.143	0.607

(20). A commonly used expression for δ is due to Biedenharn and Rose¹⁷⁾, who defined δ in the context of directional correlation theory. However, their definition contains an ambiguity with respect to the sign.

Suppose we have a gamma cascade of the following form:

$$j_0 \xrightarrow{\gamma_1} j_1 \xrightarrow{\gamma_2} j_2 \xrightarrow{\gamma_3} j_3 \quad (24)$$

where $j_0 \dots j_3$ are the spins of the states involved. Suppose further that the second transition, γ_2 , is a mixed multipole transition, with multipolarities L and $L+1$, and mixing ratio δ . Applying the formalism of Biedenharn and Rose to the first cascade, (γ_1, γ_2) , gives:

$$\delta = \frac{\langle j_2 || L+1 || j_1 \rangle}{\langle j_2 || L || j_1 \rangle}, \quad (25)$$

where the numerator and denominator are so called reduced matrix elements, as defined by Biedenharn and Rose.

On the other hand, if we apply the same formalism to the second cascade, (γ_2, γ_3) , the roles of the states $|j_1\rangle$ and $|j_2\rangle$ are interchanged, because now $|j_2\rangle$ is the intermediate state, as was $|j_1\rangle$ in the first case.

Accordingly we must write

$$\delta = \frac{\langle j_1 || L+1 || j_2 \rangle}{\langle j_1 || L || j_2 \rangle}. \quad (26)$$

These two expressions differ in sign, as can be seen from the following relation, which is valid for the reduced matrix elements of Biedenharn and Rose:

$$(2j_2+1)^{\frac{1}{2}} \langle j_1 || L || j_2 \rangle = (-1)^{j_1-j_2+L} (2j_1+1)^{\frac{1}{2}} \langle j_2 || L || j_1 \rangle . \quad (27)$$

Clearly, the adopted sign for δ depends on whether the gamma ray in question is first or second in the gamma cascade. This has been demonstrated experimentally for the first time by Ofer¹⁸⁾.

We now have to establish the relation between δ , as given in (19) and in the two expressions for δ given above. A comparison of the two formalisms commonly used to describe directional correlation and directional anisotropy of gamma ray emission from oriented nuclei, reveals that δ as appearing in (19) is defined according to expression (25), that is, as if the gamma ray is second in a cascade. This has been demonstrated in the case of the 122 keV transition in ⁵⁷Fe by the nuclear orientation results of Bishop et al.¹⁹⁾, who derive a value for δ which differs in sign from the value obtained in the directional correlation measurements, where the 122 keV transition is first in the observed cascade. We conclude that the definition of δ used in our experiments can be given as

$$\delta \equiv \frac{\langle j_f || L+1 || j_i \rangle_{B.R.}}{\langle j_f || L || j_i \rangle_{B.R.}} . \quad (28)$$

where j_i and j_f are the spins of the initial and final states, respectively, and the reduced matrix elements are defined according to Biedenharn and Rose. Given in terms of the matrix elements of Fraunfelder and Steffen²⁰⁾ our definition is

$$\delta \equiv \frac{\langle j_i || L+1 || j_f \rangle_{F.S.}}{\langle j_i || L || j_f \rangle_{F.S.}} = - \frac{\langle j_f || L+1 || j_i \rangle_{F.S.}}{\langle j_f || L || j_i \rangle_{F.S.}} . \quad (29)$$

Rose and Brink²¹⁾ have given a careful description of the angular distribution of gamma rays, using different definitions of the reduced matrix elements. Their definition of δ differs from ours with respect to the sign. Our definition is identical to those of Krane and

Steffen²²), who also give an expression for δ in terms of explicitly defined reduced matrix elements.

2.3. Gamma anisotropy parameters for ^{58}Co .

The decay scheme of ^{58}Co is given in fig. 4. The directional distribution of the 810 keV gamma rays can be expressed by

$$W(\alpha) = 1 - \frac{15}{7} N_2(j_i) U_2 f_2(I) P_2(\cos \alpha) - 5 N_4(j_i) U_4 f_4(I) P_4(\cos \alpha), \quad (30)$$

where $I = 2$ is the spin of the parent nucleus, and $j_i = 2$. The expressions for U_2 and U_4 depend on the character of the preceding beta transition, which is predominantly of the Gamow-Teller type. The ratio of

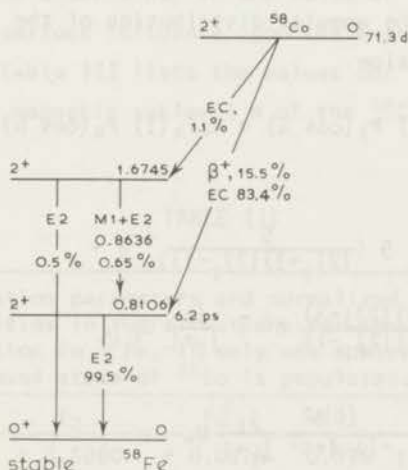


fig. 4. Nuclear decay scheme for ^{58}Co . All energies are given in MeV. The half-lives and the spins of the various states are indicated.

the Fermi and Gamow-Teller matrix elements $X \equiv C_F^M / C_A^M$ has been measured by several techniques; for a summary see ref. 23. Although the results are not compatible with each other in all cases, there is general agreement that $|\lambda| \equiv \left| \frac{X^2}{1 + X^2} \right| < 0.01$. This means that the

Fermi admixture can be neglected for the present purposes. Accordingly we can write

$$U_k = 1 - \frac{k(k+1)}{2I(I+1)}, \quad (31)$$

which gives $U_2 = 0.500$ and $U_4 = -0.667$. Substituting this into (30) together with the values for N_2 and N_4 , we obtain

$$W(\alpha) = 1 - 0.714 f_2(I) P_2(\cos \alpha) + 8.89 f_4(I) P_4(\cos \alpha) \quad (32)$$

for the 810 keV gamma transition.

However, in our experiment we could not distinguish between gammas originating from the 810 keV transition and those from the weak 864 keV transition, as a consequence of the poor energy resolution of our scintillation counters. Therefore we must correct expression (32) for this effect. For the angular distribution of the 864 keV gamma rays we use the expression

$$W(\alpha) = 1 + A_2 f_2(I) P_2(\cos \alpha) + A_4 f_4(I) P_4(\cos \alpha), \quad (33)$$

where

$$A_2 = \frac{1}{1+\delta^2} \left[-\frac{3}{2} - 9 \left\{ \frac{5}{(2j_i+3)(2j_i-1)} \right\}^{\frac{1}{2}} \delta + \frac{15}{14} \frac{(2j_i+5)(2j_i-3)}{(2j_i+3)(2j_i-1)} \delta^2 \right] \frac{j_i}{j_i+1} U_2, \quad (34)$$

$$A_4 = -\frac{30}{(2j_i+3)(2j_i-1)} \frac{\delta^2}{1+\delta^2} \frac{j_i^3}{j_i+1} U_4, \quad (35)$$

in which $j_i = 2$. Since it is reasonable to assume that the beta transition to the 2^+ state at 1.674 MeV in ^{58}Fe is also of the Gamow-Teller type, we have again $U_2 = 0.500$ and $U_4 = -0.667$. The obtained values for the mixing ratio δ differ widely. Angular correlation measurements on the 864 keV - 810 keV cascade have been done by three different groups²⁴⁻²⁶; the results are in agreement with each other and give the average result $\delta = +1.6 \pm 0.2$.

On the other hand, angular correlation studies on the same cascade,

produced by neutron capture in ^{57}Fe , resulted in $\delta = +0.57(7)^{27}$. The reason for this discrepancy is not clear. In order to apply these results to the angular distribution formula (33), the opposite sign for δ must be used, For $\delta = -1.6$ we find $A_2 = +0.63$ and $A_4 = +1.8$; whereas for $\delta = -0.57$ these quantities are $A_2 = +0.29$ and $A_4 = +0.63$. For the combined gamma anisotropy of the 810 keV and 864 keV transitions we find:

$$W(\alpha) = 1 - 0.705 f_2(I) P_2(\cos \alpha) + 8.82 f_4(I) P_4(\cos \alpha) \quad (36)$$

for $\delta = -1.6$,

or

$$W(\alpha) = 1 - 0.707 f_2(I) P_2(\cos \alpha) - 8.83 f_4(I) P_4(\cos \alpha) \quad (37)$$

for $\delta = -0.57$.

Thus we see that the uncertainty in the value of δ for the 864 keV transition has no serious influence upon the expression for the total gamma anisotropy. Table III lists the values for f_2 , f_4 , $W(0)$ and $W(\pi/2)$ if only one magnetic sublevel m of the ^{58}Co ground state is occupied.

TABLE III

Orientation parameters and normalized gamma intensities in two directions for the 810 keV transition in ^{58}Fe , if only one sublevel m of the ground state of ^{58}Co is populated.				
m	f_2	f_4	$W(0)$	$W(\pi/2)$
± 2	+ 0.5000	+ 0.0214	0.836	1.247
± 1	- 0.2500	- 0.0857	0.420	0.628
0	- 0.5000	+ 0.1286	2.486	1.429

2.4. Gamma anisotropy parameters for ^{60}Co .

The very simple decay scheme is given in fig. 5. Both gamma transitions have a pure E2 character. The directional distribution of both transitions is the same, and can be written as

$$\begin{aligned}
 W(\alpha) &= 1 - \frac{15}{7} N_2(I) f_2(I) P_2(\cos \alpha) - 5 N_4(I) f_4(I) P_4(\cos \alpha) \\
 &= 1 - 1.190 f_2(I) P_2(\cos \alpha) - 2.48 f_4(I) P_4(\cos \alpha), \quad (38)
 \end{aligned}$$

where $I = 5$ is the spin of the ground state of ^{60}Co . In Table IV, the values for f_2 , f_4 , $W(0)$ and $W(\pi/2)$ are given for the case that only one sublevel of the ^{60}Co ground state is populated.

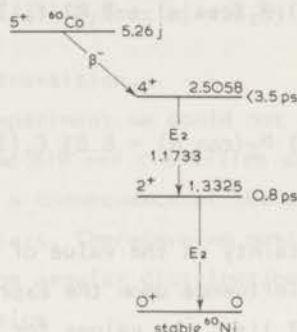


fig. 5. Nuclear decay scheme for ^{60}Co . All energies are given in MeV. The half lives and the spins of the various states are indicated.

TABLE IV

Orientation parameters and normalized gamma intensities in two directions for the 1.17 MeV and the 1.33 MeV transitions in ^{60}Ni , if only one sublevel m of the ground state of ^{60}Co is populated.

m	f_2	f_4	$W(0)$	$W(\pi/2)$
± 5	+ 0.6000	+ 0.1152	0.000	1.250
± 4	+ 0.2400	- 0.1152	1.000	1.250
± 3	- 0.0400	- 0.1152	1.333	1.083
± 2	- 0.2400	- 0.0192	1.333	0.875
± 1	- 0.3600	+ 0.0768	1.240	0.714
0	- 0.4000	+ 0.1152	1.190	0.655

3. Experimental arrangements

Our experimental set up has been described extensively in I. It consists of an adiabatic demagnetization apparatus, made of glass, in which our crystals can be cooled to ≈ 0.02 K. Two magnets are available. One magnet, serving for nuclear polarization, yields a field of 5 kOe and has hollow pole pieces, so that both $W(0)$ and $W(\pi/2)$ can be measured. The other magnet is used for the demagnetizations, but was incidentally used for nuclear polarization measurements. Its maximum field is 18.3 kOe; counters can be placed only along a direction perpendicular to that of the magnetic field.

Using scintillation counters, it is impossible to distinguish between the 136 keV transition and the 122 keV transition in ^{57}Fe . For these experiments a 20 cc Ge(Li) detector was available. It was coupled via a Canberra 1408 C preamplifier and a 1416 B amplifier/DC restorer to a Nuclear Data 2200 analyser system, which has a 50 MHz analog to digital converter and a memory of 1024 channels. The energy resolution of the system was 2.45 keV FWHM (full width at half maximum) at the 1.33 MeV transition in the decay of ^{60}Co , and was 1.55 keV FWHM for the 122 keV and 136 keV transitions in the decay of ^{57}Co . The Ge(Li) detector could be mounted in one of the hollow pole pieces of the small magnet. In this way $W(0)$ could be measured very conveniently. With the detector in this position, the magnetic field at the Ge(Li) crystal was always smaller than 1 kOe, and directed perpendicular to the electric field in the Ge(Li) crystal). We could detect no influence of this magnetic field on the energy resolution of the detector. If $W(\pi/2)$ had to be measured, the detector crystal was placed in a region where the maximum value of the magnetic field was between 3 kOe and 5 kOe, its direction being mainly parallel to the electric field. In this case the width of the 122 keV photopeak increased from 1.55 keV to 1.60 keV FWHM. In addition, the amplitude of the photopeak pulses was found to increase about 0.2% if the Ge(Li) detector was moved from the parallel to the perpendicular direction.

The samples consisted of single crystals of $(\text{La-Ce})_2\text{Mg}_3(\text{NO}_3)_{12} \cdot 24\text{H}_2\text{O}$. The Ce/La ratio in the solution from which the crystals were

grown was 0.1%. The crystals were grown at a constant temperature of 4°C in a refrigerator. Carrier free ^{57}Co , ^{58}Co or ^{60}Co was added to the solution. For the ^{60}Co experiments we used a crystal weighing 1.36 g and having an activity of 8 μCi . The measurements on ^{58}Co were carried out on two LMN crystals weighing 0.94 g and 2.2 g. The activities were 3 μCi and 1.5 μCi respectively at the time of the measurements. The ^{57}Co -LMN crystal used weighed 2.1 g and had an activity of ≈ 50 μCi . All crystals were optically bright, except the ^{57}Co -LMN sample, which had some cloudy parts. The crystals were mounted with the c-axis horizontally.

The experimental procedure to obtain nuclear orientation was the same as in I. Using the 5 kOe magnet, which could be rotated in a horizontal plane, and a vertical coil around the cryostat, we could vary the resultant magnetic field in a plane containing the c-axis of the crystal, so that the Ce splitting could be varied between $g_{\parallel}\mu_B H$ and $g_{\perp}\mu_B H$. Nuclear orientation could be accomplished for magnetic field values H so that $g\mu_B H \leq \frac{1}{2} A$. For ^{60}Co the maximum field was about 2 kOe; for ^{58}Co it was 6 kOe and for ^{57}Co 4 kOe.

During the resonance measurements we observed considerable r.f. heating in some cases. For instance, we measured a resonance-like phenomenon in the r.f. heating versus frequency curve, with a peak at 241 MHz. This could be attributed to warming up of the coil foils on the shielding tube of the apparatus, although these were made of copper and glued with GE 7031 varnish, so that no considerable r.f. heating could be expected. Probably the heating was due to impurities in the copper wires used. In other cases, the source of the r.f. heating remained unclear. In general we were not hampered seriously by the r.f. heating during the measurements; only in the case of ^{57}Co did we have troubles at some frequencies.

4. Experimental results on ^{60}Co .

4.1. *Nuclear orientation by means of cross relaxation with Ce spins.*

Cross relaxation of ^{54}Mn and Ce spins in LMN has been studied

extensively by Lubbers and Huiskamp²⁸). Therefore we will describe it only briefly on the basis of fig. 6, in which examples of this type of measurements are shown. After precooling to about 0.05 K with the magnetic field H of 1280 Oe perpendicular to the c -axis, the field was rotated in one step to a direction which was about 5° out of the

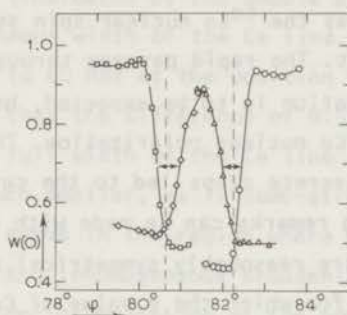


Fig. 6. Results of cross relaxation experiments on the system ^{60}Co -Ce.

The normalized gamma intensity in the direction of the magnetic field, $W(0)$, is plotted as a function of φ , the angle between the magnetic field direction and a fixed (but otherwise arbitrary) horizontal direction. The strength of the magnetic field was 1280 Oe. The four curves give the results of the thermal mixing experiments described in the text. The dashed lines indicate the values of φ for which the Ce Zeeman splitting equals the energy difference of the lowest two hfs levels of the ^{60}Co ion. The double arrows indicate the homogeneous width of the Ce line.

c -axis, after which the angle ρ between the field direction and a fixed (but otherwise arbitrary) horizontal direction was varied every 20 s in discrete steps. After each step, $W(0)$ was measured. The results of these measurements are given by the two outer curves (points denoted by \odot and \square). The inner curves were produced by the following method: after precooling of the Ce spins and rotating the field to a direction in which θ , the angle between field direction and c -axis, was about 5° , a vertical field was applied to the sample, cor-

responding to a rotation of the resultant magnetic field of about 5° in a vertical plane. The horizontal field was then rotated to a direction corresponding to $\rho = 81.5^\circ$, after which the vertical field was turned off by interrupting the current through the vertical coil. In this way it was possible to obtain a situation in which the Zeeman splitting of the Ce ions was smaller than the hfs splittings in the ^{60}Co system, whereas the ^{60}Co nuclear spin system was oriented only to a small extent. The rapid passage through the angular region where cross relaxation is to be expected, had apparently not produced a significant ^{60}Co nuclear polarization. Thereafter increasing or decreasing φ in discrete steps led to the curves indicated by Δ and \diamond . The following remarks can be made with respect to fig. 6:

- a. The two outer curves are reasonably symmetrical and can be used to obtain the value of φ for which the g value of Ce is lowest: $\varphi = 81.42^\circ$. Since the c-axis will not, in general, be perfectly aligned in the horizontal plane (in which the magnet is rotated), we varied the vertical field for a fixed direction of the horizontal field, i.e. $\varphi = 81.4^\circ$. In this way we could determine the angle θ_v between the c-axis and the horizontal plane. In the measurements of fig. 6 the c-axis appeared to be precisely in the horizontal plane, which meant that the direction given by $\varphi = 81.42^\circ$ coincided with the direction of the c-axis.
- b. From the other two curves the direction of the c-axis could also be determined; the result is $\varphi = 81.48^\circ$. Combining this with the precision with which θ_v was determined, we may conclude that the direction of the c-axis could be established with an accuracy of $\approx 0.1^\circ$.
- c. According to ref. 28, a large decrease of $W(0)$ occurs if the Ce splitting is equal to the difference between the lowest two hfs energy levels of the ^{60}Co ions at a certain lattice site. Consequently the mixing angle could be calculated, using the g values of the Ce ion: $g_{\perp} = 1.8264$ ²⁹⁾ and $g_{\parallel} = 0.0235$ ²⁸⁾, and the hfs parameters of the ^{60}Co ions at site 11 (section 4.3.). The result is indicated in fig. 6 by the vertical dashed lines. The agree-

ment with the position of the steep descent of the experimental curves is satisfactory. We may conclude that the drastic change in $W(0)$ is explained by cross relaxation between Ce ions and ^{60}Co ions at site II.

- d. The differences of about 0.5° between the positions of the inner and outer curves (indicated by the double arrows in fig. 6) reflect the homogeneous width of the Ce line. The Ce Zeeman splitting corresponds to 60 MHz at the position of the dashed line and we can calculate that the difference of 0.5° between the curves corresponds to a full width of the Ce line of about 6 MHz. (The ^{60}Co lines are much smaller, as is demonstrated in section 4.4.). The slope of the curve in the region where $W(0)$ decreases gives an impression of the inhomogeneous broadening of the Ce line. It is of the same order of magnitude as the homogenous broadening.
- e. $W(0)$ is already smaller than 1.0 at the moment that the mixing region is approached. One is tempted to attribute this to cross relaxation between Ce ions and ^{60}Co ions at site I. The mechanism of the thermal mixing process has been described in ref. 28; from there it may be learned that the mixing essentially takes place between the electron spins of ^{60}Co and Ce, and that the mixing rate is proportional to $(B/g\mu_B)^2$. For type I ions $B = 0$, which means that the dipole-dipole coupling between the Ce and the ^{60}Co electron spins gives no contribution to the transition probability. Therefore, only the direct coupling between the Ce electron spins and the ^{60}Co nuclear spins is able to produce cross-relaxation. Order of magnitude calculations along the lines of ref. 28 indicate that this mechanism can provide a measurable orientation of the ^{60}Co nuclei if the mixing time is of the order of one second.

Experimentally, in nearly all cases we observed some nuclear orientation before the final mixing between ^{60}Co ions at site II and Ce ions occurred, but the results were quite irreproducible. If one keeps in mind that we varied the field direction in discrete steps, and that consequently $d\theta/dt$ could vary some orders of magnitude

over the region where thermal mixing between Ce spins and ^{60}Co spins at site I would occur, we may conclude that probably the dipole-dipole coupling between Ce spins and ^{60}Co spins at site I is responsible for the nuclear orientation before the final thermal mixing. In section 4.5, we will present evidence that ^{60}Co ions at site I are indeed partially oriented.

4.2. Nuclear spin-lattice relaxation times.

The spin-lattice relaxation times of ^{60}Co nuclei in LMN were studied, mainly with the intention of investigating for which values of H and T the ^{60}Co nuclei could be regarded as to be thermally isolated from the lattice. After orientation of the ^{60}Co nuclei, H was set at the desired value and direction. Heat was applied to the metal system by means of a resistance heater to obtain the desired stationary temperature of the LMN lattice, after which $W(0)$ was observed as a function of time. The observed dependence of $W(0)$ on t was roughly exponential, with a time constant τ . The results of the measurements are shown in fig. 7, where τ is given as a function of $1/T$ for two values of H and θ . The straight lines are fits to the data of the

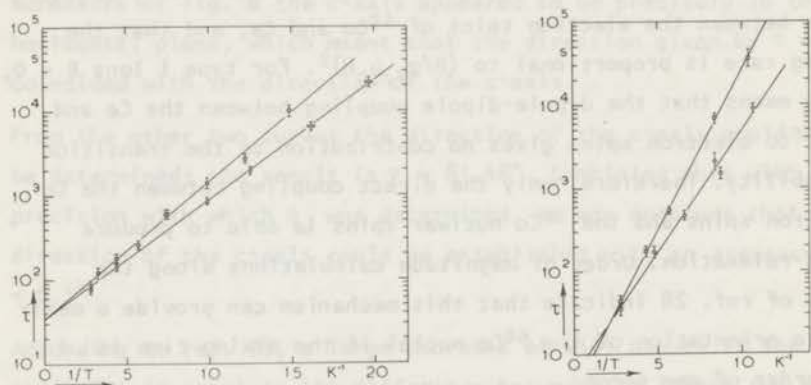


fig. 7. Results of nuclear spin-lattice relaxation measurements on ^{60}Co in LMN. The relaxation time τ is given as a function of $1/T$ for two magnetic field strengths, left: $H = 1280$ Oe, right: $H = 2800$ Oe.

○ $\theta = 5^\circ$ □ $\theta = 90^\circ$

TABLE V

Values of the parameters describing the nuclear spin-lattice relaxation times of ^{60}Co in LMN; $\tau = A \exp\{\lambda/T\}$.

H(Oe)	θ	A(s)	λ (K)	$g\mu_B H/k$ (K)
1280	5°	34	0.33	0.35
1280	90°	34	0.38	0.38
2800	5°	5.6	0.68	0.76
2800	90°	3.5	0.89	0.83

form $\tau = A \exp\{\lambda/T\}$. The parameters of these fits are given in Table V. The following comments can be made:

- A proper treatment would involve a detailed discussion of the relation between the observed $dW(0)/dt$ and the relaxation rates $W_{m \rightarrow m+1}$ between two hfs levels in the $S_z = -\frac{1}{2}$ manifold. Here we will only remark that the observed relaxation rate τ^{-1} will be mainly a measure of the transition probability $W_{5 \rightarrow 4}$, since that transition is accompanied by the largest change in $W(0)$ per ion, and since the lowest two states, of which the wave functions are predominantly characterized by $|S_z = -\frac{1}{2}, I_z = +5\rangle$ and $|S_z = -\frac{1}{2}, I_z = +4\rangle$, have the highest population densities.
- The fact that the data can be fitted by means of an exponential expression indicates that excitation of electronic states plays a role in the observed relaxation. An illustration of the mechanism is sketched in fig. 8. It is rather analogous to the Orbach process in electronic spin-lattice relaxation³⁰⁾, and the temperature dependence can be written as $\tau = A \exp\{\Delta E/kT\}$, where $\Delta E \approx g\mu_B H$ is the energy difference between the states $|\psi_1\rangle$ and $|\psi_3\rangle$ of fig. 8. To compare this with the experiment, we have also tabulated the values of $\Delta E/k = g\mu_B H/k$ (Table V). We see that there is reasonable agreement with the experimental coefficients α , in view of the rough nature of the experiments.

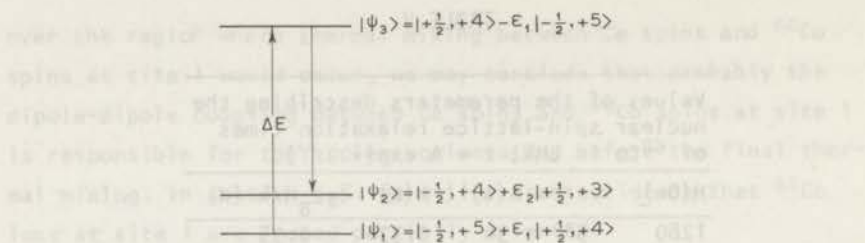


fig. 8. Illustration of the mechanism responsible for the nuclear spin-lattice relaxation of ^{60}Co in LMN. The exact values for the coefficients ϵ_1 and ϵ_2 can be obtained by applying perturbation theory to the Hamiltonian given in expressions (10) and (11). For $\theta = 0^\circ$, for instance, we calculate

$$\epsilon_1 = - \frac{B\sqrt{10}}{2(g_{\parallel} \mu_B H + \frac{9}{2} A)}, \quad \epsilon_2 = - \frac{B\sqrt{18}}{2(g_{\parallel} \mu_B H + \frac{7}{2} A)}$$

The temperature dependence of the probability for an upward transition is determined by the number of phonons of frequency $\nu = \Delta E/h$:

$$p(\nu) \propto \frac{\nu^2}{e^{h\nu/kT} - 1}. \quad \text{In the low temperature limit } (\Delta E \gg kT),$$

the temperature dependence is thus given by $e^{-\Delta E/kT}$.

4.3. Line positions and hfs parameters.

The following section describes the crux of the whole experiment. Resonance transitions between different hfs levels were induced by varying the frequency of the r.f. field through the resonance region at a rate of ≈ 1 KHz/s, meanwhile observing $W(0)$ as a function of time. This was done by accumulating the counts in the 1.17 MeV and 1.33 MeV photopeaks during intervals of 20 s, using the multichannel analyser in the multiscaling mode. An example of such a measurement is shown in fig. 9. The resonance frequencies are labeled by means of a superscript, indicating the transition in the hfs spectrum, starting with the lowest transition $(-\frac{1}{2}, +5) \rightarrow (-\frac{1}{2}, +4)$. The subscript denotes the crystallographic site. At one setting of H , two resonance transitions could be measured; the changes in $W(0)$ accompanying the other transitions were too small to be discernible.

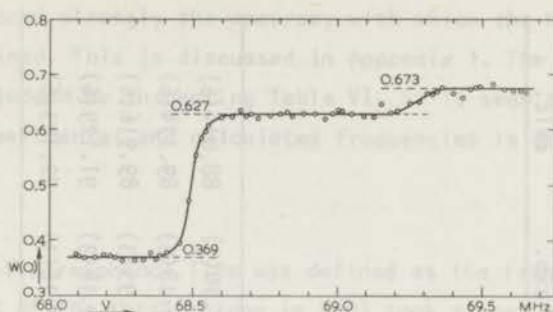


fig. 9. Example of a NMR-ON experiment on ^{60}Co in LMN. $H = 4704 \text{ Oe}$, $\theta = 0^\circ$. Two resonance transitions are clearly visible. The values for $W(0)$ before and after each transition are indicated.

In table VI the results of the measurements are shown, together with the results of computer calculations using the spin Hamiltonian parameters appearing in the lower part of Table VI. The g values were taken from ref. 2 (see Table I). The accuracy of the experimental results was determined mainly by the resonance linewidth, which depended strongly on θ (see section 4.4.). For $\theta = 90^\circ$, it was impossible to determine $\nu_{||}^1$ and $\nu_{||}^2$ separately; only one broad line was observed. To compare this with the theoretical values, we must know the changes in $W(0)$ while saturating $\nu_{||}^1$ and $\nu_{||}^2$ respectively. From section 4.5., we know that the ratio $\Delta W(0)_2 / \Delta W(0)_1 = 1/6$; therefore we compared the experimental values with the theoretical values of $\frac{6}{7} \nu_{||}^1 + \frac{1}{7} \nu_{||}^2$. This procedure was sufficiently accurate in view of the precision with which the resonance could be determined experimentally.

The errors assigned to the calculated frequencies were due to uncertainties in the determination of H and θ . The angle θ could be established with an accuracy of $\approx 0.1^\circ$. For $\theta = 0^\circ$ or 90° , this error had no serious consequences; for other angles, however, the influence on the resonance frequencies was so strong that this effect was the main source of error. H could be estimated with an accuracy of 0.1% (see the discussion in I); the accompanying uncertainty in the calculated frequencies was comparable to the experimental error.

The fact that only two of the ten resonance transitions could be

TABLE VI

Experimental and theoretical resonance frequencies for ^{60}Co , site II together with the hfs parameters used for the fit.							
H(Oe)	θ	$\nu_{ }^1$ (MHz)		$\nu_{ }^2$ (MHz)		$\frac{6}{7}\nu_{ }^1 + \frac{1}{7}\nu_{ }^2$ (MHz)	
		exp.	calc.	exp.	calc.	exp.	calc.
2078	5°	63.725(8)	63.743(4)	65.147(15)	65.159(12)		
2609	5°	65.205(8)	65.214(12)	66.380(15)	66.411(12)		
2609	0°	64.930(5)	64.932(7)	66.150(15)	66.144(6)		
3025	0°	65.840(5)	65.839(6)	66.925(15)	66.926(5)		
3823	0°	67.235(5)	67.234(6)	68.158(15)	68.154(5)		
4700	5°	68.728(5)	68.740(12)	69.510(15)	69.527(11)		
4704	0°	68.488(5)	68.480(6)	69.285(10)	69.277(5)		
2077	90°		87.906(6)		88.649(6)	87.90(3)	88.014(6)
2604	90°		89.090(6)		89.680(6)	89.18(3)	89.174(6)
3021	90°		89.844(6)		90.347(5)	89.93(3)	89.916(6)
3846	90°		91.075(6)		91.456(5)	91.14(3)	91.129(6)
4704	90°		92.151(6)		92.447(5)	92.18(3)	92.193(6)
Hfs parameters							
A	B	P	$(1+\sigma_{ })g_N\mu_N$	$(1+\sigma_{\perp})g_N\mu_N$			
+136.22(7) MHz	+179.08(8) MHz	+0.113(5) MHz	$+8.01(12)\times 10^{-4}\text{MHz/Oe}$	$+8.13(12)\times 10^{-4}\text{MHz/Oe}$			
$+45.44(3)\times 10^{-4}\text{cm}^{-1}$	$+59.74(3)\times 10^{-4}\text{cm}^{-1}$	$+0.0377(17)\times 10^{-4}\text{cm}^{-1}$	$+2.67(4)\times 10^{-8}\text{cm}^{-1}/\text{Oe}$	$+2.71(4)\times 10^{-8}\text{cm}^{-1}/\text{Oe}$			

observed influenced strongly the accuracy with which the hfs parameters could be determined. This is discussed in Appendix 1. The quality of the fit can be judged by inspecting Table VI. It is seen that the agreement between experimental and calculated frequencies is good.

4.4. Linewidths.

The width of a resonance line was defined as the frequency interval in which 68% of the total change in $W(0)$ took place. Assuming that the resonance line is a purely Gaussian curve, this is identical to the distance between the inflexion points. The assumption of Gaussian lineform is justified, since the line was broadened inhomogeneously, as demonstrated by the following experiment. The frequency was kept constant in the center of the line ν_{11}^1 , the r.f. field being equal to the value used in the experiments in which the frequency was swept. No change in $W(0)$ could be detected under these circumstances, within a time interval of five minutes. This shows that homogeneous broadening is negligible, in accordance with estimates of this broadening along the lines of Chapter I.

The results obtained for the first transition, ν_{11}^1 , are shown in Table VII. The error is of the order of 10% of the linewidth. As can be seen, the linewidth is strongly dependent on the angle θ and not on the magnetic field value H . The impression that the field inhomogeneity does not play an important role in the linewidth (as was the case in the Mn resonance lines) is confirmed by inspecting the derivative $\partial\nu_{11}^1/\partial H$, tabulated also in table VII. We know that the field inhomogeneity is roughly 0.2% of the field in the center, and consequently this type of broadening is small compared to the observed linewidths. Therefore we must assume that the broadening is caused by a spread in the hfs constants A and B : $\Delta A \approx 140$ MHz and $\Delta B \approx 1.14$ MHz. The linewidth for $\theta = 5^\circ$ is clearly larger than for $\theta = 0^\circ$, which cannot be due to the spread in A and B . We have no explanation for this difference in linewidth.

TABLE VII

Width of the lowest resonance line, $\Delta v_{||}^1$, in ^{60}Co
as a function of H and θ .

H (Oe)	θ	$v_{ }^1$ (MHz)	$\Delta v_{ }^1$ (kHz)	mean value of $v_{ }^1$ (kHz)	$\partial v_{ }^1 / \partial H$ (kHz/Oe)
2609	0°	64.930	78		2.34
3025	0°	65.840	63	70	1.96
3823	0°	67.235	72		1.54
4704	0°	68.488	68		1.28
2078	5°	63.725	95		3.18
2609	5°	65.205	115	101	2.34
4700	5°	68.728	93		1.28
4704	20°	72.298	250	250	1.25
2077	90°	87.90	650		2.55
2604	90°	89.18	620		1.94
3021	90°	89.93	520	570	1.65
3846	90°	91.09	460		1.34
4704	90°	92.18	560		1.17

4.5. Changes in $W(0)$.

By using a frequency sweep rate of about 1 kHz/s and an r.f. field of about 1 mOe, it was possible to saturate the resonance lines, since no further change in $W(0)$ could be induced by going to higher r.f. fields or lower sweep rates. Given in Table VIII is a survey of those experiments for which we expect saturation of $v_{||}^1$ and $v_{||}^2$. The quantities in the table have been defined according to:

$$W(0)_1 \xrightarrow[v_{||}^1]{\Delta W(0)_1} W(0)_2 \xrightarrow[v_{||}^2]{\Delta W(0)_2} W(0)_3.$$

We see that $\Delta W(0)_2$ scatters around a mean value $\Delta W(0)_2 = 0.0470(11)$. This result can be used to obtain the fraction f of Co ions at lattice

TABLE VIII

Changes in $W(0)$ of ^{60}Co , due to resonance transitions.

H(Oe)	θ	$W(0)_1$	$\Delta W(0)_1$	$W(0)_2$	$\Delta W(0)_2$	$W(0)_3$	$W(0)_1$	$W(0)_1, \text{calc.}$
4704	0°	0.369	0.258	0.627	0.0464(25)	0.674	0.79	0.377
4704	0°	0.411	0.258	0.669	0.0430(25)	0.713	0.88	0.419
4700	5°	0.444	0.234	0.678	0.0457(22)	0.724	0.92	0.428
4704	20°	0.396	0.245	0.641	0.0508(50)	0.691	0.82	0.391
3823	0°	0.461	0.247	0.708	0.0487(23)	0.757	0.98	0.458
2078	5°	0.394	0.256	0.650	0.0517(30)	0.712	0.84	0.400

site II: $f = 0.577 \pm 0.014$. A derivation of this value is presented in Appendix 2. The relative fraction of type II sites is $2/3$, therefore the value for f obtained indicates that for the ^{60}Co ions there exists a slight preference for site I.

From the measurements, also the normalized gamma intensity $W(0)_1$ for the ^{60}Co nuclei at site I could be obtained (see Appendix 2). The values for $W(0)_1$ vary irregularly between 0.8 and 1.0 (Table VIII), which means that, before thermal mixing, the value of $W(0)$ has been between 0.92 and 1.0. This behaviour is in accordance with the results of the thermal mixing experiments (section 4.1.).

Using the values for $W(0)_1$, we can calculate the values of $W(0)_1$ to be expected if the population densities a_m of the subsystem of ^{60}Co ions at site II could be described by $a_m \propto e^{-\beta m}$, with $2.5 < \beta < 4.0$. This gives an error of 0.012 in the calculated values for $W(0)_1$. The agreement with the experimental values suggests that this assumption is correct, meaning that the thermal mixing process is equally effective in polarizing the ^{60}Co nuclear spins as in polarizing the ^{52}Mn and ^{54}Mn nuclei.

5. Experimental results on ^{58}Co .

5.1. Nuclear orientation by means of cross relaxation with Ce spins.

To achieve nuclear orientation, the same experimental procedure

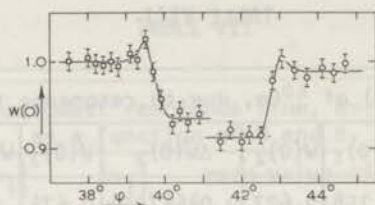


fig. 10. Results of cross relaxation experiments on the system $^{58}\text{Co-Ce}$. The two curves were obtained by varying the direction of the magnetic field in discrete steps and measuring $W(0)$ after each step. The magnetic field strength was 1980 Oe.

was used as in the case of ^{60}Co in LMN. Figure 10 shows a typical experiment. In general, the changes in $W(0)$ are much lower, in accordance with the formulas for the gamma anisotropy (36) and (37). The rise in $W(0)$ preceding the final descent indicates that the Ce spin system does not "feel" all ^{58}Co hfs splittings at the same time, because these splittings are unequal. The rise must be associated with the preferred population of the $m = 0$ level (compare Table III).

5.2. Line positions and hfs parameters.

The isotope ^{58}Co appeared to be very suitable for NMR-ON measurements, because three of the four possible transitions could be detected. This is due mainly to the exceptionally high value of $W(0)$

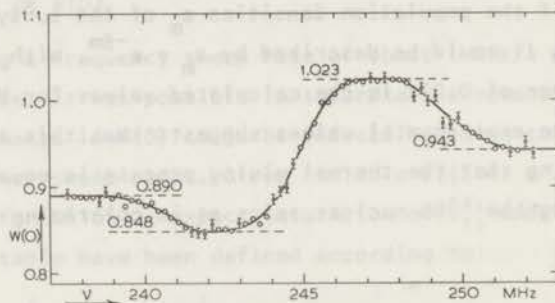


fig. 11. Example of a NMR-ON experiment on ^{58}Co in LMN. $H = 3052$ Oe, $\theta = 90^\circ$. The values for $W(0)$ before and after each transition are indicated.

corresponding to ions in the state $m = 0$. A typical experiment is shown in fig. 11. The measurement was done at an angle $\theta = 90^\circ$. Although the linewidth is relatively large, three transitions can be seen quite clearly. For $\theta = 0^\circ$, the linewidths were much smaller, as in the ^{60}Co measurements. The three transitions were also observed, although less easily, when the counters were placed along the perpendicular direction, so that $W(\pi/2)$ was measured. In this way we measured the resonances up to $H = 18$ kOe in the big magnet. This was especially useful for the determination of the parameters $(1 + \sigma_{//})g_N\mu_N$ and $(1 + \sigma_{\perp})g_N\mu_N$.

The results of the measurements can be found in table IX. The errors in the calculated values are the result of the errors in the determination of H and θ . The error in θ ($\approx 0.1^\circ$) dominates in the points for which $\theta = 5^\circ$, and played a role also if $\theta \approx 2^\circ$. For fields up to 5 kOe the error in H was estimated to be 0.1%. The higher fields were produced by the big magnet, which was calibrated up to 7 kOe using an NMR method, and above 7 kOe by means of a flip coil, coupled to an electronic integrator. In this region, the field was calibrated with a precision of 0.2%. As can be seen from the table, this error determined the accuracy with which the parameter $(1 + \sigma_{//})g_N\mu_N$ could be derived.

The uncertainty in the parameter P had not such important consequences for those in A and B as in the case of ^{60}Co . This is due to the fact that we measured three of the four possible transitions in the hfs spectrum. The (pseudo) Zeeman terms could be derived most easily by means of the field dependence of the resonances in the high field region, because there the field dependence caused by perturbation terms of the form $A^2/g\mu_B H$ was negligible. Consequently all parameters in the spin Hamiltonian were determined with greater accuracy than in the case of ^{60}Co .

5.3. Linewidths.

The widths of the three resonance lines were determined in the same way as in the case of ^{60}Co ; the accuracy was $\approx 10\%$. The results are summarized in table X. There is again a big difference between

TABLE IX

Experimental resonance frequencies for ^{58}Co , Site II, compared to calculated frequencies, using the indicated set of hfs parameters.							
H (Oe)	θ (degrees)	ν_{11}^1 (MHz)		ν_{11}^2 (MHz)		ν_{11}^3 (MHz)	
		exp.	calc.	exp.	calc.	exp.	calc.
2104 (5)	5.03	175.360 (10)	175.479 (43)	185.226 (10)	185.250 (29)	195.855 (15)	195.885 (23)
3052 (4)	5.03	180.63 (2)	180.640 (35)	187.726 (8)	187.741 (27)	195.255 (10)	195.257 (23)
3820 (4)	1.95	183.11 (3)	183.095 (15)				
4694 (5)	2.03	186.005 (15)	185.999 (15)	190.996 (10)	190.994 (11)	196.180 (15)	196.163 (8)
4714 (5)	1.95	186.085 (20)	186.062 (15)	191.075 (15)	191.039 (11)	196.205 (20)	196.189 (8)
7560 (10)	0.03	193.705 (10)	193.715 (25)	197.15 (4)	197.210 (22)	200.72 (5)	200.688 (20)
10810 (20)	0.15	201.59 (2)	201.559 (45)				
14790 (30)	0.15	210.62 (3)	210.642 (65)				
18330 (40)	0.2	218.485 (20)	218.537 (85)	220.354 (20)	220.446 (85)	222.38 (5)	222.366 (85)
2079 (3)	90.0	236.13 (15)	236.16 (2)	242.31 (8)	242.29	242.22 (12)	249.14
3052 (4)	90.0	240.68 (15)	240.73 (1)	244.85 (8)	244.87	249.51 (12)	249.35
4720 (5)	90.0	246.10 (15)	246.21	248.75 (8)	248.79	251.68 (12)	251.51
10840 (20)	88.8	261.70 (15)	261.53 (5)				
10970 (20)	89.8	261.80 (15)	261.85 (7)				
18210 (40)	89.8	278.46 (10)	278.40 (9)				
Hfs parameters							
A	B	P	$(1 + \sigma_{//})g_{N^{58}\text{Co}}$	$(1 + \sigma_{\perp})g_{N^{58}\text{Co}}$			
362.73 (4) MHz	476.75 (20) MHz	+ 0.41 (2) MHz	$2.155(6) \times 10^{-3}$ MHz/Oe	$2.21(1) \times 10^{-3}$ MHz/Oe			
$120.994(13) \times 10^{-4} \text{ cm}^{-1}$	$159.03(7) \times 10^{-4} \text{ cm}^{-1}$	$0.137(7) \times 10^{-4} \text{ cm}^{-1}$	$0.719(2) \times 10^{-7} \text{ cm}^{-1}/\text{Oe}$	$0.737(3) \times 10^{-7} \text{ cm}^{-1}/\text{Oe}$			

TABLE X

Width of the three resonance lines in ^{58}Co , as a function of H and θ							
H (Oe)	θ (degrees)	$\Delta\nu_{11}^1$ (MHz)	$\Delta\nu_{11}^2$ (MHz)	$\Delta\nu_{11}^3$ (MHz)	$\partial\nu_{11}^1/\partial H$ (kHz/Oe)	$\partial\nu_{11}^2/\partial H$ (kHz/Oe)	$\partial\nu_{11}^3/\partial H$ (kHz/Oe)
3052	5.03	0.17	0.17	0.18	+ 4.4	+ 2.4	+ 0.02
4694	2.03	0.19	0.15	0.16	+ 3.1	+ 2.2	+ 1.3
4714	1.95	0.18	0.22	0.20	+ 3.1	+ 2.2	+ 1.3
10810	0.15	0.25			+ 2.4	+ 2.2	+ 1.9
14790	0.15	0.25			+ 2.2	+ 2.2	+ 2.1
18330	0.2	0.28	0.29		+ 2.2	+ 2.2	+ 2.1
2079	90.0		1.8	2.0	+ 5.8	+ 2.9	- 0.7
3052	90.0		1.7	1.9	+ 3.8	+ 2.4	+ 0.7
4720	90.0		1.3	1.3	+ 2.8	+ 2.2	+ 1.5
10970	89.8	1.6			+ 2.3	+ 2.2	+ 2.0
18210	89.8	1.5			+ 2.2	+ 2.2	+ 2.1

linewidths measured at 0° and at 90° . From the results at $\theta = 0^\circ$ we see that the linewidth is the same for the three transitions. The field inhomogeneity is unimportant for fields up to 5 kOe, as can be seen from the table. The resonances measured in the big magnet are distinctly broader. If we ascribe this to the magnetic field inhomogeneity ΔH , then ΔH must be roughly 100 Oe over the sample. This is not impossible, although from experiments on the calibration of the magnetic field we would expect that ΔH would be lower by a factor two.

The linewidths at $\theta = 90^\circ$ were roughly constant. An exception was the point at 4720 Oe, where narrower lines were found; but this is probably caused by the fact that the three lines were not completely separable at this field, so that we may have somewhat underestimated the linewidth. Assuming that the linewidths are due to a spread in A and B (which is clearly indicated by the measurements), we derive $\Delta A = 0.36$ MHz, and $\Delta B = 3.4$ MHz.

5.4. Changes in $W(0)$ and $W(\pi/2)$.

For ^{58}Co large changes in $W(0)$ and in $W(\pi/2)$ took place, while saturating the resonance transitions. To be able to observe $W(0)$ and $W(\pi/2)$ simultaneously, we placed two counters parallel and two perpendicular to the magnetic field. After nuclear orientation had been accomplished, we set $H = 4700$ Oe in the direction of the c -axis of the crystal, after which the gamma intensities in both directions were measured during 400 s before the r.f. field was turned on, using the analyser in the pulse height mode (point 1). The first transition, $\nu_{||}^1$, was saturated by sweeping slowly through the resonance three times, using a high r.f. power level. Then the gamma intensities were remeasured during 400 s (point 2). Points 3 and 4 were measured after $\nu_{||}^2$ and $\nu_{||}^3$ had saturated in the same way. Finally, the system was warmed up to 1 K and measurements were done to normalize the observed intensities. The results are shown in Table XI. An analysis on the

TABLE XI

Changes in $W(0)$ and $W(\pi/2)$ of ^{58}Co due to resonance transitions, compares to calculations according to the model explained in the text.					
point	state of ^{58}Co spin system	experimental values		calculated values, assuming $f = 0.577$	
		$W(0)$	$W(\pi/2)$	$W(0)$	$W(\pi/2)$
1	after nucl. orientation	0.882(5)	1.110(4)	0.893(3)	1.116(10)
2	after $\nu_{ }^1$	0.812(5)	0.975(4)	0.813	0.973
3	after $\nu_{ }^2$	1.066(5)	1.047(4)	1.069	1.047
4	after $\nu_{ }^3$	0.932(5)	1.012(4)	0.941	1.009

basis of the model described in Appendix 2 yielded for the fraction f of ^{58}Co ions at site II: $f = 0.577 \pm 0.013$. This is in excellent agreement with the value obtained from the measurements on ^{60}Co (section 4.5.). Further analysis showed that the ions at lattice site I were not appreciably oriented during the cross relaxation process. The calculated values for $W(0)$ and $W(\pi/2)$ are also shown in Table XI. For

point 1, they were obtained by assuming - as usual - that the population densities of the hfs levels of type II ions could be described by $a_m \propto e^{-\beta m}$, with $2.5 < \beta < 4.0$. The agreement with the experimental values is very satisfactory.

For Co^{2+} in $\text{La}_2\text{Mg}_3(\text{NO}_3)_{12} \cdot 24\text{H}_2\text{O}$, no other determination of f is given in the literature. For the isomorphous $\text{La}_2\text{Zn}_3(\text{NO}_3)_{12} \cdot 24\text{H}_2\text{O}$, however, Culvahouse et al.³¹⁾ derived from EPR measurements for the ratio of both types of ions: $f/(1-f) = 1.8 \pm 0.2$, whereas our measurements yield $f/(1-f) = 1.36 \pm 0.06$. The difference may be ascribed to the fact that different host crystals were used. If this is the case, then it is not justified to use the ratios $f/(1-f)$ found for the lanthanum double nitrates in analyzing nuclear orientation experiments performed on the corresponding cerium salts, as has been done by various authors³²⁻³⁴⁾.

6. Experimental results on ^{57}Co .

6.1. Nuclear orientation by means of cross-relaxation with Ce spins.

Quite analogous to the measurements on the other isotopes, we observed a decrease in $W(0)$ of the 136 keV transition in ^{57}Fe if we rotated the magnetic field through the region where ^{57}Co -Ce thermal mixing could be expected. However, $W(0)$ decreased only to ≈ 0.8 , a value which is much higher than could be expected on the basis of Table II. This must be attributed to a disorientation in the excited state at 136 keV in ^{57}Fe , a phenomenon that has also been observed by Bishop et al.¹⁹⁾ for ^{57}Co in $\text{CoRb}_2(\text{SO}_4)_2 \cdot 6\text{H}_2\text{O}$. Nevertheless it was possible to establish the direction of the c-axis with a precision of $\approx 0.1^\circ$.

6.2. Line positions and hfs parameters.

From Table II, it can be seen that a measurement of $W(0)$ is not suitable to detect the resonance transition v_{11}^1 . For this transition, a measurement of $W(\pi/2)$ is necessary. Therefore v_{11}^1 and v_{11}^2 had to be measured with the Ge(Li) detector at different positions, which

was very inconvenient, and made it impossible to obtain normalization points for the gamma intensity in both directions.

The observed change in $W(\pi/2)$, associated with ν_{11}^1 , was very small, mainly due to the attenuation of the gamma anisotropy, already observed in the thermal mixing experiments. In fact, only one reliable measurement was made on this transition. Moreover, during the measurements, serious r.f. heating was observed at various frequencies. Especially the measurements at $\theta = 90^\circ$, which inevitably took much time because of the large linewidth at this angle, were hampered seriously by this phenomenon. We therefore obtained only one result at this angle. An example of the data is given in fig. 12.

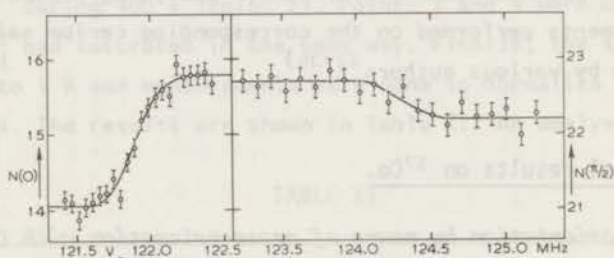


fig. 12. Example of a NMR-ON experiment on ^{57}Co in LMN. $H = 4666$ Oe, $\theta = 0^\circ$. For the first resonance transition, the gamma intensity in the direction of the magnetic field is plotted on an arbitrary scale. For the second transition, the gamma intensity perpendicular to the magnetic field direction was measured.

The results of the resonance measurements are given in Table XII, together with the deduced hfs parameters and the calculated values for the resonance frequencies. The errors in the calculated values are due to errors in H and θ . Because we had only one point at $\theta = 90^\circ$, we had to choose a value for the parameter $(1 + \sigma_{\perp})g_N\mu_N$. In view of the results on ^{60}Co and ^{58}Co , we took this parameter 0.2% higher than $(1 + \sigma_{\parallel})g_N\mu_N$. The fact that ν_{11}^2 was measured only once, with a relatively large error, was the main source of error in the hfs parameters (see Appendix 1).

TABLE XII

Experimental resonance frequencies and linewidths for ^{57}Co , site II, compared to calculated frequencies, using the hfs parameters given below						
H (0e)	θ (degrees)	ν_{11}^1 (MHz)		$\Delta\nu_{11}^1$ (MHz)	ν_{11}^2 (MHz)	
		exp.	calc.		exp.	calc.
1577(2)	3.00	108.430(35)	108.485(30)	0.27		
2082(2)	2.76	112.530(25)	112.490(20)	0.23		
2090(2)	3.00	112.575(40)	112.571(20)	(0.22)		
3037(3)	2.03	117.075(30)	117.092(15)	0.26		
3950(4)	1.95	120.070(25)	120.075(15)	0.22		
4666(5)	0.00	121.905(25)	121.890(12)	0.27	124.30(8)	124.284(10)
4712	90.0	163.14(15)	163.141(10)	1.3		
Hfs parameters						
A	B	P	$(1 + \sigma_{//})g_N\mu_N$	$(1 + \sigma_{\perp})g_N\mu_N$		
+243.46(48) MHz	+317.7(5) MHz	+0.28(4) MHz	+1.428(13) $\times 10^{-3}$ MHz/0e	+1.46 $\times 10^{-3}$ MHz/0e		
+81.21(16) $\times 10^{-4}$ cm $^{-1}$	+105.97(17) $\times 10^{-4}$ cm $^{-1}$	+0.093(13) $\times 10^{-4}$ cm $^{-1}$	+0.476(4) $\times 10^{-7}$ cm $^{-1}$ /0e	+0.487 $\times 10^{-7}$ cm $^{-1}$ /0e		

6.3. Linewidths.

In Table XII the measured linewidths are also listed. The lines were broader than could be expected on the basis of the results on the other two isotopes. This was probably caused by the rather poor quality of the ^{57}Co -LMN crystal. The field dependence of the resonance lines appeared to be so small that the field inhomogeneity did not contribute appreciably to the resonance linewidths. We can therefore conclude that the linewidth is caused by a spread in A and B:

$$\Delta A = 0.50 \text{ MHz and } \Delta B = 2.6 \text{ MHz.}$$

6.4. Multipole mixing ratio of the 122 keV gamma transition in ^{57}Fe ; reorientation in the 136 keV state.

For the purpose of obtaining the mixing ratio $\delta(E2/M1)$ of the 122 keV transition, we performed the following experiment. After demagnetization, the crystal was precooled in a magnetic field of 5 kOe in the direction of the c-axis. Under these circumstances, the nuclear spin-lattice relaxation time is practically infinite, so that no nuclear orientation occurred. In this situation, a normalizing point was taken with the Ge(Li) detector parallel to the magnetic field, measuring the intensities of the 122 keV and the 136 keV lines simultaneously during 1000 s. Next, nuclear orientation was produced in the usual way, and a second point was taken under circumstances otherwise identical to those in point 1. This yielded $W(0)$ for both gamma transitions. To measure $W(\pi/2)$, the detector was moved to the perpendicular position, keeping the rest of the equipment undisturbed. Point 3 was taken at this position, and finally the crystal was warmed up to 1 K and a normalizing point for $W(\pi/2)$ was taken. The results of these measurements are given in Table XIII.

To analyse the results, we note that, in spite of the reorientation in the 136 keV excited state, we can measure the orientation parameters $f_2(5/2)$ and $f_4(5/2)$ of this state by using the values of $W(0)$ and $W(\pi/2)$ for the 136 keV transition. This is a pure E2 transition, for which the directional anisotropy is given by expressions (14), (17) and (18). To apply these formulae, we must add the solid

TABLE XIII

Results of gamma anisotropy measurements on ^{57}Co ,
used to obtain the multipole mixing ratio δ of the 122 keV transition

136 keV transition		f_2 (5/2)	f_4 (5/2)	122 keV transition		
$W(0)$	$W(\pi/2)$			$W(0)$	$W(\pi/2)$	A_2
0.8067(18)	1.0623(25)	+0.120(2)	+0.0070(5)	1.0486(8)	0.9763(10)	0.419(10)

angle factors $Q_2 = 0.956$ and $Q_4 = 0.857$ to $P_2(\cos \alpha)$ and $P_4(\cos \alpha)$. The results for f_2 and f_4 are also given in Table XIII; they can be substituted into the expression for the directional anisotropy of the 122 keV transition, because both transitions have the same initial state. The result for the coefficient A_2 in (14) is given in Table XIII, A_4 is negligible. Using (19) we find for the multipole mixing ratio:

$$\delta = + 0.1071 \pm 0.0022.$$

We have illustrated this by plotting A_2 versus δ in fig. 13. The result for δ can be used to check that the fourth rank term in (14) is negligible compared to the other terms.

To compare our result for δ with the directional correlation results on the 122 keV - 14.4 keV gamma cascade, we recall that the angular correlation function can be written as ¹⁷⁾

$$W(\alpha) = 1 + A_2^1 \cdot A_2^2 \cdot P_2(\cos \alpha) \quad (39)$$

where A_2^1 and A_2^2 are coefficients depending on the characteristics of the first and second gamma respectively. For the 14.4 keV transition, $A_2^2 = 0.500$, so that the coefficient A_2^1 can be found directly from the measurements. The dependence of A_2^1 on δ is also sketched in fig. 13. The values for δ which are found from these measurements are negative, as could be expected in view of the discussion in section 2.2.; they are $\delta = - 0.131(6)$ ¹²⁾ and $\delta = - 0.121(3)$ ¹³⁾ respectively. The agreement with our result is poor in view of the stated accuracies. We see from fig. 13 that we should expect a lower value of A_2^1 if we assume that

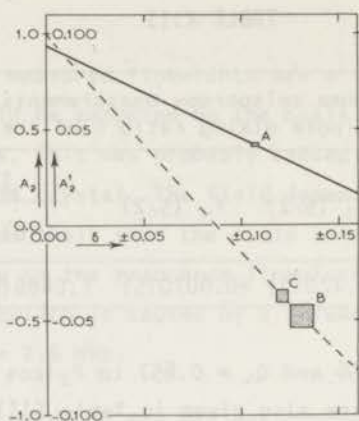


fig. 13. Results of measurements to determine the multipole mixing ratio δ of the 122 keV gamma transition in ^{57}Fe . The full line refers to the relation between δ and A_2 , the coefficient in the angular distribution of the 122 keV gamma rays, as appearing in expression (14). The positive sign for δ must be used. The dashed line refers to the relation between δ and A_2^1 , a coefficient appearing in the directional correlation of the 122 and 14.4 keV gamma rays, expression (39). In this case the negative sign for δ must be used.

A: our experiment; B: Lindqvist and Heer, ref. 12;

C: Hohenemser et al., ref. 13.

our measurement is correct. This excludes an explanation of the discrepancy in terms of the attenuation of the correlation during the 98 ns lifetime of the 14.4 keV level. It is a well known fact, however, that selfabsorption of the 14.4 keV gamma ray can lead to a too high value of the angular correlation coefficient $A_2^1 \cdot A_2^2$ (12), so this could be the origin of the discrepancy. We will only remark here that the nuclear orientation experiment is free from the experimental difficulties related to the long lifetime and the low energy of the 14.4 keV state.

So far we have analyzed the nuclear orientation in terms of the orientation parameters $f_k(5/2)$ of the excited state at 136 keV. It is interesting to compare the obtained values of $f_k(5/2)$ with those to be expected from the nuclear orientation of the ground state of ^{57}Co .

Assuming that after orientation the populations a_m of the hfs sublevels of the ^{57}Co ground state can be described again by the Boltzmann factor $a_m \propto e^{-\beta m}$ with $2.5 < \beta < 4.0$, we obtain $f_2(7/2) = 0.546(17)$ and $f_4(7/2) = 0.69(7)$. The relation between $f_k(5/2)$ and $f_k(7/2)$ can be written as (see also formula (21)):

$$f_k(5/2) = 0.577 \cdot G_k \cdot U_k \cdot f_k(7/2), \quad (40)$$

where the factor 0.577 is introduced to allow for the fact that only the ^{57}Co ions at site II are oriented. The factors U_k describe the influence of the preceding beta decay; from section 2.2. we have $U_2 = 0.933$ and $U_4 = 0.549$. The factors G_k allow for the attenuation of the gamma anisotropy during the 8.7 ns lifetime of the 136 keV state. They can thus be found by substituting the values of $f_k(5/2)$ and $f_k(7/2)$ in expression (40). The result is:

$$G_2 = 0.41 \pm 0.02, \quad \text{and} \quad G_4 = 0.32 \pm 0.04.$$

This result will be discussed in section 7.3.

6.5. Changes in $W(0)$ and $W(\pi/2)$.

The results of the previous section can be used to analyze the observed changes in $W(0)$ and $W(\pi/2)$ while crossing the resonance transitions. In the resonance measurements, the source-detector distance was 5 cm, which yields $Q_2 = 0.921$ and $Q_4 = 0.76$. Using the results of section 2.2. together with expression (40), we find for the directional distribution of the 136 keV gamma rays:

$$\begin{aligned} W(\alpha) &= \left[1 - \frac{15}{7} \cdot 0.577 N_2(5/2) G_2 U_2 f_2(7/2) Q_2 P_2(\cos \alpha) \right. \\ &\quad \left. - 5 \cdot 0.577 N_4(5/2) G_4 U_4 f_4(7/2) Q_4 P_4(\cos \alpha) \right] \quad (41) \\ &= 1 - 0.270 f_2(7/2) P_2(\cos \alpha) - 0.51 f_4(7/2) P_4(\cos \alpha). \end{aligned}$$

Using this expression, we can calculate the values of $W(0)$ and $W(\pi/2)$ for the case that only one sublevel m of the ^{57}Co ground state is populated, whereby it is assumed that the ions at site I give rise

TABLE XIV

Orientation parameters and normalized gamma intensities for the 136 keV transition in ^{57}Fe , if only one sublevel m of the ground state of ^{57}Co is populated, using the results of section 6.4.

m	f_2	f_4	$W(0)$	$W(\pi/2)$
$\pm 7/2$	+ 0.5714	+ 0.0800	0.805	1.062
$\pm 5/2$	+ 0.0816	- 0.1485	1.054	1.038
$\pm 3/2$	- 0.2449	- 0.0343	1.085	0.974
$\pm 1/2$	- 0.4082	+ 0.1028	1.058	0.925

to an isotropic contribution, which is included in the values listed in table XIV. After saturation of ν_{11}^1 , we thus expect $W(0) = 0.930$ and $W(\pi/2) = 1.050$; whereas saturation of ν_{11}^2 will lower $W(\pi/2)$ by only 0.016 and raise $W(0)$ by 0.008. This explains why this transition was so difficult to observe. The experimental values are given in Table XV. We see that in none of the cases complete saturation of ν_{11}^1

TABLE XV

Changes in $W(0)$ and $W(\pi/2)$ of ^{57}Co , due to resonance transitions.

transition ν_{11}^1				
H(0e)	θ (degrees)	$W(0)_i$	$W(0)_f$	$\Delta W(0)$
1577	3.00	0.807(5)	0.879(5)	0.072(5)
2090	3.00	0.836(4)	0.884(4)	0.048(4)
3037	2.03	0.819(3)	0.916(4)	0.097(3)
3950	1.95	0.827(3)	0.913(3)	0.086(3)
4712	90.0	0.823(3)	0.885(3)	0.062(4)
transition ν_{11}^2				
H(0e)	θ (degrees)	$W(\pi/2)_i$	$W(\pi/2)_f$	$\Delta W(\pi/2)$
4666	0.00	1.045(4)	1.023(4)	-0.022(4)

was obtained, probably by poor impedance matching in the r.f. power line. The only measurement of $\nu_{||}^2$ gives a remarkably high value for $\Delta W(\pi/2)$, which indicates that the previous resonance transition $\nu_{||}^1$ was completely saturated in that case. We could not check this, because we could not take a normalization point for $W(0)$ if we measured $\nu_{||}^1$ and $\nu_{||}^2$ in sequence.

7. Discussion.

7.1. Hfs parameters and nuclear moments.

The obtained hfs parameters can be combined with the ENDOR results of De Beer²⁾ on stable ^{59}Co in LMN, in order to derive values for the magnetic dipole and electric quadrupole moments of the radioactive isotopes. In Table XVI, the hfs parameters for Co ions at site

TABLE XVI

Summary of resonance measurements on four Co isotopes				
isotope	parameter	A/hc (10^{-4} cm^{-1})	B/hc (10^{-4} cm^{-1})	P/hc (10^{-4} cm^{-1})
^{57}Co	a)	+ 81.21 (16)	+105.97 (17)	+ 0.093 (13)
^{58}Co	a)	+120.994 (13)	+159.03 (7)	+ 0.137 (7)
^{59}Co	b)	+ 79.096 (4)	+103.911 (4)	+ 0.0720 (4)
^{60}Co	a)	+ 45.44 (3)	+ 59.74 (3)	+ 0.0377 (17)
ratios of hfs parameters				
	$^{57}\text{Co}/^{59}\text{Co}$	+ 1.0267 (20)	+ 1.0198 (16)	+ 1.29 (18)
	$^{58}\text{Co}/^{59}\text{Co}$	+ 1.5297 (2)	+ 1.5304 (7)	+ 1.90 (11)
	$^{60}\text{Co}/^{59}\text{Co}$	+ 0.5745 (3)	+ 0.5749 (3)	+ 0.52 (3)
moment ratios		g_N	μ	Q
	$^{57}\text{Co}/^{59}\text{Co}$	+ 1.023 (3)	+ 1.023 (3)	1.29 (18)
	$^{58}\text{Co}/^{59}\text{Co}$	+ 1.5298 (2)	+ 0.87417 (15)	0.54 (3)
	$^{60}\text{Co}/^{59}\text{Co}$	+ 0.5747 (2)	+ 0.8210 (3)	1.11 (6)

a) this work

b) measurements of De Beer, ref. 2.

II are listed. The moment ratios of, for instance, ^{58}Co and ^{59}Co nuclei can be calculated by means of the following formulae:

$$\frac{^{58}\text{A}}{^{59}\text{A}} = \frac{^{58}\text{B}}{^{59}\text{B}} = \frac{^{58}\text{g}_\text{N}}{^{59}\text{g}_\text{N}} = \frac{^{58}\mu^{59}\text{I}}{^{59}\mu^{58}\text{I}}, \quad (42)$$

and

$$\frac{^{58}\text{P}}{^{59}\text{P}} = \frac{^{58}\text{Q}}{^{59}\text{Q}} \frac{^{59}\text{I}(2 \times ^{59}\text{I} - 1)}{^{58}\text{I}(2 \times ^{58}\text{I} - 1)}. \quad (43)$$

These formulas are correct only if we can neglect hyperfine anomalies. A hfs anomaly, presumably connected with the nuclear charge distribution interacting with core s electrons, will depend on the spin angular momentum contribution to the g value. Hence the anomaly will not scale according to the B/A ratio in going from the z- to the x-axis. Experimentally we find that the ratio of the A's equals that of the B's within the experimental error, indicating that hfs anomalies are unimportant. ^{57}Co forms an exception; the measurements on this isotope are less reliable, however, because the determination of B depends on only one point. We therefore assigned a rather large error to the ratio $^{57}\text{g}_\text{N}/^{59}\text{g}_\text{N}$. The results are shown in Table XVI. They will now be compared with other measurements.

- a. $^{57}\text{Co}/^{59}\text{Co}$. The magnetic moment ratio has been determined by Baker et al.³⁵⁾ from EPR measurements on ^{57}Co and ^{59}Co in $\text{ZnK}_2(\text{SO}_4)_2 \cdot 6\text{H}_2\text{O}$. They found $^{57}\mu/^{59}\mu = 1.00(1)$. We note that this result is derived from the absence of any ^{57}Co spectrum, and consequently it must be taken with considerable reserve. The ratio of the quadrupole moments has not been determined before.
- b. $^{58}\text{Co}/^{59}\text{Co}$. Dobrov and Jeffries³⁶⁾ have performed EPR measurements on ^{58}Co in $\text{ZnK}_2(\text{SO}_4)_2 \cdot 6\text{H}_2\text{O}$. Their result is: $^{58}\mu/^{59}\mu = 0.8734(24)$, which is less accurate by a factor of 15, but in agreement with our measurement. The quadrupole moment ratio has not been measured before.
- c. $^{60}\text{Co}/^{59}\text{Co}$. Dobrowolski et al.³⁷⁾ have measured the magnetic moment ratio to be $^{60}\mu/^{59}\mu = 0.8191(16)$, by means of EPR measurements

TABLE XVII

Summary of nuclear moments and pseudo Zeeman coefficients								
iso- tope	μ (n.m.)	Q (barns)	g_N	$g_N\mu_N/hc$ ($10^{-8}\text{cm}^{-1}/0e$)	$(1+\sigma_{//})g_N\mu_N/hc$ ($10^{-8}\text{cm}^{-1}/0e$)	$\sigma_{//}$	$(1+\sigma_{\perp})g_N\mu_N/hc$ ($10^{-8}\text{cm}^{-1}/0e$)	σ_{\perp}
^{59}Co	+4.616 (9)	+0.38(4)	+1.319 (3)	+3.353 (7)		+0.406 (3)		+0.438 (5)
^{57}Co	+4.722(17)	+0.49(9)	+1.349 (5)	+3.430 (12)	+4.76(4)	+0.388(12)	+4.87 *	+0.420 *
^{58}Co	+4.035 (8)	+0.21(3)	+2.018 (4)	+5.131 (10)	+7.19(2)	+0.401 (5)	+7.37(3)	+0.436 (7)
^{60}Co	+3.790 (8)	+0.42(5)	+0.7580(16)	+1.927 (4)	+2.67(4)	+0.39 (2)	+2.71(4)	+0.41 (2)

* values not obtained from the measurements, but used to fit resonance frequencies.

in $\text{Zn}(\text{NH}_4)_2 \cdot (\text{SO}_4)_2 \cdot 6\text{H}_2\text{O}$. Their result is in agreement with ours, although less accurate by a factor of 5. Again the quadrupole moment ratio has not been determined before.

Using the nuclear moments of ^{59}Co as a reference, we can derive values for the nuclear moments of the three radioactive isotopes. The most reliable value for the magnetic moment of ^{59}Co is $^{59}\mu = 4.616(9)$ n.m.³⁸⁾. For the quadrupole moment of ^{59}Co several values are quoted³⁹⁾; as a mean value we adopt $^{59}Q = +0.38$ barn. In Table XVII, the resulting values of the nuclear moments of the other isotopes are listed, together with the nuclear g values $g_N = \mu/I$. It should be emphasized, however, that the derived values for the nuclear moments of the three radioactive isotopes may be subject to shifts, arising from systematic errors in the nuclear moment values for the stable isotope ^{59}Co . This holds especially for the electric quadrupole moments, where systematic errors in the order of 20% are possible due to the uncertainty in the atomic Sternheimer shielding correction used to obtain $Q(^{59}\text{Co})$.

From the nuclear magnetic moments, we can derive the values for $g_N \mu_N / hc$, where μ_N / hc is the nuclear magneton, expressed in $\text{cm}^{-1}/0e$: $\mu_N / hc = 2.5428 \times 10^{-8} \text{cm}^{-1}/0e$. Comparison with the experimental values for the gyromagnetic ratios $(1 + \sigma_{//})g_N \mu_N / hc$ and $(1 + \sigma_{\perp})g_N \mu_N / hc$ yields values for the "pseudo Zeeman" coefficients $\sigma_{//}$ and σ_{\perp} . These are listed also in Table XVII, together with the values for ^{59}Co , as found by De Beer²⁾. There is reasonable agreement between the several determinations of $\sigma_{//}$ and σ_{\perp} , although the mean values of our data are somewhat lower than the values for ^{59}Co .

7.2. Comparison of linewidths.

In sections 4, 5 and 6, we have ascribed the measured linewidths to a spread in the hyperfine parameters A and B. In Table XVIII, we have summarized the results; also the fractional widths $\Delta A/A$ and $\Delta B/B$ have been derived from the experiments. These fractions appear to be constant for the optically bright ^{58}Co -LMN crystals (two samples) and the ^{60}Co -LMN crystal, whereas the cloudy ^{57}Co -LMN sample gives larger fractional widths, especially for the parameter A.

TABLE XVIII

Comparison of the spread in the
hfs parameters A and B of three Co isotopes

isotope	A (MHz)	ΔA (MHz)	$\Delta A/A$	B (MHz)	ΔB (MHz)	$\Delta B/B$
^{57}Co	243.46	0.50	2.1×10^{-3}	317.7	2.6	8.2×10^{-3}
^{58}Co	362.73	0.36	0.99×10^{-3}	476.75	2.4	7.1×10^{-3}
^{60}Co	136.22	0.14	1.03×10^{-3}	179.08	1.14	6.4×10^{-3}

These results, combined with the absence of any appreciable spread in the hfs parameters in the case of the Mn isotopes, suggest that the spread in A and B is caused by random variations in the crystalline field from site to site. For Mn^{2+} , these variations do not affect the hfs interaction, because in that case the interaction is caused by core polarization, entering the hfs Hamiltonian through the Fermi contact term. This core polarization is caused by the electronic spin angular momentum, the latter being practically independent from crystalline field effects. For Co^{2+} , however, the orbital term P_{\perp} plays an important role in the hfs coupling. This term is directly related to the electronic orbital angular momentum in the ground state, and hence to the crystalline field.

Following Abragam and Pryce⁵⁾, the orbital contribution to the hfs parameters A and B can be written as

$$A_{\perp} = P g_{\perp}^L, \quad (44)$$

$$B_{\perp} = P g_{\perp}^L, \quad (45)$$

$$\text{where } P = 2\mu_B g_N \mu_N \langle r^{-3} \rangle, \quad (7)$$

and g_{\perp}^L and g_{\parallel}^L are the orbital contributions to the g values of the ground doublet. These last two quantities can be found, using the value for a cubic environment $g^L = \frac{2}{3} \bar{g}_L \approx 0.970$, and applying corrections for the departure from cubic symmetry⁴⁰⁾. The obtained values are

$g_{//}^L = 0.901$ and $g_{\perp}^L = 1.004$. P is estimated to be 0.0254 cm^{-1} for stable ^{59}Co , using $\langle r^{-3} \rangle = 6.04 \text{ a.u.}^{10}$. Inserting these values in (44) and (45), we obtain $^{59}A_L = 0.023 \text{ cm}^{-1}$ and $^{59}B_L = 0.026 \text{ cm}^{-1}$, which can be compared to the experimental values: $A = 0.00791 \text{ cm}^{-1}$ and $B = 0.01038 \text{ cm}^{-1}$ (2).

Using these values, we have for the relative spread in the hfs parameters of ^{58}Co and ^{60}Co :

$$\Delta A/A_L = 3.5 \times 10^{-4} \quad ; \quad \Delta B/B_L = 2.7 \times 10^{-3} .$$

It is instructive to compare this with the results of Choh and Seidel¹¹⁾, who performed NMR measurements on ^{59}Co in $\text{Co}(\text{NH}_4)_2 \cdot (\text{SO}_4)_2 \cdot 6\text{H}_2\text{O}$, in a situation in which the electron spins were polarized to a high degree. Assuming that the observed linewidths in their experiments ($\Delta\nu/\nu \approx 2.5 \times 10^{-3}$ for $\theta = 0^\circ$, and $\Delta\nu/\nu \approx 5 \times 10^{-3}$ for $\theta = 90^\circ$) were caused by the same phenomenon, we calculate for this case, using the values for A_L and B_L obtained by Abragam and Pryce:

$$\Delta A/A_L = 1.5 \times 10^{-3} \quad \text{and} \quad \Delta B/B_L = 1.0 \times 10^{-2} .$$

The absolute values for both quantities are about a factor 4 higher than in our experiment. It is remarkable, however, that in both experiments $\Delta A/A_L$ is about a factor of 7 smaller than $\Delta B/B_L$. The source of this difference is not clear, but is possibly related to local strains causing a departure from axial (i.e. trigonal) symmetry.

7.3. Intermediate state reorientation after electron capture.

The attenuation parameters $G_2 = 0.41(2)$ and $G_4 = 0.32(4)$, as measured in section 6.4., are of interest for the problem of reorientation during the 8.7 ns lifetime of the 136 keV state in ^{57}Fe . In this section we want to discuss the results in connection with the events following the capture of an inner shell electron in the ^{57}Co nucleus, leading to the formation of an excited state of ^{57}Fe at 136 keV. Several discussions of this subject are given in the literature⁴¹⁻⁴³). The sequence of events is the following. The electron

capture creates a hole, usually in the K shell, which is filled by an electron from an outer electronic shell, so that the hole moves outwards. A hole in the K shell decays predominantly by Röntgen emission; for other shells, however, the Auger effect determines mainly the transition probability. In this process additional holes are created, because when one electron from an outer shell drops into an inner shell, a second electron is ejected from the atom (ion) in order to carry off the excess energy.

The total time required for the holes to move out to the outermost shell can be estimated to be 10^{-14} s for cobalt. However, once the holes have reached the valence shell, they will decay more slowly. In metals, the conduction electrons will fill the holes in the valency band in a very short time ($\leq 10^{-12}$ s), but in insulators, these high valency states can exist much longer. In the case of ^{57}Co , Mössbauer experiments on several hydrated salts⁴⁴⁻⁴⁵⁾ have shown that excited Fe ions exist as Fe^{2+} and Fe^{3+} for about equal fractions, the lifetime of the latter being $10^{-6} - 10^{-8}$ s, which is longer than the half life of the 136 keV state, $T_{1/2} = 8.7$ ns. States of higher charge decay in a time less than 10^{-9} s. This means that the excited ^{57}Fe nucleus will see a constant hyperfine field during most of its lifetime, the magnitude depending on the electronic configuration.

One can ask which of these subsequent events give rise to attenuation of the gamma anisotropy. It is generally believed that the first step, the rapid filling of the holes in the inner shells, does not influence the gamma anisotropy. Experimentally, this has been demonstrated by the absence of attenuation for intermediate states having lifetimes shorter than 10^{-10} s (see, for instance, Lubbers and Huiskamp²⁸⁾). The second step, however, in which the high valency states exist, may have noticeable influence on the gamma anisotropy if the ^{57}Co nuclei are incorporated in an insulator. The same holds for the third period, in which the nuclear spin precesses around a constant hyperfine field set up by the electrons in the configurations Fe^{2+} and Fe^{3+} , which are stable during the lifetime of the excited state at 136 keV. For the case of ^{57}Co in $\text{Ce}_2\text{Zn}_3(\text{NO}_3)_{12} \cdot 24\text{H}_2\text{O}$, Daniels and

Misra⁴¹⁾ and recently Misra⁴⁹⁾ have calculated the time evolution of the density matrix in this period. For Fe^{2+} , no attenuation is to be expected, because probably $g_{\perp} = B = 0$ in this case, causing the nuclei to precess around the trigonal axis of the crystal. For Fe^{3+} , however, serious attenuation effects will occur. Unfortunately, the results of Daniels and Misra cannot be compared directly with our experiment, because they assume a magnetic field of 150 G to be present at site 11, arising from the Ce ions. This field is clearly absent in our case. The influence of this difference can be estimated and leads to the conclusion that for our case the calculated value for G_2 would be about 0.5 for Fe^{3+} . Recalling that it is very unlikely that all Fe ions would have the configuration Fe^{3+} during the lifetime of the 136 keV state, we may conclude that this mechanism cannot explain the observed attenuation $G_2 = 0.41 \pm 0.02$. Therefore, time dependent interactions during the second period, in which the high valency states decay, probably have a noticeable influence on the attenuation of the gamma anisotropy.

Finally, the difference in behaviour between metallic and non-metallic samples may be mentioned. In a metal such as iron, high valency states will decay in about 10^{-12} s, and the electronic configuration will reach its final state in a time which is very short compared to 8.7 ns, the half life of the intermediate state. For iron, the hyperfine field will be collinear with the external field, and no disturbance of the nuclear orientation will occur. This is confirmed experimentally by gamma anisotropy measurements on polarized ^{57}Co nuclei in metallic iron⁴⁶⁾ and Mössbauer experiments on the same system^{47,48)}. In contrast, in an insulator the electronic configuration will reach its final state much slower, so that probably the electron shell will be completely depolarized during the lifetime of the intermediate state^{41,49)}.

8. Conclusion

The method of magnetic resonance on radioactive nuclei, oriented in a dilute paramagnetic crystal, has been applied in Chapter I to two Mn isotopes in LMN. In this Chapter we described the application of

the technique to three Co isotopes, thereby establishing the general usefulness of the method. The main features of the Co experiments appeared to be the same as those of the Mn experiments: nuclear orientation by means of cross relaxation with a cooled Ce spin system, very long nuclear spin-lattice relaxation times, provided that the Co electron spins were sufficiently polarized, and the feasibility of inducing (and saturating) several hfs transitions separately. The obtained line-widths were found to be larger than in the case of the Mn isotopes, and could be ascribed to a spread in the hfs constants A and B. As was expected on the basis of the resonance mechanism, only Co ions at site II of the LMN lattice could be observed in the resonance measurements, although in the case of ^{60}Co evidence was found that the Co ions at site I could be partially oriented at low magnetic fields. The fraction of Co ions at site II was determined from the ^{58}Co and ^{60}Co measurements to be $f = 0.577$, which means that there was a slight preference for lattice site I, just as in the case of the Mn isotopes.

The method of nuclear orientation also proved to be very advantageous in the study of the directional anisotropies of the 122 keV and 136 keV gamma transitions in ^{57}Fe . The multipole mixing ratio in the former transition could be determined in a very simple experiment, using the anisotropy of the other transition to determine the nuclear orientation parameters. The result is surprisingly low compared to the results obtained from angular correlation measurements using the 122 keV - 14.4 keV cascade. Moreover, detailed information was obtained about the attenuation of the anisotropy during the 8.7 ns lifetime of the 136 keV state in ^{57}Fe .

Appendix 1 - Analysis of errors in the obtained hfs parameters and in the calculated resonance frequencies.

The errors in the hfs constants were determined mainly by the circumstance that only two transitions in the hfs spectrum could be measured. This can be seen with the aid of the perturbation expres-

sions (12) and (13). From (12), we obtain for a resonance transition, measured at $\theta = 0^\circ$:

$$E_{-\frac{1}{2},m} - E_{-\frac{1}{2},m-1} = \frac{1}{2} A - \frac{B^2(m-1)}{2\{g\mu_B H + (m-1)A\}} - (2m-1)P + (1+\sigma_{//})g_N\mu_N H. \quad (46)$$

Suppose that we have measured ν_{11}^1 for $\theta = 0^\circ$, that is, $m = +I$. We can fit this measurement with a certain set of hfs parameters (A, B, P). Now if we raise the quadrupole coupling constant P by an amount ΔP , we can keep the calculated energy difference constant by lowering A by $\Delta A = -2(2I - 1)\Delta P$. From (13), it can be derived in the same way that raising P by an amount ΔP can be compensated at $\theta = 90^\circ$ by raising B by an amount $\Delta B = + (2I - 1)\Delta P$. These statements are true only if we can neglect the second term in (46) with respect to the first term. For the magnetic fields used in our experiments, this is a reasonable assumption.

We conclude that it is impossible to obtain the three hfs parameters A, B and P in an unambiguous way, as long as only ν_{11}^1 is measured. However, the situation is better if we measure both ν_{11}^2 and ν_{11}^1 under identical conditions. For $\theta = 0^\circ$, we calculate from (46)

$$h(\nu_{11}^2 - \nu_{11}^1) = \frac{B^2}{2\{g\mu_B H + (I - 3/2) A\}} - 2P. \quad (47)$$

From this equation P can be obtained independently from A, with an accuracy determined by the experimental error in $\nu_{11}^2 - \nu_{11}^1$. To use this expression, B has to be known only to a first approximation, obtained from the results at $\theta = 90^\circ$. The error in P determines those in A and B. The experimental error in ν_{11}^1 is very small compared to the error in the quadrupole term $(2m - 1)P$ in (46), so that we obtain from the measurement of ν_{11}^1 :

$$\Delta A = -2(2I - 1)\Delta P \quad \text{and} \quad \Delta B = (2I - 1)\Delta P.$$

Thus we see that for a high value of I the situation is very unfavourable with respect to the accuracy with which A and B can be determined. Using the experimental determination of ν_{11}^2 gives no improvement, because these determinations are in most cases much more inaccurate than

those of ν_{11}^1 . Only in the case of ^{58}Co was the situation different, because there three of the four transitions could be easily determined.

The parameters $(1 + \sigma_{//})g_N\mu_N$ and $(1 + \sigma_{\perp})g_N\mu_N$ were determined by inspection of the field dependence of the resonance lines. The parameters A and B appear in the third term of (12) and in the third and fourth term of (13) respectively, and consequently influence the field dependence. Therefore the errors in A and B were the main source of error in the parameters $(1 + \sigma_{//})g_N\mu_N$ and $(1 + \sigma_{\perp})g_N\mu_N$ for the ^{57}Co and ^{60}Co isotopes. For ^{58}Co , the error introduced by ΔA and ΔB was much smaller, because in that case the measurements could be extended up to 18 kOe, causing these terms to become very small.

Appendix 2 - Analysis of changes in $W(0)$ during saturation of resonance transitions.

For ^{58}Co and ^{60}Co , saturation of the resonance lines was observed, i.e. the population of the two hfs levels involved, were equalized. The accompanying changes in $W(0)$ were analyzed using the following model. It was assumed that, after the nuclear orientation process had been completed, only the lowest two levels of the hfs spectrum were significantly populated as far as Co ions at site II were concerned. From the results on the Mn isotopes, we know that this is a reasonable assumption. After saturation of ν_{11}^1 , we will have the population numbers $a_5 = a_4 = 0.5$ for the subsystem of Co ions at site II. Saturation of ν_{11}^2 leads to $a_5 = 0.5$, $a_4 = a_3 = 0.25$, etc.

Thus, for all transitions except ν_{11}^1 , the populations before and after saturation were known. The changes in $W(0)$ accompanying these transitions were compared to calculations, to obtain the fraction f of Co ions at site II. This was done by writing

$$W(0) = fW(0)_{11} + (1 - f)W(0)_I, \quad (48)$$

where $W(0)_I$ and $W(0)_{11}$ are the gamma intensities in the direction of the field for the two subsystems of Co ions at site I and II, respec-

tively. The expected changes in $W(0)_{II}$ could easily be calculated, using tables II and IV, and the population numbers given above. From a comparison with the observed changes in $W(0)$, f was obtained. Small solid angle corrections were included in the comparison. The value for f could be used thereafter to analyse the values of $W(0)$ after saturation of, say, ν_{II}^1 . In this way, $W(0)_I$ was found, the normalized gamma intensity for Co ions at site I. This quantity differed from 1 only in the case of ^{60}Co .

Finally, the assumption concerning the state of the nuclear spin system after thermal mixing could be checked. This was done by calculating the value of $W(0)$ to be expected after thermal mixing, on the basis of the obtained value for $W(0)_I$ and the assumption that the populations of the hfs subsystem for site II ions could be described by a Boltzmann factor: $a_m \propto e^{-\beta m}$, with $2.5 < \beta < 4.0$.

The general agreement between the experimental and the calculated values indicates that the population of the higher lying levels is indeed negligible.

References

1. Niesen, L. and Huiskamp, W.J., *Physica* **50** (1970) 259, (Commun. Kamerlingh Onnes Lab. Leiden No. 379b); Chapter I of this thesis.
2. De Beer, R., private communication.
3. Gager, W.B., Jastram, P.S. and Daunt, J.G., *Phys. Rev.* **111** (1958) 803.
4. Zalkin, A., Forrester, J.D. and Templeton, D.H., *J.Chem.Phys.* **39** (1963) 2881.
5. Abragam, A. and Pryce, M.L.H., *Proc.Roy.Soc. A* **205** (1951) 173.
6. Thornley, J.H.M., Windsor, C.G. and Owen, J., *Proc.Roy.Soc. A* **284** (1965) 252.
7. Abragam, A. and Bleaney, B., *The Theory of EPR in Transition Metal Ions*, Clarendon Press (Oxford, 1970).
8. Rei, D.K., *Sovjet Physics Solid State* **3** (1962) 1613.
9. Ref. 7, p. 693.
10. Freeman, A.J. and Watson, R.E., *Magnetism*, Vol. IIA, ed. G.T. Rado and H. Suhl, Academic Press (New York, 1965), p. 167.
11. Choh, Sung Ho and Seidel, G., *Phys. Rev.* **174** (1968) 385.
12. Lindqvist, T. and Heer, E., *Nucl. Phys.* **2** (1956) 680.
13. Hohenemser, C., Reno, R., Benski, H.C. and Lehr, J., *Phys.Rev.* **184** (1969) 298.

14. Nuclear Data Sheets B 3, 3 - 4 (1970) p. 103-145.
15. Ewan, G.T., Graham, R.L. and Geiger, J.S., Nucl.Phys. 19 (1960) 221.
16. De Groot, S.R., Tolhoek, H.A. and Huiskamp, W.J., Alpha- Beta- and Gamma-Ray Spectroscopy, ed. K. Siegbahn, North-Holland Publ. Co. (Amsterdam, 1965) p. 1199 c.f.
17. Biedenharn, L.C. and Rose, M.E., Rev.Mod.Phys. 25 (1953) 729.
18. Ofer, S., Phys.Rev. 114 (1959) 870.
19. Bishop, G.R., Grace, M.A., Johnson, C.E., Knipper, A.C., Lemmer, H.R., Perez Y Jorba, J. and Scurlock, R.G., Phil.Mag. 46 (1955) 951.
20. Frauenfelder, H. and Steffen, R.M., Alpha- Beta- and Gamma-Ray Spectroscopy, ed. K. Siegbahn, North-Holland Publ. Co. (Amsterdam, 1965) p. 997.
21. Rose, H.J. and Brink, D.M., Rev.Mod.Phys. 39 (1967) 306.
22. Krane, K.S. and Steffen, R.M., Phys.Rev. C 2 (1970) 724.
23. Nuclear Data Sheets B 3, 3 - 4 (1970), p. 145 - 186.
24. McArthur, D., Goodman, R., Artna, A. and Johns, M.W., Nucl. Phys. 38 (1962) 106.
25. Malmkog, S., Nucl.Phys. 51 (1964) 690.
26. Ramamohan, R.V., Reddy, K.V., Raju, B.V. and Janananda, S., Ind. J. Pure Appl.Phys. 4 (1966) 420.
27. Fanger, U., Michaelis, W., Schmidt, H. and Ottmar, H., Nucl.Phys. A 128 (1969) 641.
28. Lubbers, J. and Huiskamp, W.J., Physica 34 (1967) 166. (Commun. Kamerlingh Onnes Lab. Leiden No. 353b).
29. Abragam, A. and Borghini, M., Progress in Low Temp. Phys. vol. 4, ed. C.J. Gorter, North-Holland Publ. Co. (Amsterdam, 1964) p. 418.
30. Orbach, R., Proc.Roy.Soc. London A 264 (1961) 458.
31. Culvahouse, J.W., Unruh, W.P. and Sapp, R.C., Phys.Rev. 121 (1961) 1370.
32. Levi, M.W., Sapp, R.C. and Culvahouse, J.W., Phys.Rev. 121 (1961) 538.
33. Strohm, W.W. and Sapp, R.C., Phys.Rev. 132 (1963) 207.
34. Mellema, J. and Postma, H., Nucl.Phys. 130 (1969) 161.
35. Baker, J.M., Bleaney, B., Llewellyn, P.M. and Shaw, P.F.D., Proc. Phys. Soc. 69A (1956) 353.
36. Dobrov, W. and Jeffries, C.D., Phys.Rev. 108 (1957) 60.
37. Dobrowski, W., Jones, R.V. and Jeffries, C.D., Phys.Rev. 101 (1956) 1001.
38. Walstedt, W., Wernick, J.H. and Jaccarino, V., Phys.Rev. 162 (1967) 301.
39. Fuller, G.H. and Cohen, V.W., Nuclear Spins and Moments, Nuclear Data Tables 5 (1969) 433.
40. Ref. 7, p. 449.
41. Daniels, J.M. and Misra, S.K., Can.Journ.Phys. 44 (1966) 1965.
42. Ref. 20, p. 1182 c.f.
43. Wickman, H.H. and Wertheim, G.K., Chemical Applications of Mössbauer Spectroscopy, ed. V.I. Goldanskii and R.H. Herber, Academic Press (New York, 1968) p. 604 c.f.

44. Wertheim, G.K. and Guggenheim, H.J., J. Chem. Phys. 42 (1965) 3873.
45. Ingalls, R., Coston, C., De Pasquali, G., Drickamer, H.G. and Pinajian, J., J.Chem.Phys. 45 (1966) 1057.
46. Holliday, R.J., Shirley, D.A. and Stone, N.J., Phys.Rev. 143 (1966) 130.
47. Dash, J.G., Taylor, R.D., Nagle, D.E., Craig, P.P. and Visscher, W.M., Phys.Rev. 122 (1961) 1116.
48. Ehnholm, G.J., Katila, T.E., Lounasmaa, O.V. and Reivari, P., Phys. Letters 25A (1967) 758.
49. Misra, S.K., Phys.Rev. B 3 (1971) 176.

CHAPTER III

HYPERFINE FIELDS ON ^{133}Xe AND ^{160}Tb NUCLEI IN Fe1. Introduction

The discovery by Samoilov¹⁾ that strong magnetic fields exist at the nuclei of diamagnetic atoms if they are incorporated in ferromagnetic metals has led to much experimental and theoretical work on this subject. In the case of iron as host material, the hyperfine fields of about 50 elements have been measured, using a considerable variety of techniques. In order to be certain that interaction effects among the impurity atoms are negligible, one has to keep the impurity concentration very low; this makes it attractive to use radioactive nuclei to measure the hyperfine field. One can choose then between three methods: Mössbauer effect, perturbed angular correlations (PAC) and nuclear orientation. None of these methods is universal in the sense that it is applicable to all nuclei; only the combination of the results of all techniques provides a reasonably complete picture of the subject.

Several techniques for sample preparation are used. If the impurity atoms are soluble in the ferromagnetic host material, samples can be made by diffusion or melting. In that case, the impurity atoms will usually occupy substitutional positions, i.e. they substitute host atoms. Serious problems arise if the impurities are not soluble. The difficulties have been overcome by shooting the radioactive atoms into the host material with kinetic energies ranging from 10 keV to 30 MeV. This technique is called ion implantation. Isotope separators have been used for energies up to about 500 keV; for higher energies one induces the implantation by means of a nuclear reaction. In the latter case the target nuclei are incorporated in a very thin foil on a backing of ferromagnetic material. The target is exposed to a beam of fast ions from an accelerator. The target nuclei are excited and they recoil into the ferromagnetic backing. Usually the subsequent decay to

the ground state is monitored with the PAC technique; the method is then called IMPACT (Implantation Perturbed Angular Correlation Technique).

The location of the implanted ions presents a difficult problem. This can be studied very beautifully by preparation of implanted sources in single crystals and using the "channeling" technique, based on differential Rutherford scattering from the impurity and the host nuclei. In this way one can obtain information about the fraction of atoms in substitutional, interstitial or more complex sites. The observation of different sites (by differences in their hyperfine interactions) is also possible in experiments using the Mössbauer effect. With the PAC and nuclear orientation methods this is much more difficult and in most cases only an average of the hyperfine fields on different sites can be measured. Several experiments have shown that it is possible, in many cases, to obtain implanted sources in which a large fraction of atoms end up in substitutional sites. Valuable information on this subject can be found in the proceedings of a discussion on ion implantation and hyperfine interactions, held in 1968²⁾.

The theory of hyperfine interactions in dilute ferromagnetic alloys is still in an embryonic state. Several mechanisms contributing to the hyperfine field are known, but in most cases it is difficult to estimate their strength. In fact, even the sign cannot always be predicted with confidence, because cancellation of several large contributions of opposite sign leads to a relatively small hyperfine field. For an outline of the theoretical aspects we refer to an article of Shirley et al.³⁾.

The nuclear orientation measurements reported here were done in close collaboration with the group of Prof. H. de Waard in Groningen. By means of their isotope separator, ^{133}Xe and ^{160}Tb ions were shot into iron foils. Various concentrations and bombarding energies were used. ^{133}Xe -Fe foils served also for Mössbauer effect measurements in Groningen. In addition, ^{161}Tb -Fe foils were made for this purpose. The Mössbauer results turned out to be very helpful in the discussion of the nuclear orientation measurements, as will be seen below.

2. Theory

2.1. Decay and magnetic moment of ^{133}Xe . Gamma anisotropy parameters.

^{133}Xe (spin 3/2, positive parity, half life 5.2 d) decays almost exclusively through a beta branch to the $5/2^+$ state at 81 keV in ^{133}Cs , which in turn decays by a mixed M1 + E2 gamma transition to the $7/2^+$ ground state of ^{133}Cs . The absolute value of the quadrupole-dipole mixing parameter δ has been carefully determined by Brown et al.⁴⁾ from K- and L-subshell conversion ratio's: $|\delta| = 0.163 \pm 0.008$.

According to the nomenclature of De Groot et al.⁵⁾, the directional distribution of the gamma ray emission from oriented nuclei is given by

$$W(\alpha) = 1 + A_2 f_2(I) P_2(\cos\alpha). \quad (1)$$

$f_2(I)$ is an orientation parameter, depending on the populations of the magnetic sublevels of the decaying ^{133}Xe nucleus and on its spin $I = 3/2$; $P_2(\cos\alpha)$ is the second order Legendre polynomial; A_2 is related to the properties of the gamma transition, and is given in ref. 5; after removal of an error in the last term the appropriate formula reads

$$A_2 = \frac{1}{1+\delta^2} \left[\frac{3}{2} + 3 \left\{ \frac{15(j_i + 2)^{\frac{1}{2}}}{j_i} \right\} \delta + \frac{15}{14} \frac{j_i + 6}{j_i} \delta^2 \right] M_2(j_i) U_2. \quad (2)$$

j_i is the spin of the initial state of the gamma transition; $j_i = 5/2$. $M_2(j_i)$ is a numerical factor depending on j_i :

$$M_2 = \frac{j_i^2}{(j_i+1)(2j_i+3)}. \quad (3)$$

The factor U_2 is included to account for the preceding beta decay. In this particular case $M_2(j_i)U_2 = M_2(3/2) = 0.15$.

Since the sign of δ is unknown, two values of A_2 are possible. For $\delta > 0$, we find $A_2 = 0.605 \pm 0.015$ and for $\delta < 0$, we find $A_2 = -0.138 \pm 0.013$. We remark that the mixing ratio used in formula (2) is defined as

$$\delta = \frac{\langle j_f || L + 1 || j_i \rangle}{\langle j_f || L || j_i \rangle}, \quad (4)$$

where j_i and j_f are the spins of the initial and final state, respectively. The definition of the reduced matrix elements is from Biedenharn and Rose⁶⁾. For a discussion of expression (4) together with the expressions used in angular correlation theory^{6,7,10)} we refer to Chapter II.

Although the dipole moment of ^{133}Xe has not been measured, a fair estimate can be made from the systematics of dipole moments of neighbouring nuclei. We inspected pairs of isotopes having neutron numbers N and $N+2$, in the region $76 \leq N \leq 82$. For these pairs, the measured magnetic moments μ of states having identical spin were compared⁸⁾. It is seen from Table I that the addition of two neutrons results in an increase in μ of the order of 0.1 n.m. in all cases except one. Because we are near a closed neutron shell ($N = 82$), we can apply the shell model, which shows that in this region pairs of neutrons probably will fill the $1h_{11/2}$ shell, giving rise to a roughly constant increase of μ . The magnetic moment of ^{131}Xe is +0.691 n.m.; we therefore estimate the magnetic moment of ^{133}Xe to be +0.8 n.m.

2.2. Decay and magnetic moment of ^{160}Tb . Gamma anisotropy parameters.

^{160}Tb (half life 72 d) has a complicated decay scheme¹¹⁾. We used the anisotropy in the emission of the strong 299 keV gamma ray to determine the nuclear orientation. This transition between the 2^- state of ^{160}Dy at 1.265 MeV and the 2^+ state at 0.966 MeV is fed by an allowed beta branch from the 3^- ground state of ^{160}Tb . Its multipolarity can be measured using the angular correlation of the 299 - 966 keV cascade, the 966 keV line being an electric quadrupole transition to the 0^+ ground state. The experimental results⁹⁻¹²⁾ scatter around the value $\delta = 0$. We will therefore assume that the 299 keV transition has a purely electric dipole (E1) character.

The directional distribution of the emission of this gamma ray can be written as

TABLE I

Spins and magnetic moments of isotopes with neutron number N between 76 and 82				
odd-proton isotopes				
isotope	N	I	μ (n.m.)	$\Delta\mu$ (n.m.)
^{129}I	76	7/2	+ 2.618	
^{131}I	78	7/2	+ 2.738(1)	+ 0.120(1)
^{133}I	80	7/2	+ 2.837(5)	+ 0.099(5)
^{133}Cs	78	7/2	+ 2.579	+ 0.150
^{135}Cs	80	7/2	+ 2.729	+ 0.109
^{137}Cs	82	7/2	+ 2.838	
^{131}Cs	76	5/2	+ 3.538(2)	- 0.10(4)
^{133}Cs	78	5/2	+ 3.44(4)	
odd-neutron isotopes				
^{135}Ba	79	3/2	+ 0.837(1)	+ 0.099(1)
^{137}Ba	81	3/2	+ 0.936	
^{131}Xe	77	3/2	+ 0.691	
^{133}Xe	79	3/2	?	

$$W(\alpha) = 1 + A_2 f_2(I) P_2(\cos \alpha), \quad (1)$$

where f_2 and $P_2(\cos \alpha)$ have been defined above.

The factor A_2 is given by⁵⁾

$$A_2 = -\frac{3}{2} \frac{j_i}{j_i + 1} U_2, \quad (5)$$

where j_i is the spin of the initial state of the gamma transition.

U_2 is given by

$$U_2 = \frac{I(2j_i - 1)}{j_i(2I - 1)}, \quad (6)$$

in which I is the spin of the ground state of the parent nucleus. For ^{160}Tb , $I = 3$, and $j_i = 2$. Substitution of the appropriate values gives $A_2 = +0.900$. The magnetic moment of ^{160}Tb has been measured by Easley et al.¹³⁾ They find $\mu = 1.685 \pm 0.008$ n.m.

2.3. Hyperfine fields on dilute impurities in iron.

In this section we will briefly discuss the mechanisms responsible for the hyperfine fields as far as they are relevant to the impurities studied. The Lorentz field, which in iron amounts to 7 kOe, will not be considered further here. We will start with a diamagnetic impurity such as ^{133}Xe , and thereafter will handle the more complicated case of a paramagnetic rare earth ion such as ^{160}Tb .

2.3.1. Hyperfine field on ^{133}Xe in Fe.

For diamagnetic impurities only the s electrons can be responsible for the magnetic field at the nucleus, which is caused by the so called "contact" interaction. We will denote the eigenfunctions of a certain type of s electron with spin up by $\psi_i(\underline{r})_+$, and the density of these s electrons as n_i^+ , with the corresponding notation for electrons with spin down. The magnetic contact field at the nucleus ($\underline{r} = 0$) can be written as

$$H_c = -\frac{8\pi}{3} \sum_i \{n_i^+ |\psi(0)_{i^+}|^2 - n_i^- |\psi(0)_{i^-}|^2\}, \quad (7)$$

in which $H > 0$ means that the magnetic field has the upward direction. The index i runs over the different types of s electrons which contribute to H_c , such as:

1. bound electrons in closed inner shells, giving rise to core polarization (CP).
2. conduction electrons of which the wave functions have s character

with respect to the impurity atom, giving rise to conduction electron polarization (CEP).

3. s electrons in the outer shells of the impurity atom which have wave functions overlapping the wave functions of the polarized d electrons of the iron host. They are responsible for overlap polarization (OP).

For diamagnetic atoms the contribution of core polarization is only a second order effect, but this mechanism is very important in the transition elements. The conduction electron polarization can be described roughly by a model due to Daniel and Friedel¹⁴). They assume that the impurity is bound as an ion having a charge equal to the valence difference $Z - Z_h$ between the impurity and the host. (For iron $Z_h = 1$). The presence of the impurity is described by means of a rectangular potential well, having a depth depending on this valence difference. Let us assume that the external polarizing field is up (\uparrow). The spins in the 3d band will then be polarized in the opposite direction (\downarrow). There will be an energy difference between conduction electrons with spin up and spin down, leading to a polarization of the conduction band. The mechanism of the coupling between the spins in the 3d band and those in the conduction band determines whether the polarization will be positive (defined by $n_{\uparrow} > n_{\downarrow}$, ferromagnetic coupling) or negative ($n_{\uparrow} < n_{\downarrow}$, antiferromagnetic coupling). In addition, the wave functions of the s conduction electrons at the impurity nucleus, $\psi(0)_{\uparrow}$ and $\psi(0)_{\downarrow}$, will be different, due to the energy difference between the "up" electrons and the "down" electrons. The conduction electron polarization at the impurity site, which can be written as $n_{\uparrow} |\psi(0)_{\uparrow}|^2 - n_{\downarrow} |\psi(0)_{\downarrow}|^2$, is determined by these two inequalities.

Assuming a conduction band containing one s electron per atom, Daniel and Friedel calculate that for high Z, the polarization at the impurity site will have the same sign as the conduction electron polarization at the host, whereas for low Z, the signs will be different. From the experimental results (fig. 1) for the hyperfine fields of 5p shell atoms in iron, Daniel and Friedel conclude that there exists a ferromagnetic coupling between the spins in the 3d band and those in the conduction band.

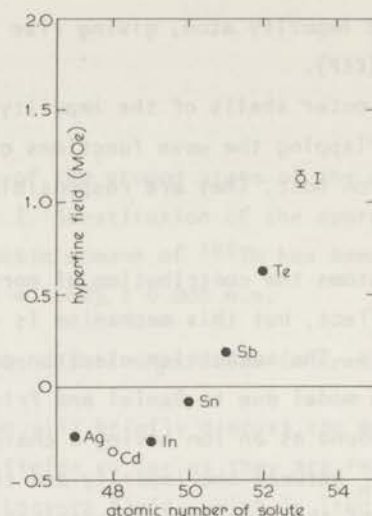


Fig. 1. Hyperfine fields at nuclei of 5p shell atoms in iron. Solid circles indicate that the sign of the field has been determined. Data are from ref. 3.

Campbell¹⁵⁾, however, has shown that if one makes the more reasonable assumption that there are only ≈ 0.25 s electrons per atom in the conduction band, the relation between the CEP polarization at the impurity site and at the host site is completely different. His calculations lead to the conclusion that there must exist an antiferromagnetic coupling between the spins of the conduction electrons and the 3d spins in order to get agreement with the experiments. For high Z the CEP contribution to the hyperfine field tends to zero; in the case of Cs, for instance, Campbell expects a small hyperfine field, the sign being unpredictable in his model.

Although the Daniel and Friedel model seems to be able to describe the experimental results for the 5p shell atoms for not too high Z, it is doubtful if it can explain the large positive hyperfine field for I and - borrowing from the experimental results of section 3.2. - that for Xe. On the basis of the model of Daniel and Friedel, the result on Xe in Fe would imply that the valence of Xe in Fe is 8, which is rather unlikely. Moreover, Shirley¹⁶⁾ has argued that the Daniel

and Friedel model leads to serious inconsistencies when applied to the case of Xe in Fe. Therefore the contribution of overlap polarization must also be taken into account.

Shirley¹⁶⁾ has made a calculation of this effect, assuming atomic orbitals for Xe in Fe. The direct exchange interaction due to overlap between the d shell of the Fe atoms and the 5s shell of the Xe atoms creates a polarization in the 5s shell. The sign of this "transferred" hyperfine field H_{OP} will always be positive and the calculation of Shirley leads to $H_{OP} \approx 3 \times 10^6$ Oe. This result is very sensitive to small variations in the distance between the Xe and Fe atoms and can only be regarded as an order of magnitude estimate. It is clear, however, that the mechanism is strong enough to account for the observed high value of the hyperfine field.

2.3.2. Hyperfine field on ^{160}Tb in Fe.

We will start the discussion of this case by mentioning the well established fact that Tb in a metallic environment usually behaves as a Tb^{3+} ion, influenced by the crystalline electric fields of the neighbouring ions and the exchange fields of other magnetic ions. For a free Tb^{3+} ion, one has $L = S = 3$ and $J = 6$; the z component of the magnetic moment is $\mu_z = -g_J \mu_B J_z$, where $g_J = 3/2$ is the Landé factor. The magnetic hyperfine interaction may be written as

$$H = + 2\mu_B g_N \mu_N \langle r^{-3} \rangle \langle J \parallel N \parallel J \rangle \underline{J} \cdot \underline{I}, \quad (8)$$

where the reduced matrix elements $\langle J \parallel N \parallel J \rangle$ for the ground state of rare earth ions have been tabulated by Elliott and Stevens¹⁷⁾. For Tb^{3+} , one has $\langle J \parallel N \parallel J \rangle = 49/90$.

A magnetic field in the z-direction will split up the ground state, the hfs multiplet $J_z = J$ being lowest in energy. For a large external field, the energy difference between the hfs sublevels can then be written as

$$\Delta E_{\text{hfs}} = g_N \mu_N H_{\text{hf}}^{\text{ion}}, \quad (9)$$

with

$$H_{hf}^{ion} = -2 \mu_B J \langle r^{-3} \rangle \langle J || N || J \rangle . \quad (10)$$

H_{hf}^{ion} is known as the "free ion" hyperfine field. It can be calculated for Tb^{3+} , using a reasonable value for $\langle r^{-3} \rangle$. If we take $\langle r^{-3} \rangle = 8.4 \pm 0.2$ atomic units¹⁸⁾, we find $H_{hf} = (3.46 \pm 0.09) \times 10^6$ Oe.

In a solid such as Fe metal, the Tb^{3+} ion will experience the crystalline fields due to the surrounding Fe ions and the magnetic exchange fields produced by the 3d electrons of the host metal. The ground manifold will be thus split in a manner determined by the relative strength of the crystalline electric field and the exchange field. However, both interactions may be expected to be much weaker than the spin-orbit coupling, so that J remains a good quantum number. Each ionic substate may be characterized by the expectation value $\langle J_z \rangle$, where z is chosen along the direction for which $\langle J \rangle$ is a maximum in the ground state. Since the hyperfine interaction is small when compared to the spin-orbit coupling of the free ion, we can neglect matrix elements of the hfs interaction between states having different J . The magnetic hyperfine interaction in one of the electronic substates can then be written as:

$$H = +2 \mu_B g_N \mu_N \langle J_z \rangle \langle r^{-3} \rangle \langle J || N || J \rangle \cdot I_z . \quad (11)$$

In this Hamiltonian, off diagonal terms of the type $A J_x I_x$ have been neglected. This can be justified for the case that one axial term is dominant in the interaction between the Tb ion and its surroundings (for instance an exchange field, or an axial crystalline electric field). If the situation is different, the off-diagonal terms cannot be neglected in general, but for the ground state their influence will be small in view of the choice of the z -axis along the direction for which $\langle J_z \rangle$ is a maximum. Comparing eq. (11) with the usual formula which defines the hyperfine field on the Tb nucleus:

$$H = -g_N \mu_N H_{hf} I_z , \quad (12)$$

we find

$$H_{hf} = - 2\mu_B \langle J_z \rangle \langle r^{-3} \rangle \langle J || N || J \rangle . \quad (13)$$

If the Tb-Fe exchange interaction is much stronger than the crystalline electric field, the resulting ground state will have $\langle J_z \rangle = J$ and the nucleus feels the ionic hyperfine field. However, if the crystalline electric field dominates the situation is much more complicated. For Tb^{3+} in a bcc lattice such as Fe, point charge calculations of Lea et al.¹⁹⁾ indicate that a singlet (Γ_2) or a non-magnetic doublet (Γ_3) would be lowest, which would give $\langle J_z \rangle = 0$ and thus zero hyperfine field. It is not at all certain, however, that a point charge calculation gives the correct signs of the fourth order and sixth order terms in the cubic potential, and therefore this result must be taken with some reserve. In general, one may say that the introduction of crystal field effects leads to a lowering of $\langle J_z \rangle$ in the ground state and consequently to a lowering of the hyperfine field compared to the free ion value.

So far we have neglected the contribution of contact terms to the hyperfine interaction. Both core polarization and conduction electron polarization will be possible. The core polarization contribution has been estimated, for instance by Bleaney²⁰⁾: $H_{CP} \approx +90 (g_J - 1)kOe$, which gives $+45 kOe$ for Tb^{3+} . The CEP contribution probably has a negative sign, and is of the order of several hundred kOe. This is estimated on the basis of the experimental value for the hyperfine field of Gd in Fe³⁾, where only contact terms contribute to the hfs interaction, since $L = 0$ in this case.

For the free ion, the interaction between the gradient of the electric field set up by the 4f electrons, denoted by q_{4f} , and the nuclear quadrupole moment Q gives rise to a quadrupole term in the Hamiltonian. We can write for this term

$$H_Q = \frac{3e^2Q}{4I(2I-1)} (1 - R_Q) q_{4f} \left\{ I_z^2 - \frac{1}{3} I(I+1) \right\} . \quad (14)$$

The factor $1 - R_Q$ is called the atomic Sternheimer factor, and accounts for the induced quadrupole moment in the closed electron shells resulting from the interaction of these shells with the electrons in the partially filled 4f shell. The magnitude of $|R_Q|$ is rather uncertain,

but of the order of magnitude of 0.1. Within a manifold of states of constant J one can write

$$\langle q_{hf} \rangle = -3 \langle J \parallel \alpha \parallel J \rangle \langle r^{-3} \rangle \{ \langle J_z^2 \rangle - \frac{1}{3} J(J+1) \}. \quad (15)$$

The matrix elements $\langle J \parallel \alpha \parallel J \rangle$ have been tabulated by Elliott and Stevens¹⁷⁾. The quadrupole term in the spin Hamiltonian for an energy state in a solid can thus be written

$$H_Q = P \{ I_z^2 - \frac{1}{3} I(I+1) \}, \quad (16)$$

with

$$P = -\frac{9e^2Q}{4I(2I-1)} (1-R_Q) \langle r^{-3} \rangle \langle J \parallel \alpha \parallel J \rangle \{ \langle J_z^2 \rangle - \frac{1}{3} J(J+1) \}. \quad (17)$$

For very low temperatures, only the lowest electronic level will be populated and the formulae (13) and (17) can be used without modifications. For elevated temperatures, however, the situation is more complicated. If the spin correlation times corresponding to transitions between the various electronic states are much shorter than the reciprocal of the nuclear Larmor precession frequency we can still use eq. (13) and (17) if we replace $\langle J_z \rangle$ and $\langle J_z^2 \rangle$ by $\langle J_z \rangle_T$ and $\langle J_z^2 \rangle_T$, in which the subscripts indicate Boltzmann averages over the various electronic states. The assumption made above holds generally for temperatures above a few Kelvin.

The measurements of H_{hf} and P as a function of T thus give information concerning the electronic energy levels in the solid, quite analogous to susceptibility measurements. If the exchange field dominates the crystalline electric field effects, it is easy to calculate H_{hf} and P as a function of the temperature. The following expressions then hold:

$$H_{hf}(T) = H_{hf}(T=0) \cdot \frac{\sum \langle J_z \rangle \exp \{ -g_J \mu_B H_{ex} \langle J_z \rangle / kT \}}{\sum \exp \{ -g_J \mu_B H_{ex} \langle J_z \rangle / kT \}}. \quad (18)$$

$$P(T) = P(T=0) \cdot \frac{\sum \{ \langle J_z^2 \rangle - \frac{1}{3} J(J+1) \} \exp \{ -g_J \mu_B H_{ex} \langle J_z \rangle / kT \}}{\sum \exp \{ -g_J \mu_B H_{ex} \langle J_z \rangle / kT \}}. \quad (19)$$

In this formulae, the summations are over the electronic states. H_{ex} is the exchange field on the Tb^{3+} ions, defined by $H_{ex} = + g_J \mu_B H_{ex} \cdot \underline{J}$, where H_{ex} is the Tb-Fe exchange interaction Hamiltonian.

3. Experimental arrangements

3.1. *Foil preparation.*

^{133}Xe can be obtained either as a fission product or by neutron irradiation of natural xenon. For the first sample, we used natural Xe that had been neutron irradiated during 5 days in the high flux reactor of the "Reactor Centrum Nederland (RCN)" in Petten. The specific activity obtained was about 0.1 mCi/mg. For the other two samples, fission produced Xe with an initial activity of 4 Ci/mg was used. To be able to handle this source, the fission gas was diluted with natural Xe so as to obtain specific activities of the order of 4 mCi/mg.

The isotope separator at the University of Groningen was used to implant the Xe atoms into a very pure iron foil. The foil was first soldered onto a flattened copper wire, which served as a heat conductor during the nuclear orientation experiments. The final Xe concentration in the foil depended on the specific activity of the starting material, the ^{133}Xe activity in the foil, and the rejection factor of the isotope separator for neighbouring Xe isotopes.

For one of the sources (used for Mössbauer experiments), a mass-spectrometric determination of the Xe content was made. The number of Xe atoms per cm^2 of foil surface was determined for each isotope, and could be compared with the natural abundance ratios to give the isotope rejection factors for the most abundant ^{132}Xe and ^{134}Xe isotopes. This factor turned out to be 2200 for both. With the aid of this figure, the total amount of Xe in the other foils could be derived, assuming a constant rejection factor for all implantations. The results for the three samples used for nuclear orientation measurements are shown in Table II.

The mean penetration depth of the implanted 50 keV Xe ions in Fe can be estimated as 160 Å with a RMS deviation in the depth distribution

TABLE II

 Characteristics of ^{133}Xe -Fe and ^{160}Tb -Fe samples

^{133}Xe in Fe			
sample	activity (μCi)	ion energy (keV)	implanted dose (atoms/ cm^2)
I	20	50	$\approx 2 \times 10^{14}$
II	8	63	$\approx 1 \times 10^{13}$
III	15	63	$\approx 2 \times 10^{13}$
^{160}Tb in Fe			
sample	activity (μCi)	ion energy (keV)	implanted dose (atoms/ cm^2)
I	20	50	$\approx 6 \times 10^{13}$
II	3	50	$\approx 2 \times 10^{12}$
III	10	150	$\approx 4 \times 10^{13}$

of about 65 \AA . This means that a dose of 10^{14} Xe atoms/ cm^2 will give a maximum local concentration of 0.3 at. % in the foil. To study the influence of the condition of the surface on the experimental results, sample III was etched in 2N HCl for 20 s. After the etching the activity of the source had decreased from 15 μCi to 12 μCi .

For the preparation of the iron samples with implanted ^{160}Tb ions the same procedures were used as in the case of ^{133}Xe . To be able to study the influence of the Tb concentration in the foil, and the influence of the implantation energy, three samples were made (see Table II).

For 50 keV ^{160}Tb ions the same penetration depth can be assumed as for ^{133}Xe ions of the same energy. The penetration depth of the 150 keV ions is $\approx 370 \text{ \AA}$; the RMS deviation is about 150 \AA . This implies that the maximum concentration at 150 keV will be lower by a factor 2.3 if the dose is the same.

3.2. Measuring equipment.

The iron foils were mounted in the adiabatic demagnetization ap-

paratus described in Chapter I. The cooling salt consisted of a mixture of Cr-K-alum powder with grain size $\approx 20 \mu$ and of a 1:1 volume mixture of glycerol and a fresh saturated solution of Cr-K-alum in H_2O . The ratio of powder to fluid was about 25:10, which gave a convenient slurry. A ball mill was used to powder the Cr-K-alum. Visible dehydration took place during the milling process; this could also be observed by Röntgen analysis. Addition of some water caused instantaneous reappearance of the violet colour. The final slurry was also analyzed by Röntgen diffraction. The observed diffraction pattern was identical with that of the starting material. The Cr-K-alum slurry was put into a perspex cylinder, which also contained a bundle of 8000 copper wires of 0.08 mm diameter. The contact area between the wires and the slurry was about 1500 cm^2 .

The heat leak to the sample amounted to about 0.2 erg/s, as determined by placing a heat switch between the sample and the cooling salt. The heat flow between the copper wires and the slurry can be described by

$$\dot{Q} = KA(T_m^4 - T_{CrK}^4) \quad , \quad (20)$$

in which A is the contact area in cm^2 , \dot{Q} is the heat flow in erg/s and T_m and T_{CrK} are the temperatures of the metal wires and the Cr-K-alum respectively. K is the so called "Kapitza resistance" coefficient. Its value was determined by applying a calibrated heat flow by means of a resistance heater, and measuring the value of T_m with a Speer resistor, calibrated against the susceptibility of a sample of cerium magnesium nitrate (CMN). A resistor has the advantage of a fast response to temperature variations. When switching off the heat flow, one makes $\dot{Q} = 0$ (apart from the small natural heat leak) and T_{CrK} could then be measured. This was done in the temperature region $0.025 \text{ K} < T_m < 0.10 \text{ K}$. The results could be reasonably described by formula (20), the value of K being $3.5 \times 10^4 \text{ erg cm}^{-2} \text{ K}^{-4}$. For comparison, we may note that the highest value of K reported in the literature is about $10^5 \text{ erg cm}^{-2} \text{ K}^{-4}$ (21).

Applying this result to the situation in which a heat leak of 0.2 erg/s is present, and taking into account that the Cr-K-alum slurry

can be demagnetized to $T_{CrK} = 10$ mK (experimentally demonstrated by, for instance, the Oxford nuclear orientation group), we expect a temperature $T_m = 11$ mK after demagnetization. This must also be the temperature of the Fe sample, because the temperature gradient in the very pure Cu rod connecting the sample and the wires is negligible. However, the lowest sample temperature obtained was 15 mK. The demagnetizations were quite reproducible, excepting the first one during a given day. In this run, we got a temperature which was generally 1 to 2 mK higher. This behaviour remained the same over a period of several months if the slurry was stored in a refrigerator at -15° C. It indicates that at this temperature deterioration is unimportant.

In view of the calculation above, it is extremely unlikely that the cooling salt is at 10 mK after demagnetization; instead $T_{CrK} = 14$ mK is very probably. No explanation was found for the failure of the apparatus to reach lower temperatures.

Using the magnet with hollow pole pieces, a field of 1.5 to 2.0 kOe was applied in the plane of the iron foils. Preliminary experiments on ^{60}Co nuclei dissolved in Fe had shown that this field was sufficient to orient the domains in the iron foil. The temperature was measured by means of the susceptibility of a cylindrical cerium magnesium nitrate (CMN) powder sample with diameter equal to height. This thermometer was calibrated against a calibrated Speer resistor in the region $0.1 \text{ K} < T < 2 \text{ K}$ under measuring conditions. (The calibration of the Speer resistor was done in the absence of the magnet, utilizing a larger CMN sample). The magnetic field on the CMN was about 30 Oe. A small correction was applied at the lowest temperatures for the deviation from the Curie law due to saturation effects.

The gamma anisotropy was determined with the aid of four NaI scintillation counters, placed along directions parallel and perpendicular to the magnetic field. Conical lead collimators were used to minimize the influence of Compton scattering at the walls of the cryostat and at the magnet. This is very important, especially for the low energy ^{133}Xe gamma ray (81 keV), because the energy loss of the gamma rays during Compton scattering is relatively small. Consequently, part of

these Compton scattered gammas would be accumulated in the photopeaks of the scintillation counters. The use of lead cones, however, made the effect of these scattered photons almost negligible. For the ^{160}Tb measurements, the lead cones were especially useful to minimize the background under the 299 keV photopeak due to scattered photons of higher energy. This background amounted to about 30% of the total number of counts under this peak. The anisotropy in the background was determined by extrapolation from the high energy side of the peak, up to about 700 keV. In this region, the anisotropy was found to vary only slightly with energy.

4. Results and discussion

4.1. ^{133}Xe in Fe.

The results of the measurements on the three samples are shown in fig. 2. From the fact that $W(0) < W(\frac{\pi}{2})$ it follows directly that we must choose the negative value for A_2 , namely $A_2 = -0.138$. Consequently δ is negative (see section 2.1.). The full curve is a theoretical fit

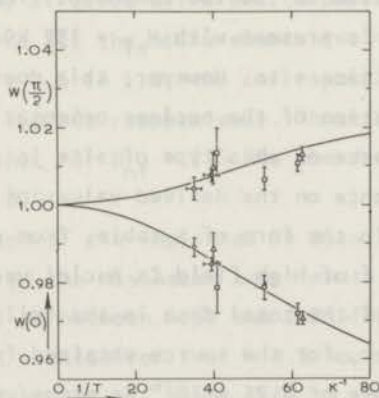


Fig. 2. Results of nuclear orientation measurements on ^{133}Xe in iron.

$W(0)$ and $W(\frac{\pi}{2})$ are the normalized gamma radiation intensities in directions parallel and perpendicular to the magnetic field, respectively.

○ sample I, □ sample II, △ sample III.

The full curve gives the result of a calculation on the basis of eq. (12) with $H_{\text{hf}} = 1.0 \text{ MOe}$.

using this value of A_2 and assuming that the Hamiltonian for all Xe nuclei can be written as

$$H = -g_N \mu_N H_{hf} I_z, \quad (12)$$

with $|H_{hf}| = 1.0 \text{ M0e}$ and $g_N = \frac{\mu}{I} = 0.53$. Within the statistical error there are no differences between the data of the various samples, and the curve fits the measurements reasonably well.

This simple result is rather surprising in view of the Mössbauer effect measurements of De Waard and Drentje²²⁾ on this gamma ray, in which the same type of source was used. From their measurements, it appears that the Xe nuclei come to rest in at least two different sites. For one of the sites the hyperfine field is less than $\approx 30 \text{ k0e}$, whereas for the other site a field of $+273 \text{ k0e}$ is measured at the ^{133}Cs nuclei, produced by the beta decay of ^{133}Xe . This last site is substitutional, as has been determined by Murnick²³⁾, whereas the other is most likely associated with vacancies in the lattice. Recent measurements²⁴⁾, with the source at various temperatures between 4 K and 70 K , indicated that in addition to the two components found previously, a medium field component is present with $H_{hf} \approx 132 \text{ k0e}$, associated with yet another type of lattice site. However, this does not alter significantly the interpretation of the nuclear orientation measurements on ^{133}Xe , since the abundance of this type of site is relatively low and has a negligible influence on the derived values of H_{hf} . We reproduce some of their results in the form of a table, from which it can be seen that the fraction f of high field Cs nuclei varies irregularly between 0.55 and 0.75 if the total dose in the foil is $\lesssim 10^{14} \text{ Xe atoms/cm}^2$ (Table III). However, for the source obtained from neutron irradiated Xe, with a total dose of $8.75 \times 10^{14} \text{ Xe atoms/cm}^2$, the fraction is much lower, $f = 0.22$.

It is clear that the assumption that all Xe atoms experience the same hyperfine field in our samples is not justified by the Mössbauer experiments. Hence the value for the hyperfine field obtained above must be regarded as a lower limit. A rough upper limit can be found by taking into account the variation in the temperature dependence of

TABLE III

Results of Mössbauer experiments on ^{133}Cs in Fe, from ref. 16		
source nr	total dose Xe atoms/cm ²	f
921	0.15×10^{14}	≈ 0.60
922	0.31 -	≈ 0.55
919	0.62 -	≈ 0.74
923	0.88 -	≈ 0.75
920	1.25 -	≈ 0.61
917	8.75 -	≈ 0.22

the calculated anisotropy if one assumes that only a fraction f experiences a large hyperfine field. For a certain value of f , one can vary H_{hf} to obtain the best fit to the experimental points. We have used sample II and III to obtain mean values for the anisotropy parameter $\epsilon \equiv W(\frac{\pi}{2}) - W(0)$ at three different temperatures. It turns out that it is possible to fit the measurements reasonably well for values of f ranging from $f = 0.6$ to 1.0 ; the corresponding best values for H_{hf} are 1.6 MOe and 1.0 MOe respectively. These two curves are drawn in fig. 3. We note that for $H_{\text{hf}} = 1.6 \text{ MOe}$ the data on sample I are compatible with $f \approx 0.5$.

From a comparison of the implanted Xe dose in our samples (Table II), and those used in the Mössbauer experiments (Table III), one might conclude that f will be between 0.55 and 0.75 for sample II and III, whereas for sample I a value for f of ≈ 0.5 would be quite possible. Using only our measurements, it seems safe to conclude that

$$1.0 \text{ MOe} < H_{\text{hf}} < 1.6 \text{ MOe}.$$

From the Mössbauer measurements one might derive that f is smaller than 0.75 . Using this result, we find for the range of H_{hf} values which are allowed by the nuclear orientation measurements:

$$1.2 \text{ MOe} < H_{\text{hf}} < 1.6 \text{ MOe}.$$

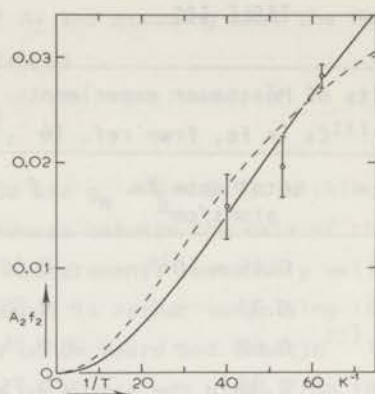


Fig. 3. ^{133}Xe in Fe. Mean experimental values of the anisotropy parameter $\epsilon \equiv W(\frac{\pi}{2}) - W(0)$ as a function of $1/T$, together with the results of calculations using the model explained in the text. Drawn curve: $H_{\text{hf}} = 1.0$ MOe, $f = 1.0$. Dashed curve: $H_{\text{hf}} = 1.6$ MOe, $f = 0.6$.

As was discussed in section 2.3., the most important contribution to H_{hf} is thought to be polarization of the 5s shell of the Xe atoms due to direct overlap with the 3d wave functions of the iron host. Shirley¹⁶⁾ calculated this contribution for the case of Xe in Fe, namely $H_{\text{hf}} \approx +3 \times 10^6$ Oe. This value is very sensitive to a variation in the interatomic distance between Xe and Fe; an increase of this distance with 5% would lower H_{hf} by a factor of two. Therefore the discrepancy between Shirley's calculation and our experimental result is not significant. The CEP contribution to the hyperfine field is difficult to estimate, because one can doubt the physical relevance of the model of Daniel and Friedel¹⁴⁾ (or the improved version of Campbell¹⁵⁾) for this case. However, most probably the CEP contribution is positive, so that there can be little doubt about the positive sign of the hyperfine field on Xe nuclei in Fe.

4.2. ^{160}Tb in Fe.

The results of the measurements on three samples are summarized in figures 4-6. Using the same model as for the analysis of the ^{133}Xe results, we were able to obtain rather accurate values for the fraction

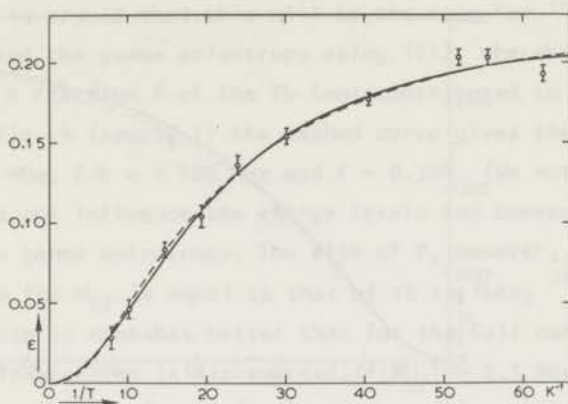


Fig. 4. Nuclear orientation measurements on ^{160}Tb in Fe. Results on sample I. The full curve gives the result of a calculation using the following parameters: $|H_{hf}| = 2.3 \text{ Moe}$, $P = 0$, $f = 0.286$. Dashed curve: $|H_{hf}| = 3.8 \text{ Moe}$, $P/h = +180 \text{ MHz}$, $f = 0.304$.

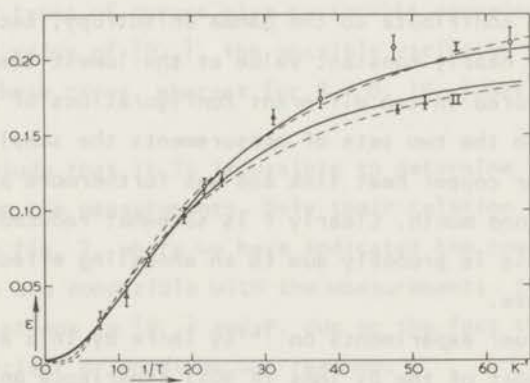


Fig. 5. Nuclear orientation measurements on ^{160}Tb in Fe. Results on sample II. Configuration II^a: experimental points denoted by \odot , calculated curves by I. Dashed curve: $|H_{hf}| = 3.8 \text{ Moe}$, $P/h = +220 \text{ MHz}$, $f = 0.345$. Full curve: $|H_{hf}| = 2.1 \text{ Moe}$, $P = 0$, $f = 0.296$. Configuration II^b: experimental points denoted by Δ , calculated curves by II. Dashed curve: $|H_{hf}| = 3.8 \text{ Moe}$, $P/h = +180 \text{ MHz}$, $f = 0.270$. Full curve: $|H_{hf}| = 2.3 \text{ Moe}$, $P = 0$, $f = 0.259$.

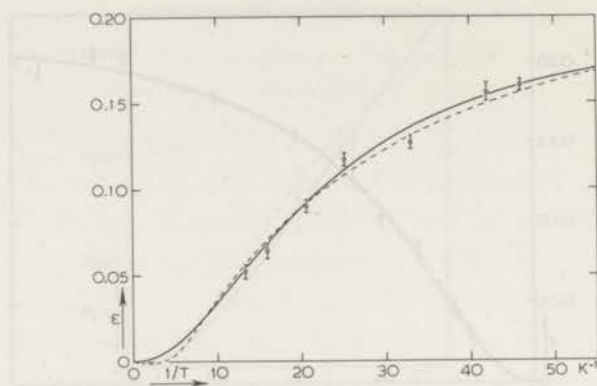


Fig. 6. Nuclear orientation measurements on ^{160}Tb in Fe. Results on sample III. The full curve gives the result of a calculation using the following parameters: $|H_{hf}| = 2.1$ MOe, $P = 0$, $f = 0.250$. Dashed curve: $|H_{hf}| = 3.8$ MOe, $P/h = +230$ MHz, $f = 0.298$.

f of ions which contribute to the gamma anisotropy, because the anisotropy reached a nearly constant value at the lowest temperatures. Sample II was measured in two different configurations of the apparatus, a and b. Between the two sets of measurements the sample was soft soldered to another copper heat link and was furthermore at room temperature for about one month. Clearly f is somewhat reduced if we compare II^a and II^b; this is probably due to an annealing effect during the soldering process.

The Mössbauer experiments on ^{161}Dy in Fe by Inia and De Waard²⁵⁾ indicate that most of the Dy ions ($\approx 90\%$) experience an appreciable electric quadrupole interaction in addition to the magnetic hfs interaction. Assuming that this will be the case also for Tb ions, the total hfs Hamiltonian must be written as

$$H = -g_N \mu_N H_{hf} I_z + P \left\{ I_z^2 - \frac{1}{3} I(I+1) \right\}. \quad (21)$$

This holds also for a polycrystalline sample if the electric field gradient at the nucleus is due to the 4f electrons, which in turn are oriented by an exchange field collinear with the external field. In

section 2.3, it is argued that this will be the case for ^{160}Tb in Fe.

We calculated the gamma anisotropy using (21), whereby it was assumed that only a fraction f of the Tb ions contributed to the gamma anisotropy. In fig. 4 (sample I) the dashed curve gives the results for $|H_{\text{hf}}| = 3.8$ MOe, $P/h = +180$ MHz and $f = 0.304$. (We note that the sign of H_{hf} does not influence the energy levels and consequently has no effect on the gamma anisotropy. The sign of P , however, is important.) The value for H_{hf} is equal to that of Tb in TbFe_2 ²⁶). The agreement with the data is somewhat better than for the full curve, where the quadrupole interaction is disregarded. ($|H_{\text{hf}}| = 2.3$ MOe, $P = 0$, $f = 0.286$). For a fixed value of $|H_{\text{hf}}|$, the variation of P/h allowed by the data is about 20 MHz.

In fig. 5 and 6 the data on samples II and III are fitted in the same way. The dashed curves give the result of fits in which $|H_{\text{hf}}|$ was kept constant, while P/h and f were optimized. The full curves show fits in which the quadrupole interaction was disregarded ($P = 0$). As can be seen, both types of curves give reasonable agreement with the data. For a fixed value of $|H_{\text{hf}}|$, the possible variation in P/h is about 30 MHz in these cases, whereas for $P = 0$, $|H_{\text{hf}}|$ may vary as much as 0.2 MOe.

We must conclude that it is impossible to determine $|H_{\text{hf}}|$ and P independently from the measurements. Only their relation can be given, as can be seen in fig. 7, where we have indicated the combinations of $|H_{\text{hf}}|$ and P which are compatible with the measurements. f is quite insensitive to variations in $|H_{\text{hf}}|$ and P , due to the fact that a very high degree of nuclear orientation was reached.

At this point we want to discuss the results of other experiments which are relevant to the measurements presented here. Inia and De Waard²⁵) have performed Mössbauer experiments on ^{161}Dy nuclei. In this case ^{161}Tb ions were implanted, so that the implantation problems are very similar. The Mössbauer spectra obtained show a clear hyperfine structure pattern. At liquid nitrogen temperature, nearly all Dy ions experience a hyperfine field $|H_{\text{hf}}| = 6.05$ MOe and a quadrupole coupling with $P/h = +122$ MHz. At room temperature these parameters are $|H_{\text{hf}}| = 4.5$ MOe and $P/h = +60$ MHz. The spectrum shows a distinct re-

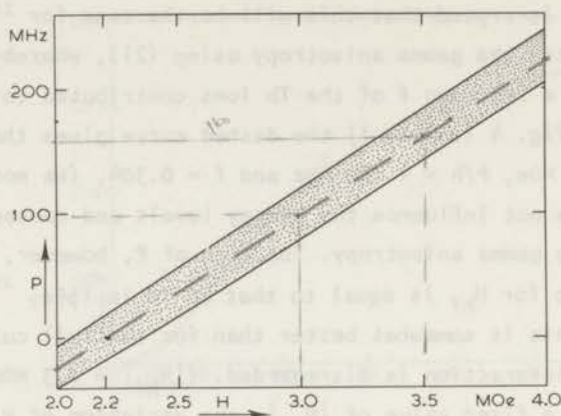


Fig. 7. ^{160}Tb in Fe. The shaded area represents the combinations of P and H_{hf} which are compatible with the nuclear orientation results.

relaxation behaviour at this temperature; in addition to the usual hfs spectrum a diffuse background plus a strong central peak is observed. It is not clear at this moment if the spectrum is build up by several fractions of Dy nuclei (associated with different sites) or if one observes the relaxation behaviour of only one fraction. A provisional analysis²⁵⁾ shows that the temperature dependence of the hfs parameters is in accordance with formulas (18) and (19), if one takes the strength of the exchange field H_{ex} as $g\mu_B H_{\text{ex}}/k \approx 100$ K. Extrapolation to $T = 0$ yields $|H_{\text{hf}}| = 7.0$ MOe and $P/h = +170$ MHz, which is somewhat higher than the free ion value calculated by Bleaney²⁰⁾, but in reasonable agreement with the values found by Bowden et al. for ^{161}Dy nuclei in DyFe_2 ²⁷⁾.

Other interesting information is gained from channeling experiments. Schmorak and Bøgh²⁸⁾ implanted 3×10^{15} Lu ions/cm² into an iron single crystal, and deduced from channeling measurements that about 40% of the Lu ions occupied substitutional sites, whereas the remaining 60% was probably located in radiation damaged zones of the crystal. The substitutional sites are not thermodynamically stable, because annealing of the samples gives a lower fraction of ions at substitutional sites²⁹⁾. One therefore may expect that after implan-

tation a considerable fraction of rare earth ions will be at non-substitutional sites.

Returning to our nuclear orientation experiments on ^{160}Tb in Fe, we notice that our value of f , 25% - 35%, is in reasonable agreement with the value for the fraction of rare earth ions at substitutional sites, as found from channeling experiments. It seems reasonable to associate the fraction f contributing to the gamma anisotropy with substitutional sites, where the exchange interaction will dominate the crystal field effects. For these ions, we expect to find the full hyperfine field, (plus) contributions from core and electron polarization, which would lead to $|H_{\text{hf}}| \approx 3.8 \text{ MOe}$, as found in TbFe_2 ²⁶⁾. We see from fig. 7 that this is compatible with our measurements, if a quadrupole interaction with $P/h \approx 200 \text{ MHz}$ is also present. This can be compared, for instance, to the value of the quadrupole interaction of stable Tb in Tb metal: $P/h = + 334 \text{ MHz}$ ^{30,31)}. From the known values of the quadrupole moments of stable ^{159}Tb ($Q = 1.32 \pm 0.13 \text{ barn}$ ³²⁾) and of ^{160}Tb ($Q = 3.0 \pm 0.5 \text{ barn}$ ¹³⁾), we calculate for the quadrupole coupling constant $^{160}P/h = + 150 \pm 30 \text{ MHz}$, which is only slightly smaller than our value, $P/h \approx 200 \text{ MHz}$. For comparison, in DyFe_2 the Dy quadrupole coupling is roughly 25% higher than in Dy metal²⁵⁾, which gives an estimate of the variation in $1 - R_Q$ for these environments. We conclude that the data are consistent with the model in which exchange effects give rise to an electronic ground state $\langle J_z \rangle = J$. However, the possibility that crystal field effects have a noticeable influence, leading to a lowering of $\langle J_z \rangle$ and thus of H_{hf} , cannot be ruled out.

In our experiments, f appeared to be insensitive to a variation in the Tb dose by a factor 20, and also insensitive to variations in the implantation energy. This has been confirmed by PAC measurements of Murnick²³⁾ and leads to the conclusion that surface effects in the target are unimportant. Our measurements show very clearly that reproducibility of the results does not necessarily mean that all ions come to rest at identical sites in the Fe lattice. Therefore, the interpretation of measurements in which one has no information about those

sites is very difficult, and may lead to ambiguous results. We suspect that many of the IMPACT measurements made on rare earth impurities in Fe suffer from this ambiguity.

The value for f obtained ($\approx 30\%$), seems to be in contradiction with the results of the Mössbauer experiments. However, the discrepancy can be removed if one supposes that non-substitutional sites probably will be associated with one or more vacancies in the iron lattice. The presence of one vacancy leads to a strong axial crystalline electric field at the position of the ion. Consequently the rare earth ion will have a ground state in which $\langle J_z \rangle \approx J$, where the z -axis is aligned along the axis of the crystalline field. In a polycrystalline sample these axes will be randomly distributed in space, so that the rare earth ions will have no net alignment and thus do not contribute to the gamma anisotropy. On the other hand, these rare earth nuclei will experience the full hyperfine field, which explains that a large fraction of the Dy ions show the full hyperfine interaction, although they do not all occupy substitutional sites. The same holds for the quadrupole interaction, if the $4f$ electrons provide the main component of the electric field gradient at the nucleus.

Finally we will discuss the sign of the hyperfine parameters. The measurements are sensitive to the sign of P , but not to that of H_{hf} .

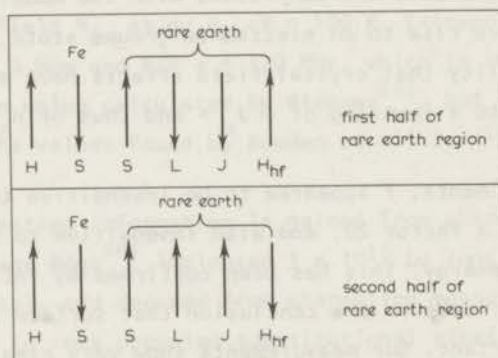


Fig. 8. Sign of the hyperfine field on rare earth impurities in iron, assuming an antiferromagnetic exchange interaction between the electron spins of the iron host and the rare earth impurity.

Nevertheless, the sign of H_{hf} for Tb can be determined from IMPACT measurements on rare earth ions in Fe^{33,34}). These measurements show that the hyperfine fields are positive in the first half of the rare earth region (Ce-Sm) and negative in the second half (Gd-Yb), which means that the coupling between the d spins of the iron host and the spin of the rare earth impurity is antiferromagnetic. This is illustrated in fig. 8. The hyperfine field on the Tb nucleus is thus negative.

References

1. Samoilov, B.N., Sklyarevskii, V.V. and Stepanov, E.P., Zh.Exp. Theor. Fis. U.S.S.R. 36 (1959) 644. (J.E.T.P. 9 (1959) 448).
2. A discussion on ion implantation and hyperfine interactions, Proc. Roy. Soc. 311 A (1968) 3-211.
3. Shirley, D.A., Rosenblum, S.S. and Matthias, E., Phys. Rev. 170 (1968) 363.
4. Brown, F., Graham, R.L., Ewan, G.T. and Uhler, J., Can.Journ. Phys. 39 (1961) 779.
5. De Groot, S.R., Tolhoek, H.A. and Huiskamp, W.J., Alpha-, Beta- and Gamma-ray Spectroscopy, ed. K. Siegbahn, North-Holland Publ. Co., (Amsterdam, 1965) p. 1199 c.f.
6. Biedenharn, L.C. and Rose, M.E., Rev.Mod.Phys. 25 (1953) 729.
7. Rose, H.J. and Brink, D.M., Rev.Mod.Phys. 39 (1967) 306.
8. Nuclear Data Tables A 5 (1969) 433 (Academic Press, New York).
9. Jaklevic, J.M., Funk, E.G. and Mihelich, J.W., Nucl.Phys. A 99 (1967) 83.
10. Krane, K.S., and Steffen, R.M., to be published.
11. Nuclear Data Sheets for A = 160, compiled by K. Way et al. (Printing and Publishing Office, Nat.Ac.Sci.-Nat.Res.Council, Washington, D.C.).
12. Günther, C., Strübe, G., Wehmann, U., Engels, W., Blumberg, H., Luig, H., Rieder, R.M., Bodenstedt, E. and Körner, H.J., Z. Phys. 183 (1965) 472.
13. Easley, W.C., Barclay, J.A. and Shirley, D.A., Phys.Rev. 170 (1968) 1083.
14. Daniel, E. and Friedel, J.J., J.Phys.Chem.Solids 24 (1963) 1601.
15. Campbell, I.A., J.Phys.C 2 (1969) 1338.
16. Shirley, D.A., Phys.Letters 25A (1967) 129.
17. Elliott, R.J. and Stevens, K.W.H., Proc.Roy.Soc. A 218 (1953) 553.
18. Watson, R.E. and Freeman, A.J., Hyperfine Interactions, ed. A.J. Freeman and R.B. Frankel, Academic Press (New York, 1967) p.80.
19. Lea, K.R., Leask, M.J.M. and Wolf, W.P., J.Phys.Chem.Solids 23 (1962) 1381.
20. Bleaney, B., J.Appl.Phys. 34 (1963) 1024.
21. Vilches, O.E. and Wheatley, J.C., Rev.Sci.Instr. 37 (1966) 819.
22. De Waard, H. and Drentje, S.A., Proc.Roy.Soc. A 311 (1969) 139.
23. Murnick, D.E., Conference on Angular Correlations, Delft, 1970.

24. De Waard, H., Schurer, P., Inia, P., Niesen, L. and Agarwal, Y.K., Proceedings Conference on Hyperfine Structure and Nuclear Radiations, Rehovoth, 1970.
25. Inia, P. and De Waard, H., Conference on Angular Correlations, Delft, 1970.
26. Atzmony, U., Bauminger, E. and Ofer, S., Nucl.Phys. 89 (1966) 433.
27. Bowden, G.J., Bunbury, D.St.P., Guimarães, A.P. and Snyder, R.E., J.Phys. C 1 (1968) 1376.
28. Schmorak, M. and Bøgh, E., Hyperfine Structure and Nuclear Radiations, ed. E. Matthias and D.A. Shirley, North-Holland Publ. Co., (Amsterdam, 1968) p. 712.
29. Deutch, B.I., comment on ref. 28, p. 717.
30. Kobayashi, S., Sata, N. and Itoh, J., J.Phys.Soc.Japan 22 (1967) 676.
31. Anderson, A.C., Holmström, B. and Krusius, M., Phys.Rev.Letters 20 (1968) 154.
32. Arnoult, C. and Gerstenkorn, S., J.Opt.Soc.Am. 56 (1966) 177.
33. Grodzins, L., Borchers, R. and Hagemann, G.B., Phys.Letters 21 (1966) 214.
34. Boehm, F., Hagemann, G.B. and Winther, A., Phys.Letters 21 (1966) 217.

SAMENVATTING

De wisselwerking tussen de kernspin en de omringende elektronen van een atoom of ion, de zogenaamde hyperfijnstructuur (hfs) interactie, kan worden onderzocht met een groot aantal technieken. In het geval van radioactieve kernen kan de hfs wisselwerking worden bestudeerd door metingen te doen aan de door deze kernen uitgezonden straling. De in dit proefschrift beschreven kernorientatie experimenten maken deel uit van dit snel groeiende gebied van onderzoek, dat een grensgebied vormt tussen de kernfysica en de fysica van de vaste stof.

In de hier beschreven onderzoeken werden radioactieve kernen tot zeer lage temperaturen ($T \approx 0.01$ K) afgekoeld, waardoor een aanzienlijke kernspinpolarisatie kon worden verkregen. Deze werd bestudeerd door de anisotropie in de richtingsverdeling van de uitgezonden gammastraling te meten. Wanneer voldoende van het verval van de radioactieve kern bekend is, geeft een meting van de gamma anisotropie als functie van de temperatuur informatie over de sterkte van de hyperfijnstructuur wisselwerking.

Deze methode geeft vrij globale en niet erg nauwkeurige resultaten. Het blijkt echter mogelijk kernorientatie te combineren met magnetische resonantie: door een magnetisch wisselveld in te stralen, waarvan de frequentie past bij het energieverval tussen twee opeenvolgende hfs niveaus, is het mogelijk overgangen tussen deze niveaus te induceren. Dit leidt tot een verandering van de kernspinpolarisatie, en daarmee tot veranderingen in de gamma anisotropie.

In Hoofdstuk I en II wordt deze methode toegepast op vijf radioactieve kernen, die zijn opgenomen in een éénkristal van lanthaan magnesium nitraat, waaraan 0.1 at.% cerium is toegevoegd. De kernspins werden georiënteerd in een magnetisch veld van enkele kOe door warmtecontact tot stand te brengen met het cerium elektronspinsysteem, dat door middel van rotatiekoeling op een zeer lage temperatuur was ge-

bracht. Dit contact komt tot stand wanneer de Zeeman opsplitsing van de Ce spins gelijk wordt aan de energiever verschillen tussen de hfs niveaus van de radioactieve kernen. Zolang hieraan niet voldaan is, en de temperatuur van het kristal beneden 0.1 K blijft, is het kernspinsysteem vrijwel geïsoleerd van de omgeving. Dit blijkt een belangrijk voordeel te zijn voor het hierop volgende resonantie experiment, omdat hierdoor de door het hoofdfrequent veld geïnduceerde veranderingen in de bezettingsgraad van de hfs niveaus niet worden tegengewerkt door de kernspin-rooster relaxatie.

Door instraling van een wisselveld, waarvan de frekwentie langzaam werd gevarieerd, konden de energiever verschillen tussen de verschillende hfs niveaus zeer nauwkeurig worden bepaald uit de optredende veranderingen in de gamma anisotropie. Uit deze metingen konden de magnetische momenten van de vijf radioactieve isotopen bepaald worden met een veel grotere nauwkeurigheid dan voorheen. Tevens konden de elektrische quadrupoolmomenten van deze kernen voor het eerst worden bepaald. Details van het resonantieproces, zoals overgangswaarschijnlijkheden en lijnbreedtes, konden bevredigend worden verklaard. Van de in het verval van ^{57}Co optredende 122 keV gamma overgang werd de multipool mengverhouding gemeten, terwijl tevens waardevolle informatie werd verkregen over de kernspin-desorientatie die bij dit verval optreedt gedurende de tijd dat de ^{57}Fe kern zich bevindt in een aangeslagen toestand op 136 keV van het grondniveau.

Hoofdstuk III beschrijft orientatie experimenten aan ^{133}Xe en ^{160}Tb kernen, die met behulp van een isotopenseparator waren geïmplanteerd in ijzerfolies. Dit werk werd gedaan in nauwe samenwerking met de groep van Prof.dr. H. de Waard in Groningen. Voor dit soort systemen hebben resonantiemethoden tot nu toe geen resultaat opgeleverd. De hyperfijnstructuur interactie werd daarom bestudeerd door de gamma anisotropie te meten als functie van de temperatuur in een veld van circa 2 kOe, groot genoeg om de Weiss gebiedjes in de ijzerfolies te richten.

Ionenimplantatie is de enig bruikbare methode om Xe en Tb ionen in een ijzerrooster te brengen. Het nadeel is echter, dat niet alle

ionen op substitutionele plaatsen terecht komen, waardoor het hyperfijnveld niet voor alle kernen hetzelfde is. Het bleek desondanks mogelijk zinnvolle resultaten uit de metingen te verkrijgen, door deze te combineren met de resultaten van Mössbauer-effect metingen aan ^{133}Cs en ^{161}Dy kernen in Fe, uitgevoerd door de groep in Groningen.

Op verzoek van de faculteit der Wiskunde en Natuurwetenschappen volgt hier een overzicht van mijn studie.

Na het behalen van het HBS-B diploma aan het Dalton Lyceum in Den Haag, waar Dr. W.P.J. Lignac mijn belangstelling voor de natuurkunde wist te wekken, ben ik in 1960 mijn studie begonnen aan de Rijksuniversiteit te Leiden. Het candidaatsexamen D¹ in de vakken natuurkunde, wiskunde en scheikunde werd in 1963 afgelegd. Sinds november van dat jaar ben ik verbonden aan de werkgroep adiabatistische demagnetisatie en kernfysica van het Kamerlingh Onnes Laboratorium, waarvan Prof.dr. C.J. Gorter de supervisie heeft, en de dagelijkse leiding berust bij Dr. W.J. Huiskamp. Hier assisteerde ik Dr. J. Lubbers, die mij de eerste beginselen van de experimentele natuurkunde op bescheiden, maar daarom niet minder doeltreffende wijze heeft bijgebracht. In september 1966 legde ik het doctoraal examen experimentele natuurkunde af.

Sinds 1964 heb ik diverse functies vervuld bij het natuurkundig practicum. De Stichting voor Fundamenteel Onderzoek der Materie, F.O.M., verleende mij in juni 1965 een candidaat-assistentschap in de werkgroep K IV. In oktober 1966 werd ik aangesteld als wetenschappelijk medewerker.

Tijdens mijn werkzaamheden heb ik van alle leden van de werkgroep veel medewerking gehad. Dr. J. Lubbers suggereerde de resonantie experimenten waaraan een groot deel van dit proefschrift is gewijd, en werkte mee aan de eerste metingen. Verder hebben drs. H.B. Brom, drs. J.A. Konter, drs. D.L. de Jong, de heer F.J. van Steenwijk en in het bijzonder drs. N. de Boo hulp verleend tijdens de experimenten. Drs. E. Lagendijk bood de helpende hand bij het oplossen van diverse numerieke problemen. Door de geregelde discussies met Dr. W.J. Huiskamp hebben inhoud en vorm van het proefschrift grote verbeteringen ondergaan.

Mijn speciale dank gaat uit naar mijn vrienden uit Groningen, in het bijzonder naar Prof.dr. H. de Waard, die de experimenten beschreven in Hoofdstuk III op stimulerende wijze heeft begeleid. Dr. S.A. Drentje, Dr. Y. Agarwal, Drs. P. Schurer en drs. P. Inia vervaardigden de geïmplanteerde bronnen. Met Dr. H. Postma had ik een aantal waardevolle discussies.

De verzorging van het technische en cryogene gedeelte van de opstelling lag in de bekwame handen van de heren J. van Weesel en J. van der Waals. De glazen apparatuur werd vervaardigd door de heren C.J. van Klink en P.J.M. Vreeburg. De heren R. Hulstman en F.J. Kranenburg verzorgden de elektronische apparatuur. Drs. P.W. Verbeek en drs. H.L. van Noort leenden mij hun radiofrequentie apparatuur en gaven een aantal waardevolle adviezen. Alle tekeningen werden gemaakt door de heer W.F. Teegelaar, terwijl het typewerk op vaardige wijze werd uitgevoerd door de administratieve staf van het laboratorium. Dr. J.K. Hoffer en Dr. R.C. Thiel ben ik erkentelijk voor het corrigeren van de Engelse tekst.

